PhD degree in Medical Nanotechnology

European School of Molecular Medicine (SEMM)

University of Milan

Faculty of Medicine

Settore disciplinare: FIS/07

Design of a high-throughput method for the assessment of enzyme activity upon adsorption on cluster-assembled nanostructured titanium oxide films

Supervisor: Prof. Paolo Milani

University of Milan

External co-Supervisor: Prof. Yosi Shacham-Diamand

Tel Aviv University

Lasma Gailite, MSc

University of Milan

Matricola n. R07958

Academic Year 2011-2012

The Mentaculus –

To my son, his father and his grandparents

1. CONTENTS

ACKNOWLEDGEMENTS

This work was kindly supported by following collaborations: i) Vimal Sharma performed the synthesis of nanostructured titanium oxide films and designed and deposited the gradient slides; ii) Marco Indrieri, Massimiliano Galluzzi and Elisa Sogne performed the AFM characterization of the nanostructured titanium oxide films; iii) Antonio Borgonovo and Luca Ravagnan created supporting software for image analysis and spectrophotometry.

I would like to acknowledge my thesis supervisor Prof. Paolo Milani for giving me the possibility to accomplish the PhD thesis project being a part of his group and for the support that he has provided to me during the years of the PhD study.

I would also like to express my gratitude to the external co-supervisor Prof. Yosi Shacham-Diamand and to Prof. Gabriella Tedeschi for the fruitful discussions.

Thanks to Pasquale Scopelliti for his fountain of ideas and friendly discussions.

Moreover, I am saying special thanks to my colleagues Vimal Sharma, Ajay Vikram Singh and Varun Vyas for the constant encouragement that they have given to me through the years of the PhD.

Thanks to Lara Pagliato and to Simona Rodighiero for the assistance and advice.

I wish to say many thanks to all of my current and ex-colleagues who have always been truly supportive and have shown interest in my work.

LIST OF ABBREVIATIONS

Activity probe:	ActivX TAMRA-conjugated fluorophosphonate serine hydrolase probe (Pierce/Thermo Scientific)
AFM:	atomic force microscopy
Alexa555-trypsin:	trypsin conjugated with Alexa Fluor 555 dye
Alexa647-BSA:	bovine serum albumin conjugated with Alexa Fluor 647 dye
Asp:	aspartate
BAPNA:	Nα-Benzoyl- DL -arginine 4-nitroanilide hydrochloride
BSA:	bovine serum albumin
FITC:	fluorescein isothiocyanate
FPQ:	fluorescence photobleaching quantification
FRAP:	fluorescence recovery after photobleaching
FWHM:	full width at half maximum
His:	histidine
Milli-Q water:	ultrapure water produced using Milli-Q filtration system (Millipore Corporation)
ns-TiO_x:	cluster-assembled nanostructured titania synthesized by supersonic cluster beam deposition method
OWLS:	optical waveguide lightmode spectroscopy
PMCS:	pulsed microplasma cluster source
PSIM:	protein-surface interaction microarrays
QCM:	quartz crystal microbalance
SCBD:	supersonic cluster beam deposition
SDS:	sodium dodecyl sulfate
Ser:	serine
SPR:	surface plasmon resonance
TAMRA:	carboxytetramethylrhodamine
TBS:	tris buffered saline
TBS-Ca^{2+}:	tris buffered saline modified by 20 mM $CaCl_2$
TE and TM modes:	transverse electric (TE) and transverse magnetic (TM) modes of a beam of electromagnetic radiation
TIRF:	total internal reflection fluorescence
Tris:	tris(hydroxymethyl)aminomethane

LIST OF FIGURES

LIST OF TABLES

ABSTRACT

Control of nanometre-scale topography of solid surfaces has opened the possibility to tailor the interactions between materials and biomolecules in a manner that allows the maintenance of the biological functions of these molecules, a crucial aspect for diverse applications of biomaterials spanning from in vitro biosensors to in vivo tissue implants. The general mechanisms that dictate protein adsorption to topographical nanostructures are however poorly understood. We have addressed this issue in our previous work uncovering the role of pore geometry in protein adsorption to random rough nanoporous surfaces. In this study, on the other hand, we have explored the catalytic activity of immobilized serine-protease trypsin as product of its adsorption properties governed by the nanometre-scale surface morphology of cluster-assembled titanium oxide films.

Both, adsorption characteristics and the catalytic activity of the surface-bound enzymes, were evaluated in parallel using an innovative microarray-based methodology developed in this PhD work. The principle of the novel approach combines the arraying of fluorescently labelled enzymes on a panel of materials of interest coated on glass microarray slides, with the subsequent on-chip binding of fluorescently labelled activity-based probes. In contrast to standard techniques for enzyme detection in microarray format, our method enables the estimation of activity of enzymes immobilized by physisorption omitting the requirement of covalent attachment and, most importantly, giving direct measure of the interaction between the biomaterial and the enzyme under investigation.

Trypsin adsorption analysis demonstrated an increase in both, the saturation uptake and the equilibrium dissociation constant, with roughness thereby exceeding the predicted contribution of the specific area. The observed trend was attributed to clustering of enzyme molecules inside the surface nanopores resulting in the filling of pore volume rather than homogenous coverage of surface area, as it has been proposed previously for protein adsorption on stochastically rough surfaces. The growth of adsorbed trypsin activity with roughness was

attributed to the increment of the specific area provided by the titania films, whereas the drop in the specific activity per mass of immobilized enzyme was associated with the steric hindrance of trypsin clustered inside titania nanopores.

This study has shed light on the topographical determinants of trypsin adsorption on nanostructured titania surfaces and the consequences of trypsin adsorption properties on its resulting catalytic activity. A novel method was developed elucidating the obstacles and specifics of protease immobilization by physisorption and suggesting possible routes to solve them. This methodology is directly applicable in biomaterial screening with respect to the functionality of immobilized enzymes and can be extended beyond the trypsin-nanostructured titanium oxide model used in this work.

OBJECTIVES

Material surfaces bearing topographical features on the nanometre scale have been shown to provide the means for selective localization, enhanced immobilization, as well as manipulation of bio-macromolecules, such as proteins, polysaccharides and lipids. Particularly in the design of biomaterial surfaces, there is an urge to synthesize disordered nanostructures capable of mimicking the naturally occurring stochastic nanometre scale morphology of the extracellular matrix. On the other hand, materials possessing a random size and shape distribution of submicron- to nanometre scale pores have found recognition as heterogeneous nucleants in protein crystallization and as media for surface-based enzymatic catalysis. The vast majority of applications though, are developed by trial-and-error methods combining the material of choice with selected immobilization techniques and surface chemistries, often grounded on empirical findings. Irrespective of the specific context of the nano-bio-interface, it is therefore of prime importance to uncover the mechanisms of protein adsorption which in turn determine the density and organization of adsorbed protein layers, as well as the conformation and the biological functionality of immobilized protein molecules.

From the perspective of solid-state enzymatic catalysis, we defined the primary objective of this thesis study: to clarify how the catalytic activity of a model enzyme trypsin is influenced by its adsorption behaviour on a disordered nanostructured surface. In order to explore the adsorption and activity characteristics of the enzyme as variables dependent on preassigned nanoscale surface properties, we exploited a bottom-up thin film synthesis method termed supersonic cluster beam deposition (SCBD). According to the SCBD method, thin solid films are grown by random stacking of clusters of atoms on solid support positioned in the path of the cluster beam. By virtue of the low temperature ballistic deposition, the resulting films are assembled of nanometre-sized clusters, whereby the average thickness, roughness and specific area are fully controllable parameters defined by the deposition settings. Furthermore, as opposed to various top-down surface fabrication methods, the nanostructure is achieved by SCBD

without the modification of surface chemistry and altering solely topographical features, thus presenting a platform for the studies of the effect of nanotopography on protein adsorption.

For protein adsorption studies, we have applied a method developed earlier by our group, the protein-surface-interaction-microarrays (PSIM), which relies on the detection of fluorescently labelled proteins dispensed as subnanoliter droplets on the material surface of choice. From the multitude of available methods, PSIM is superior for protein adsorption studies in the case of nanostructured surfaces since it is not limited to optically smooth surfaces and does not require a prior knowledge of the optical constants of the surface. Moreover a range of surface parameters and protein concentrations are probed within each single experiment.

Owing to the advantages of the PSIM technique, we have set the second objective to this thesis study: the further development of the PSIM methodology to enable detection of the catalytic activity of surface-bound enzymes. One must remark that virtually all of the enzyme activity assays are targeting free enzymes in solution and hence – in the case of physisorbed enzymes – the resulting activity signal can be biased by undesired side effects, such as leakage of the enzyme molecules from material surface. In contrast to conventional activity assays, the fraction of activity signal that originates from enzyme species detached from material surface is excluded in PSIM methodology. In line with this assumption, we adapted activity-based probes originally designed for activity-based protein profiling in proteomic research, to the detection of physisorbed enzyme activity in microarray format by PSIM method.

Taken together, the two main objectives of this doctoral study were: 1) to elucidate the relation between the catalytic activity of a physisorbed model enzyme and the nanoscale topography parameters of cluster-assembled solid thin films; and 2) to establish a methodology capable of detection of the activity of physisorbed enzyme molecules in microarray format.

1. INTRODUCTION

1.1. Protein adsorption on solid surfaces

1.1.1. Adsorption models

Protein adsorption to solid surfaces can be mediated by multiple interactions, including electrostatic, hydrophobic, van der Waals and hydrogen bonding, owing to the variety of surface-exposed side chains of the amino acid constituents and the complex behaviour of the biopolymer molecules. The interaction between proteins and solid substrates is further affected by the physicochemical properties of the solid interface, e.g., hydrophobicity versus hydrophilicity, smooth versus rough topography, along with the characteristics of the surrounding medium, e.g., the composition, pH and ionic strength of the buffer. Despite of the complex interplay of the various factors governing protein adsorption, it is often well described with simplistic models, among which the most widely used are the Langmuir model and the Random Sequential Adsorption model.

The Langmuir model (Langmuir, 1918) that was initially developed for the adsorption kinetics of perfect gas molecules on solid surface scan be generalized in terms of equilibrium statistical mechanics to approximate the reversible adsorption of any non-interacting particles. The reversibility of the adsorption implies the possibility of desorption and surface mobility of the adsorbed molecules. To sum up, Langmuir model combines the principles of perfect gas kinetics with geometric assumptions for the covered adsorbent surface: the non-interacting adsorbate molecules can bind to the homogenous adsorbent surface via single type of adsorption sites, the number of which is definite, reaching one complete monolayer (Dabrowski, 2001). Thus, the adsorption can be viewed as filling of the adsorption sites (vacancies) on the available surface with the corresponding fractional coverage θ proportional to the adsorbed density Γ as: $\Gamma = m/a \cdot \theta$, where m is the mass of the adsorbate molecule and a is the surface area covered by a single

adsorbate molecule (adsorption cross-section or the footprint in case of proteins). The evolution of the adsorbed density with time can then be expressed as:

$$\frac{d\Gamma}{dt} = k_{on} C(\Gamma_{\mathrm{m}} - \Gamma) - k_{off}\Gamma$$

where C is the bulk concentration of the adsorbate molecules, Γ_m is the maximum adsorbed density corresponding to the maximum fractional coverage θ_m, i.e., one full monolayer, k_{on} and k_{off} are the adsorption and desorption rate constants, respectively. Assuming a state of dynamic equilibrium between adsorption and desorption implies that the adsorption rate is equal to the desorption rate:

$$k_{on} C(\Gamma_m - \Gamma) = k_{off}\Gamma$$

Equilibrium dissociation constant can be defined as: $k_D = k_{off}/k_{on}$. Deriving the steady state dependence of the adsorbed density from the bulk concentration of the adsorbate molecules leads to the Langmuir isotherm (Fig. 1.1.1.1.) that can be written in the following form:

$$\Gamma = \frac{\Gamma_m}{1 + \frac{k_D}{C}}$$

Γ_m or the maximum adsorbed density is often termed “saturation uptake” or shortly, *SU*, when expressed in the units of mass per area to characterize the loading capacity of a particular surface with the adsorbate molecules. As evident from the equation, the equilibrium dissociation constant k_D is equivalent to the adsorbate bulk concentration at which the adsorbed density has reached the half of the saturation uptake. The reciprocal of the equilibrium dissociation constant $K = 1/k_D$ or respectively, the equilibrium binding constant K, is directly proportional to the affinity of the adsorbate molecules to the adsorbent surface, giving the strength of the binding interaction in terms of thermodynamics.

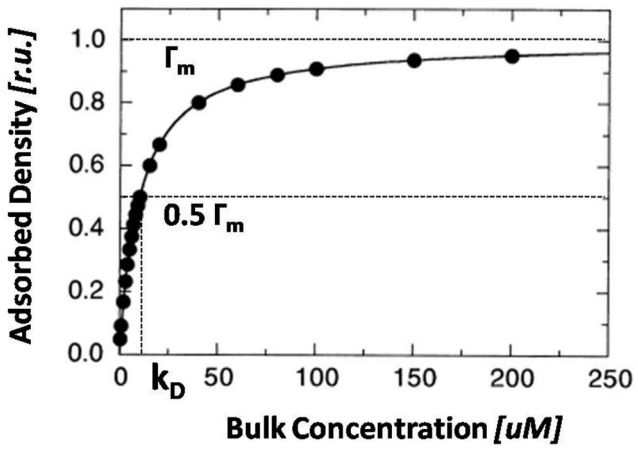

Fig. 1.1.1.1. Langmuir isotherm with the characteristic parameters: equilibrium dissociation constant k_D and maximum adsorbed density Γ_m (also denoted as SU or saturation uptake).

According to the reversibility assumption, the Langmuir model can account for protein adsorption caused by interactions the energy of which is on the order of magnitude of thermal energy, i.e., the weak intermolecular bonding, including van der Waals forces and the weak hydrogen bonding (Senger et al., 2000). Numerous studies have been proven however, that the practical applicability of the Langmuir model oversteps the limitations set by the theory. Satisfying approximation and explanation of the adsorption behaviour by the Langmuir isotherm has been demonstrated in diverse systems that do not obey the preconditions of Langmuir model, including electrostatic bonding accompanied by change of protein conformation (Jackson et al., 2000), as well as protein binding to non-planar heterogeneous surfaces, e.g., nanoparticles (Roach et al., 2006) and even porous media where the adsorption is ascribed to the filling of pore volume rather than the layer-by-layer adsorption on the solid surface (Miyahara et al., 2006). Nevertheless, extensions of the Langmuir model have been required to interpret the additional factors playing role in adsorption process and not regarded by the Langmuir model. In particular, the Langmuir equilibrium dissociation constant k_D represents the net attractive interaction between the adsorbate and adsorbent, neglecting three important possible contributions to the adsorption mechanism: (i) multiple binding sites per adsorbate molecule, as in the case of macromolecules, (ii) the heterogeneity, i.e., several types of binding sites, on the adsorbent

surface and (ii) interactions between the adsorbate molecules. The attempts to incorporate the contributions of several types of binding sites have been solved by the multi-component Langmuir model where the net adsorption is given by the superposition of two or more Langmuir isotherms (Langmuir, 1918). This approach has been justified in cases when it can be distinguished between high versus low affinity binding of the adsorbate to the two major classes of adsorption sites on the surface (Chang et al., 1995).

More often however, an alternative version of the Langmuir isotherm is used, namely, the Hill model, which was at first dedicated for the description of the binding between haemoglobin and oxygen but later, applied for the characterization of loading of agarose gels with proteins (Jennissen, 1976). In Hill model, the adsorbed density was initially substituted by the more general term "fractional saturation" θ that coincides with the fractional occupied area in case of solid surfaces:

$$\frac{\theta}{1-\theta} = K \cdot C^n$$

For protein adsorption on solid surfaces, Hill equation can be rewritten in a form analogous to the Langmuir isotherm:

$$\Gamma = \frac{\Gamma_{mH}}{1 + \frac{k_{DH}}{C^n}}$$

where letter "H" in lowercase stands for Hill model as opposed to Langmuir model. The main distinction of Hill equation from the Langmuir isotherm arises from the bulk concentration *C* raised to the power of *n*. By replacing *C* with C^n, the value of the variable power n called the Hill coefficient, foresees additional concentration-dependent interactions in the mechanism of adsorption not comprised in the Langmuir model. Accordingly, the value of the Hill coefficient $n > 1$ indicates additional attractive interaction that can be caused either by the presence of more than one binding sites on the adsorbent surface or by the attractive interactions between the adsorbate molecules and is therefore termed cooperative adsorption (Luo and Andrade, 1998). By contrast, value of Hill coefficient $n < 1$ signifies non-cooperative adsorption, i.e., the presence of repulsive protein-protein or protein-surface interactions. If Hill equation is viewed as equivalent

to multi-component Langmuir model, the Hill's equilibrium dissociation constant k_{DH} corresponds to the weighted average of the individual equilibrium dissociation constants. In case the Hill coefficient equals 1, the Hill model is reduced to the simple Langmuir isotherm. Hill model has been successfully applied to account for the effects of surface heterogeneity and the lateral interactions in the adsorption of proteins on hydroxyapatite (Dolatshahi-Pirouz et al., 2011; Luo and Andrade, 1998). On the other hand, adsorption phenomena that promote irreversible binding and hence, shift the system away from the thermodynamic equilibrium exceed the scope of Langmuir and Hill models. Primarily, the heterogeneity of protein molecule surface itself acts to facilitate the formation of multiple bonds that have to be broken for the protein to desorb (Roth and Lenhoff, 1993), thus diminishing the probability of protein release from the surface. Furthermore, such effects as changes in protein conformation upon adsorption caused by hydrophobic interactions with the sorbent surface or alternatively, clustering of protein molecules on the sorbent surface lead to the irreversibility of adsorption (Calonder et al., 2001). To explain this so called "history dependence", a class of related methods is used that relies entirely on statistical and geometrical assumptions, the simplest and most widely used being the random sequential adsorption model (RSA) (Talbot et al., 2000). According to RSA, the interpretation of adsorption kinetics is based on two major postulates: (i) adsorption is irreversible and (ii) adsorption occurs on the surface area not excluded by previously adsorbed particles. The adsorption process is modelled as sequential addition of particles at random positions of the surface; an adsorption event takes place unless the incoming particle overlaps with previously adsorbed particles. The temporal evolution of the adsorbed density ρ is described with the aid of the available surface function Φ(θ) that can be viewed as the probability of a particle to adsorb on the surface occupied by other particles at time t and coverage θ, where the fractional coverage θ is equal to the ratio of covered surface area to the total area (Senger et al., 2000). The adsorption kinetics can be represented by a general equation:

$$\frac{\partial \rho(t)}{\partial t} = k_{on}\Phi(\theta)$$

Where ρ is the surface density, k_{on} is the adsorption rate and Φ(θ) is the available surface function. Assuming that the incoming particle interacts with the other already deposited particles via pair potential u(rij), at any random location the interaction energy is characterized by the Boltzmann factor exp(-U(r)/kT), where U(r) is the total potential energy, k is the Boltzmann constant and T is the absolute temperature. The available surface function Φ(θ) can therefore be expressed as the mean value of the Boltzmann factor along the surface (Senger et al., 2000):

$$\Phi(\theta) = \langle exp(-U(r)/kT \rangle$$

The form of Φ(θ) can be further specified depending on the shape and properties of the adsorbing particles (spherical versus elongated, hard versus soft) and on the adsorption regime (diffusion limited versus reaction limited). In the simplest case of the two-dimensional random sequential adsorption, hard, i.e., non-interacting disks adsorb on a homogenous surface in the reaction limited regime. The available surface function Φ(θ) is then equivalent to the probability of finding a circular area the size of two disk diameters with no centres of adsorbed disks on it (Fig. 1.1.1.2. A.) (Talbot et al., 2000). It has been shown that Φ(θ) can be expressed as power series of θ (Calonder et al., 2001; Senger et al., 2000):

$$\Phi(\theta) = A_0 + A_1\theta + A_2\theta^2 + \ldots$$

Most importantly, it was demonstrated that the first three coefficients of the power series are identical for both, the random sequential adsorption and the equilibrium adsorption model, implying that the available surface function is equivalent in both cases at low coverage values (θ < 0.25). At high coverage values, the consequences of the adsorption away from equilibrium become prominent, one of the main effects being the maximum RSA coverage or the so called jamming limit θ(∞). The value of the jamming limit for hard sphere deposition on a surface has been estimated by computer simulations as θ(∞) = 0.547, a rather low value compared to the hexagonal close packing where θ(∞) = π/2√3 ≈ 0.91. The physical interpretation of the low jamming limit is linked to the irreversible nature of the random sequential adsorption process. Namely, in random sequential adsorption, the adsorbed particles are not allowed to desorb or diffuse along the sorbent surface hence, the relaxation to a “crystalline” hexagonal close packing

arrangement is not possible and the configuration of the adsorbed particles remains stochastic with a correspondingly lower maximum reachable coverage.

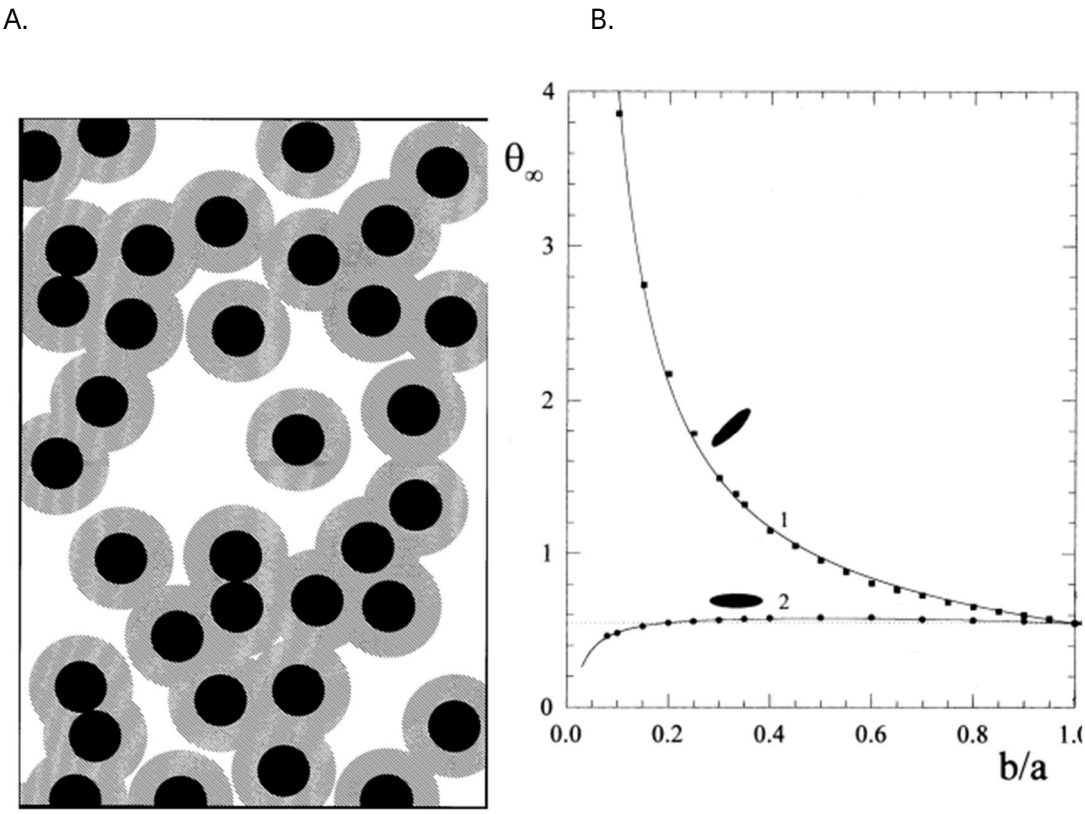

Fig. 1.1.1.2. Random Sequential Adsorption modelling of the surface coverage.

A) Geometric interpretation of the available surface area as the free white space between the already adsorbed hard disks and the gray area excluded for the centre of an incoming disk. The available surface area function corresponds to the ratio of the white area to the total surface area. From Senger et al. (Senger et al., 2000).

B) Numerical modelling of the jamming limit θ_∞ dependence from the orientation and the shape of rotation ellipsoids characterized by the parameter A = b/a equal to the axial aspect ratio of the ellipsoids. Data points mark the numerical simulation results, while the lines follow analytical functions interpolating numerical data in the case of side-on adsorption (1) and unoriented adsorption (2). When the aspect ratio tends to 1, the jamming limit approaches the saturation coverage predicted for the adsorption of hard disks, namely, $b/a \rightarrow 1$: $\theta_\infty \rightarrow 0.547$. From Adamczyk et al. (Adamczyk et al., 2002).

In the context of protein adsorption, an explanation is related to the post-adsorption changes in protein conformation leading to an extended footprint and reducing the available surface area. Jamming limit is often implemented to calculate the theoretical monolayer coverage of proteins thus giving an estimate on the adsorption regime (isotherm foot versus isotherm plateau, monolayer versus multi-layer adsorption) (Hovgaard et al., 2008; Koutsopoulos et al., 2007; Lavalle et al., 2000). Values of the jamming limit have been assessed numerically for a variety of cases, including special particle shapes, such as ellipses, rectangles and needles (Viot et al., 1992) as well as for soft particles modelling the lateral interactions (Adamczyk et al., 2002). In the work presented here, an analytical function was used for monolayer coverage estimation that was derived by Adamczyk et al. by the interpolation of the numerical results of the jamming limit dependence on the aspect ratio of unoriented hard rotation ellipsoids (Fig. 1.1.1.2. B.) (Adamczyk et al., 2002):

$$\theta = 0.304 - 0.123 \cdot A + \frac{0.365}{A}$$

where A = b/a is the axial aspect ratio of the rotation ellipsoid.

1.1.2. Protein adsorption on nanomaterials

Substrates possessing tailored features on the nanometre scale or shortly, nanomaterials have been proven versatile as platforms in biotechnology owing to the possibility of fine control and interaction on the length scale of biomolecular and cellular events (Gray, 2004; Nakanishi et al., 2001). Another motivation to implement nanofabricated interfaces for a wide range of biotechnological applications is the trend of miniaturization allowing the development of high content and high throughput methods with a minimal requirement for the quantity of materials and reagents (Hook et al., 2010; Sobek et al., 2006). Nanostructures have often been designed to render particular functionality to the liquid-solid interface with regards to protein immobilization: (i) control of protein binding by specific chemical groups organized in nanoscale patterns on the substrate surface (Hung et al., 2011) or (ii) perturbation of protein adsorption by nanometric

topographical features (Muller et al., 2001), including nanoparticles as the sorbent surface. The regulatory effect of nanostructures can be positive, resulting in the enhancement of protein immobilization (Galli et al., 2002), as well as negative, thus obtaining the so-called anti-fouling surfaces inert to non-specific protein adsorption (Holmlin et al., 2001). Concerning the mechanisms of interaction between proteins and nanostructures, in the case of nanoscale arrangement of selected chemical groups, e.g., self-assembled monolayers, specific adsorption can be supported by targeting a range of protein surface residues that exhibit particular characteristics such as charge, polarity, hydrophilicity or chemical affinity towards the moieties of the substrate surface. In contrast, the nanoscale topography has been shown to affect the adsorption in a non-specific manner, i.e., irrespectively of the involved protein residues. Namely, protein binding is altered on the basis of purely geometric grounds, as well as the interplay between the nanotopography and the superficial chemical groups that leads to an altered surface energy, respectively, wettability, compared to smooth substrates of identical chemical composition (Badre et al., 2007). Typically, adsorption is promoted by the augmentation of surface energy linked to increased specific surface area (nanoporous and nanorough substrates (Huckel et al. 1996; Dolatshahi-Pirouz et al. 2009) and to the surface to volume ratio and curvature in case of nanoparticles (Chen et al., 2008; Vertegel et al., 2004). In practice, however, it is complicated to assess separately the contribution of topography, since the fabrication of topographic nanostructures usually leads to the modification of physicochemical properties of the substrate. Depending on the fabrication method, the created nanotopography features bear additional surface defects; hence the enhancement of non-specific protein adsorption can be attributed to the defect energy localized in the nanostructures, as it was demonstrated by human serum albumin binding to the rims of nanopits produced on GaAs surface by Finely Focused Ion Beam technique (Bergman et al., 1998). As a side effect to the obtained nanostructures, the chemical composition of the treated surfaces is contaminated when using top-down methods, such as acid and alkaline etching, reported in numerous studies on titanium (Linderbäck et al., 2010; Sanz and et al., 2010; Sela et al., 2007), in this way biasing the selective evaluation of the

effect of nanotopography on protein adsorption. On the other hand, bottom-up methods such as diverse deposition techniques, including physical vapour deposition, chemical vapour deposition and cluster beam deposition of thin films, enable the control of surface roughness while retaining a constant surface chemical composition. Khang et al. presented an original approach to the problem of maintaining invariant surface chemistry while varying the nanoroughness: a mixture of carbon nanotubes in a polymer matrix was deposited as thin films on glass by spin coating or evaporation (Khang et al., 2007). In this way, Khang et al. investigated the independent effect of nanoroughness on the adsorption characteristics of fibronectin on hydrophilic polymer films. The study demonstrated a linear correlation between the surface energy and surface roughness; furthermore, the amount of immobilized fibronectin was expressed as a linear function of surface roughness excluding the fraction of surface energy not associated with topography. Using substantially different nanofabricated substrates in combination with various proteins, several groups have come to the conclusion that the adsorbed amount to nanostructured surfaces grew non-linearly with the specific surface area exceeding the value predicted by the increase in the geometric area (Dolatshahi-Pirouz et al., 2009; Muller et al., 2001; Rechendorff et al., 2006; Scopelliti et al., 2010). Two of the authors (Dolatshahi-Pirouz et al., 2009; Rechendorff et al., 2006) ascribed the observed effect to specific changes in the structure of the adsorbed protein layers related to the orientation (side-on versus end-on) and the conformation (native versus extended) of the adsorbed protein molecules. In particular, fibrinogen was demonstrated to favour end-on adsorption with increasing roughness of tantalum films, thus supporting a higher number of adsorbed molecules additionally to the increase of the geometric surface area associated with nanoroughness. In the study of immunoglobulin G adsorption on germanium surface, roughness variation was achieved by the growth of various densities of uniformly distributed well defined Ge islands on Si(001) (Muller et al., 2001). The increase of adsorption beyond the rise in the specific surface area was attributed to the presence of different adsorption sites on the nanostructured versus smooth substrates; the nature of the hypothetic adsorption sites was however not specified. The changes in the conformation caused by the rough

substrates, although not discussed by the authors, are plausible since the antibody recognition of the adsorbed immunoglobulin G was impaired with increasing sample roughness. In contrast to the aforementioned papers, Scopelliti et al. demonstrated in their study of protein adsorption on nanorough titania films that protein binding to the surface was boosted by the geometrical constraints of the surface pores on the nanometre-scale; the authors proposed an adsorption mechanism of pore volume filling by protein clustering (Scopelliti et al., 2010). A special class of solid substrates that provide an improved adsorption of proteins by the mechanism of pore volume filling are the nano- to meso- porous media including such diverse materials as polymer resins, sol-gels and mesoporous silicates of ordered and disordered porous networks, where the size and the shape of the pores is crucial for the maximum loading capacity of proteins (Miyahara et al., 2006; Suh et al., 2004).

Besides the increment of protein adsorption, there are studies reporting no effect (Cai et al., 2006; Denis et al., 2002; Han et al., 2003) or reduced adsorption (Hovgaard et al., 2008) of proteins on nanostructures – the latter findings have been attributed to particular changes in protein conformation upon adsorption that lead to spreading, respectively, the increase of protein footprint and hence, a lower adsorbed density. These results imply that factors other than surface topography have to be taken into consideration, such as the type of interaction between the solid substrate and protein molecules and lateral protein-protein interactions. To summarize, the binding of proteins to nanostructured features of solid substrates is governed by the interplay of both, the physicochemical interactions and the purely geometrical constraints dictated by the surface topography.

1.1.3. An overview of methods for protein adsorption studies

There are a number of physical variables that can be measured in order to explore protein adsorption at liquid/solid interfaces: the adsorbed mass per time, i.e., adsorption kinetics; the adsorbed mass in the steady state; mobile fraction; surface diffusion; thickness and structure of the adsorbed layer; changes in protein conformation upon adsorption; interaction force between

protein and surface; bonding energy etc. Various methods have been developed to assess some of the listed aspects, and complementary methods are often used to gain a satisfying interpretation of the adsorption mechanisms.

The simplest method for the estimation of the adsorbed amount of proteins on the surface is the depletion method where the adsorbed mass is assessed as the difference between the bulk concentration in the protein solution before and after adsorption. Protein concentration is measured by a number of label-free methods, such standard spectrophotometry-based assays as Lowry or Bradford method (Orschel et al., 1998) or alternatively, methods requiring protein markers, often radiolabelling with ^{125}I. However, due to the relatively low adsorbed density – typically on the order of nanograms per square centimetre, a large surface area is necessary for protein adsorption to take place in order to reach a detectable difference and accuracy of the concentration before and after adsorption. Usually, micro- and nanoparticles are applied as sorbent surfaces based on their large specific surface area. Equilibrium adsorbed mass on the surface upon homogenous adsorption, exchange and desorption, as well as competitive adsorption has been extensively studied by the groups of Voegel and Schaaf using the depletion method combined with radiolabelling (Ball et al., 1996; Ball et al., 1994; Bentaleb et al., 1997; Bentaleb et al., 1998; Huetz et al., 1995).

Measurement of the amount of irreversibly adsorbed protein on the surface is carried out by direct detection of labelled protein molecules (radiolabelling or fluorescent labelling) (Kurosawa et al., 2007) or by immunodetection of enzyme-linked immunosorbent assays (ELISAs) (Sela et al., 2007) that can be performed in microtiter plate or microarray format enabling the high-throughput assessment. The drawback of these methods is the loss of information on a certain fraction of reversibly bound molecules due to the rinsing and/or blocking steps prior to the detection. One of the techniques used in this work – the Protein-Surface Interaction Microarrays (PSIM) belongs to this class of methods (Scopelliti et al., 2010). We managed to perform long-term desorption studies despite of the limitations of the method, however the information of the initial desorption rate cannot be recovered with this approach and only the

irreversibly adsorbed fraction of proteins can be determined with accuracy. (For more details on PSIM method, please, see the section 1.2.3., as well as the "Materials and Methods" chapter).

Direct visualization and characterization of the adsorbed amount of fluorescently labelled proteins can be achieved by methods based on fluorescence microscopy. In particular, the confocal microscopy approach is justified in cases when the exact localization and distribution of proteins or mixtures of proteins on heterogeneous surfaces is of major importance, e.g., porous substrates and surfaces of particles (Balme et al., 2006; Baschong et al., 2001; Suh et al., 2004). However, these methods give a relative estimate of the adsorbed amount of proteins; in order to obtain quantitative values, calibration standards or additional methods are necessary. Our group has developed a confocal microscopy approach that includes both, the probed signal and the calibration fluorescence signal, within the same image, whereby the absolute values of the fluorescence signal are obtained by an additional method (spectrophotometry) (detailed description in the section 1.2.2., as well as the "Materials and Methods" chapter).

Depletion and microscopy-based techniques require the labelling of proteins, where the fluorescent labelling is preferred over radiolabelling due to the convenient preparation and safe handling. Although labelling of proteins gives the possibility to study competitive adsorption along with time-resolved monitoring and direct visualization of the adsorbed protein localization, the label can perturb the adsorption behaviour of proteins and, in case of fluorophores, the signal can be affected by the environment. A number of label-free methods offer the possibility for time-resolved *in situ* monitoring of adsorption kinetics, the most widely used among them are the optical techniques ellipsometry, optical waveguide lightmode spectroscopy (OWLS) and surface plasmon resonance (SPR), all of which are based on the detection of change in the refractive index caused by protein adsorption, as well as the quartz crystal microbalance (QCM) technique which detects the changes in the oscillation frequency of a quartz crystal upon protein binding. Although this class of methods was not used in our work, owing to their importance in the field of protein adsorption, we will briefly describe each of the mentioned techniques.

The primary area of application of the surface plasmon resonance (SPR) has been the detection of biomolecular recognition exploring the binding of analytes to a layer of preadsorbed ligands, rather than the non-specific protein adsorption (Homola, 2003). The reason behind it is the narrow choice of the substrate materials assigned by the principles of the SPR method. Changes in surface plasmon wave propagating at the boundary of a metal and a dielectric are measured, that are caused by the binding of analyte molecules at the interface. In the optical wavelength region, the boundary conditions for surface plasmon propagation are fulfilled for several metals, whereby gold is used as the standard. Furthermore, any dielectric layer between the metal surface and the adsorption plane has to possess a nanometre-scale thickness for the adsorption to be detectable, since the electromagnetic field of a surface plasmon wave decreases exponentially with the distance from the metal surface. The increase of the refractive index of the dielectric upon protein adsorption leads to an increase in the surface plasmon propagation constant, measured as amplitude or phase shift of the reflected light from which the thickness and the refractive index of the adsorbed film can be deduced. In the field of protein adsorption, surface plasmon resonance method is mainly applied for the investigation of protein binding to selected chemical groups of sensor surfaces functionalized with the self-assembled monolayers (Mrksich et al., 1995). An interesting approach to the investigation of protein-nanostructured material interaction by SPR, was demonstrated by Cedervall et al.: they studied protein adsorption on nanoparticles attached to the SPR sensor surface via thiol linkage (Cedervall et al., 2007).

The principle of ellipsometry is the measurement of the changes in the polarization angles of elliptically polarized light reflected from the planar surface under investigation (Neal and Fane, 1973). The theoretical basis of ellipsometry is formed by the extension of the general Fresnel equations dictated by the characteristics of the reflecting interface. Essentially, from the two measured ellipsometric angles Δ and Ψ, the refractive index and the thickness of a non-absorbing (optically transparent) thin film can be derived, whereby the precondition is the knowledge of the refractive index of the substrate and the refractive index of the surrounding (incidence) medium.

In case of absorbing thin film, the refractive index becomes a complex magnitude including two optical constants to be determined besides the film thickness; therefore additional information is necessary to derive the three unknown parameters from the two measured polarisation angles. There are several approaches to overcome this complication: often, polarization change of the probed film is measured in different surrounding media; alternatively, various angles of incidence or different thickness values of the studied film are employed. In case of protein adsorption on the liquid/solid interface, the refractive index of the adsorbed protein films is close to 1.5 allowing an accurate estimation of the film thickness (Hook et al., 2002). To render a more precise physical meaning to the ellipsometry data, the adsorbed amount is often expressed in terms of the surface density Γ, calculated from the thickness d, the difference between the refractive indices of the film n_f and the liquid medium n_s (buffer), and the increment of the film refractive index with protein concentration (Elwing, 1998). It was shown that the refractive index of protein (and synthetic polymer) films increases linearly with the adsorbed concentration up to high adsorbed density values, thus leading to a simple relation between the adsorbed density Γ, film thickness d_f and the refractive indices n_f and n_s, de Feijter's formula (De Feijter et al., 1978):

$$\Gamma = d_f \frac{n_f - n_s}{dn/dc}$$

where dn/dc is the constant increment of the refractive index with concentration. Real-time adsorption of proteins to the substrate can be observed, followed by the binding of antibodies to the adsorbed protein film and/or desorption studies. Historically and up to the present, important studies have been done by means of ellipsometry and related methods on the antibody recognition of surface-bound antigens (Langmuir and Schaefer, 1937; Nygren et al., 1986), as well as the blood coagulation mechanisms in contact with solid surfaces (Vroman and Adams, 1969). The major drawback of the ellipsometry method is the requirement of smooth reflective surfaces with known optical properties, thus setting limitations to the range of biomaterials that can be tested by this class of methods. Moreover, for heterogeneous, optically anisotropic or absorbing films, the theory for the expression of the optical parameters and film

thickness can be rather complicated (Hook et al., 2002). Ellipsometry, as well as SPR, despite of their limitations, have been further developed towards imaging either by implementing large area detectors or scanning modules (Harke et al., 1997; Jin et al., 1995; Steiner, 2004).

Another label-free optical method sharing several basic assumptions with ellipsometry is the optical waveguide lightmode spectroscopy (OWLS). Similarly as in ellipsometry, de Feijter's formula is used in OWLS for the quantification of the adsorbed mass per unit area knowing the refractive index and the thickness of the adsorbed layer (Vörös, 2004). In contrast to ellipsometry, the changes in the refractive index upon protein adsorption and the adsorbed film thickness are derived from the measured phase shifts of the TE and TM modes propagating by total internal reflection within a waveguide coated with a thin film of the material of interest (Kurrat et al., 1997; Vörös, 2004). The requirements to the materials for coating of the OWLS sensor surfaces include: thickness on the order of tens of nanometres, as well as the value of the refractive index similar or lower compared to the waveguide material (usually $Si(Ti)O_2$), for a sensitive detection of the interaction of the adsorbate with the evanescent wave. The OWLS method has been used independently to reveal the kinetics of adsorption and desorption (Tie et al., 2003); more often however it has been used in combination with additional methods to gain more detailed information on the structure of adsorbed layers and the conformation of proteins (Roba et al., 2009; Scott and Elbert, 2007; Vörös, 2004).

With the quartz crystal microbalance technique (QCM) the adsorbed surface density Γ is directly related to the shift Δf in the resonance frequency of a quartz crystal loaded with the mass of the adsorbed proteins, as expressed by the Sauerbrey equation (Dixon, 2008):

$$\Gamma = -\frac{C}{n}\Delta f$$

where C is the mass sensitivity constant and n is the overtone number. In a medium other than vacuum, for protein adsorption, typically, buffer solution, the mechanical oscillations of the sensor and the adsorbed protein layer are coupled with the adjacent layer of the aqueous medium. Consequently, the calculated surface density includes the water molecules of the protein hydration shells, as well as water and buffer ions trapped in the adsorbed layer, termed

the “wet mass” as opposed to the “dry mass” detected by ellipsometry and OWLS. Similarly as in other methods, the quartz crystal sensor can be coated or deposited with a film of the material of interest. Additionally, in the quartz crystal microbalance with dissipation monitoring (QCM-D) setup, the shift in the energy dissipation ΔD can be estimated, the parameter ΔD/Δf being a relative measure of the amount of the coupled water and the viscoelastic properties of the adsorbed layer (Dolatshahi-Pirouz et al., 2011; Vörös, 2004).

1.2. Introduction to the methods used in this work

1.2.1. Fluorescence recovery after photobleaching

Fluorescence recovery after photobleaching (FRAP) is a confocal microscopy-based method for the assessment of the mobility of fluorescent molecules by confocal imaging of a bleached region of interest. From the rate of recovery and the asymptotic value of the fluorescence signal, parameters associated with the motion of the fluorescent moieties can be derived. The FRAP technique was initially applied for the characterization of protein transport in living cells, modelled as diffusion versus uniform concentration flow of the fluorescent molecules across the area of a focused laser beam (Axelrod et al., 1976). The temporal recovery of the mean fluorescence signal f(t) across a circular bleached spot of radius w can be expressed in the following form (Axelrod et al., 1976; Sprague et al., 2004):

$$f(t) = e^{-\frac{w^2}{2Dt}}\left[I_0\left(\frac{w^2}{2Dt}\right) + I_1\left(\frac{w^2}{2Dt}\right)\right]$$

where D is the diffusion coefficient of freely diffusing fluorescent molecules of one kind with the corresponding diffusion time $\tau_D = w^2/D$, and I_0 and I_1 are modified Bessel functions.

The FRAP approach was further extended to characterize any binding reactions where a certain population of the fluorescent molecules becomes immobile upon binding, including the non-specific binding of proteins on solid surfaces. For the description of binding reaction kinetics, two distinct kinetic regimes are introduced, namely, the diffusion limited (Axelrod et al., 1976) versus the reaction limited model (Bulinski et al., 2001; Kaufman and Jain, 1992), while the

experiment can correspond to a binding reaction perturbed by diffusion. Therefore the full diffusion binding model was proposed by Sprague et al. that considers the influence of diffusion to binding reactions (Sprague et al., 2004). In case of a uniform circular bleached area, diffusion is characterized by the ratio of the diffusion coefficient D to the square of the radius of the bleached spot w, namely, D/w^2. Kinetics of the binding can be described by the on- and off- rate constants k_{on} and k_{off}, where the pseudo-on-rate constant $k_{on}^* = k_{on} \cdot [B]$ accounts for the concentration of the binding sites [B] at equilibrium. Then, a parameter $k_{on}^* w^2/D$ can be introduced to distinguish between the kinetic regimes. Accordingly, the kinetics can be classified into four submodels to facilitate the interpretation of the recovery curves, as follows (Kang and Kenworthy, 2008; Sprague et al., 2004):

(i) Pure diffusion limited model, when the $k_{on}/k_{off}, << 1$, corresponding to a negligible bound population of molecules;

(ii) Pure reaction limited model, when $k_{on}^* w^2/D << 1$, describing a situation, when binding is slow compared to diffusion, respectively, diffusion is too fast to be detected in the time-scale of the recovery monitoring.

(iii) Effective diffusion model, when $k_{on}^* w^2/D >> 1$, if the time-scale of binding is comparable to that of diffusion. In this case, kinetics is conveniently described by the diffusion equation introducing an effective diffusion coefficient D_{eff} that includes the on and off rate constants of binding: $D_{eff} = D/(1 + k_{on}^*/k_{off},)$.

(iv) Full model.

In the special case of pure reaction dominant, kinetics can be reduced to the equilibrium rate equation of the free and bound populations of the fluorescent molecules:

$$\frac{d[\mathrm{AB}]}{dt} = k_{on}^* [A] - k_{off} [AB]$$

where [A] and [AB] denote the concentration of the free and the bound populations, respectively. Several assumptions are made, namely: (i) the concentration of the free population [A] is a constant owing to the fact that the reaction is significantly slower than the diffusion resulting in an instantaneous equilibration of the free molecules. (ii) Steady state condition claims

the equality of the on- and off- rates: $k_{on}^{*}[A] = k_{off}[AB]$. Considering the listed statements, fluorescence recovery can be derived from the rate equation as:

$$f(t) = [A]_{\infty} + [AB]_{\infty}(1 - e^{-k_{off}t})$$

where $[A]_{\infty}$ and $[AB]_{\infty}$ signify the equilibrium concentrations of the free and the bound population, where $[AB]_{\infty}$ approaches its asymptotic value when $t \rightarrow \infty$. If the recovery signal is set to f(0) = 0 at the instant of the bleaching event (t = 0), and the fractional fluorescence $f_n(t)$ is normalized to the signal intensity f(-) before bleaching as $f_n(t) = f(t)/f(-)$, then the term $[AB]_{\infty}$ denotes the mobile fraction, respectively, the part of the bound population of molecules that can exchange with the free molecules.

In the studies of protein adsorption, FRAP technique has mostly been used to estimate the lateral diffusion of already adsorbed proteins, especially in combination with total internal reflection fluorescence (TIRF) microscopy, in order to exclude the contribution of binding reaction of molecules from the bulk and to enable the reduction of the model to diffusion dominant or effective diffusion (Tilton et al., 1990; Yuan et al., 2003). Burghard and Axelrod (Burghardt and Axelrod, 1981) have addressed the problem of coupling the binding kinetics with surface diffusion by approximating the adsorption of BSA on quartz glass with a model that describes the adsorbing molecules as three independent populations, i.e., one irreversibly bound immobile population and two reversibly bound populations, the most rapidly reversible of which is perturbed by surface diffusion (Thompson et al., 1981). From the studies of BSA dynamics on quartz glass surface in the bulk concentration range covering three orders of magnitude, the authors found that the fraction of reversibly adsorbed molecules increased with the bulk concentration. They hypothesized that the occurrence of two populations of reversibly bound molecules, one of which can diffuse along the surface, can be attributed to multi-layer adsorption regime confirmed by the quantitative amount of the adsorbed molecules exceeding the theoretical monolayer value. The analytical approach proposed by Thompson, Burghard and Axelrod has been used in several studies of lateral diffusion of macromolecules on solid substrates by patterned FRAP, where

bleaching is localized in a fringe pattern formed by a standing evanescent wave of the TIRF microscopy setup (Chan et al., 1997).

In our work, we utilized the FRAP approach with the aim to characterize the adsorption of trypsin on the ns-TiO_x surfaces according to the reaction dominant kinetic regime. We considered the contribution of bulk diffusion as negligible, since desorption occurred at longer time scales than the theoretical diffusion time given by the bulk diffusion coefficient D calculated according to Stokes-Einstein relation:

$$D = \frac{kT}{6\pi r\eta}$$

where k = 1.38 × 10^{-23} J/K is the Boltzmann constant, T = 293 K is the temperature in Kelvin, r = 2.6× 10^{-9} m is the hydrodynamic radius of trypsin according to (Kunitz et al., 1934; Scherp, 1933) and η = 1 mPa·s is the viscosity of water (or aqueous solutions) at room temperature. Plugging the calculated value of the diffusion coefficient D = 8.26×10^{-11} m^2/s, as well as the size of the bleached region w = 15×10^{-6} m, in the equation of the diffusion time $\tau_D = w^2/D$, gives the typical diffusion time $\tau_D \approx 2.7$ seconds, as opposed to the average recovery halftime τ = 162 ± 18 seconds, as detected in the FRAP exchange studies (for more details on FRAP experiments, please, see the chapters of "Materials and Methods" and "Results").

1.2.2. Fluorescence photobleaching quantification

Recently, our group has developed a confocal microscopy-based method for the quantification of the adsorbed amount of proteins on solid substrates, termed the fluorescence photobleaching quantification (FPQ) (Scopelliti et al., 2010). The drive to develop this approach was the failure of straightforward quantification of adsorbed proteins on nanorough surfaces with the conventional methods, such as ellipsometry and QCM, related to the complex theoretical assumptions for the treatment of the optical properties of rough substrates in case of ellipsometry, as well as high percentage of trapped water versus adsorbed protein inside the nanopores of the cluster-assembled films in case of QCM. As an alternative, our group proposed a

robust and self-sufficient approach, the principle of which is the bleaching of a region of the adsorbed fluorescent protein layer and immediate imaging of the transverse plane (cross-section) of the layer revealing both, the bleached and the intact regions of the layer in presence of a bulk protein solution of known concentration. By the virtue of the bleaching step, two crucial issues are solved:

(i) the bleached region of the layer uncovers the fluorescence signal of the bulk solution adjacent to the surface of the film and therefore the least perturbed by spherical aberration, the consequence of which is a decrease of the detected intensity with increasing depth of focus, typically observed when imaging objects in aqueous media with high numerical aperture oil immersion objectives (Diaspro et al., 2002; Hell et al., 1993; Hibbs et al., 2006) (Fig. 1.2.2.1.).

(ii) The difference between the intact and the bleached signals of the protein layer serves for the quantitative estimation of the adsorbed surface density by using the signal of the bulk solution of known concentration as the calibration standard.

For the calibration, bulk concentration is estimated by spectrophotometry measurements prior to adsorption experiment. Due to the relatively low total surface area of the specimen equal approximately to 1 cm^2, the adsorbed mass of proteins is on the order of magnitude of ng per cm^2 and cannot be detected by means of spectrophotometry. We verified that the change in the bulk concentration upon protein adsorption did not result in changes of the fluorescence intensity beyond the limits of the standard deviation. The bulk concentration was therefore considered constant in the whole applied range from 0.5 to 20 µM, with a total sample volume of 200 µl. Adsorbed surface density ρ was calculated according to the equation:

$$\rho = \frac{L}{B}\frac{V_{res}}{S_{res}}C$$

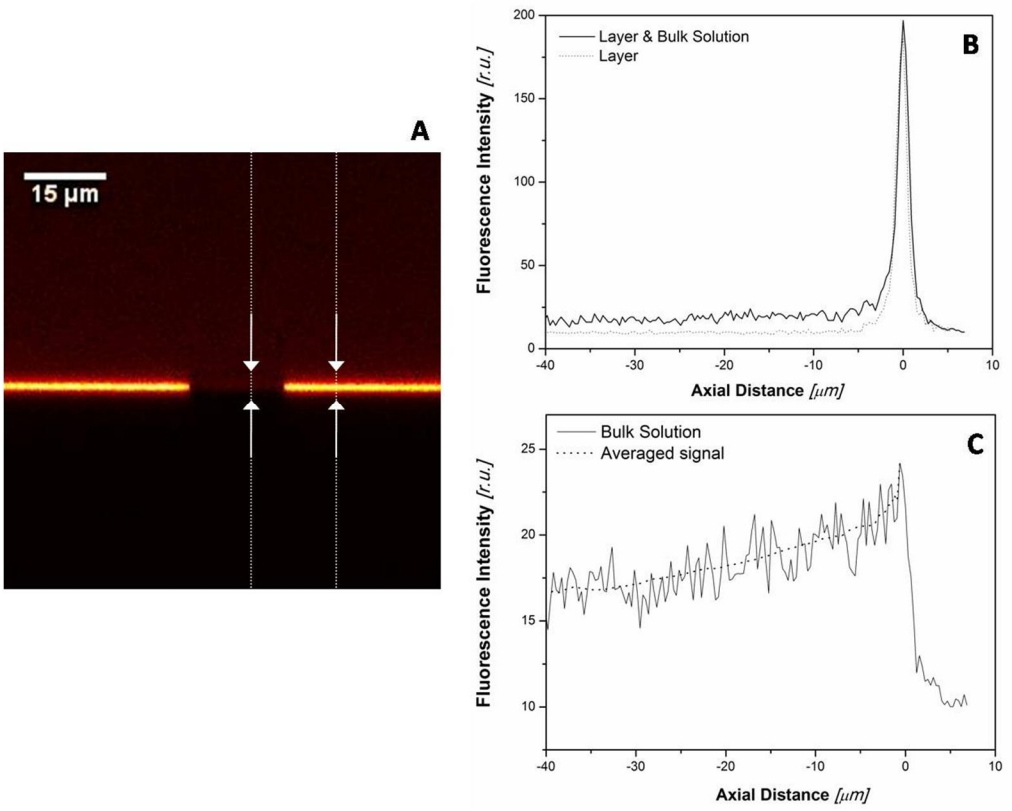

Fig. 1.2.2.1. Principles of the FPQ method.

A) Image of the axial XZ plane capturing the fluorescence of the adsorbed layer, the bleached region of the layer and the signal of the bulk solution adjacent to the bleached region. Signal of the adsorbed layer L is determined as the difference between the intact layer signal (which includes the contribution of bulk solution B) and the signal B of bulk solution of known concentration serving as calibration standard.

B) Axial profile of the intensity distribution along the white dotted line in the image A. Fluorescence peak of the layer is shown with and without the contribution of bulk solution.

C) Signal of the bulk solution as a function of the axial distance from the cover slip surface demonstrating the effect of the aberration caused by refractive index mismatch. (Experiment details in the chapter "Materials and Methods").

Here, the calibration factor to convert the concentration units to surface density units consists of two ratios: (i) the ratio of the fluorescence signals detected on the adsorbed layer L and the bulk solution B, and (ii) the ratio of the resolution volume V_{res} versus the resolution

surface S_{res} where V_{res} can be defined as the 3D volume of the point spread function or the product of the squared lateral resolution and the axial resolution. Accordingly, S_{res} corresponds to squared lateral resolution. L is the fluorescence intensity of the adsorbed layer determined as the difference between the measured intact layer signal and the bulk solution signal B adjacent to the bleached layer. An analogous expression was given by Pertaya et al. (Pertaya et al., 2007) who derived a similar equation for the estimation of the surface density of antifreeze proteins bound on surfaces of ice crystals calibrated by the fluorescence of solution. To account for the signal originating from the proteins adsorbed on the surface of a single crystal of ice, Pertaya et al. used a complex computational routine to estimate the convolution of the point spread function with the lateral surface of a single crystal. In contrast to the case reported by Pertaya et al., the advantage of the FPQ setup that makes the calculations rather simple is the imaging in the transverse XZ plane, thus reducing the adsorbed protein layer to a single sub-resolution line the width of which depends on the axial resolution of the optical system. In this way, the first expression can be simplified as:

$$\rho = \frac{L}{B} z_{min} \cdot C$$

where z_{min} is the axial resolution and ρ is expressed as mass per unit area.

The theoretical axial resolution of a diffraction-limited system can be defined as the distance of the first diffraction minimum from the central maximum of the image of a point source produced by a lens with an angular aperture, modelled by Linfoot and Wolf and reproduced by Inoue as (Inoue et al., 2006; Linfoot and Wolf, 1953):

$$z_{min} = \frac{2\lambda n}{(NA)^2}$$

where λ is the wavelength, n is the refractive index of the object medium and NA is the numerical aperture of the objective. Given the λ = 565 nm emission wavelength used in this work, n = 1.33 refractive index of the aqueous buffer and NA = 1.4 the numerical aperture of the 63× objective, yields axial resolution of z_{min} = 769 nm. We tested experimentally the axial resolution and estimated the full width at half maximum of the fluorescence intensity profile of the sub-

resolution adsorbed protein layer, $(FWHM)_z$ = 1.32 ± 0.06 μm (please, see "Materials and Methods"), a value 1.7 times higher than the theoretically predicted axial resolution z_{min}. This observation can be ascribed to the spherical aberrations arising from the mismatch of refractive indices of the objective and the immersion medium (n = 1.52) and the aqueous protein solution (n = 1.33). It has been shown that both, the axial and the lateral resolution are influenced by the spherical aberrations, however the effect on the axial resolution is more pronounced, evident both, as the broadening of the point spread function and as the decrease of detected intensity with increasing focus depth, mentioned earlier in this section (Diaspro et al., 2002; Hell et al., 1993).

Slightly similar setup has been presented by Togashi et al. (Togashi et al., 2009) where the quantification was performed by comparing the average fluorescence detected from the adsorbed protein layer after the removal of bulk solution, to the calibration curves obtained by measuring the average fluorescence of bulk solutions of known concentrations. Togashi et al. presented a generally equivalent expression for the determination of the adsorbed surface density with the difference that they included the compensation for the fluorescence quantum yield on the surface, although the authors assumed that this parameter does not change between bulk and surface. Most importantly however, Togashi et al. carried out the image acquisition in the lateral XY plane, thus not compensating for the spherical aberrations. We would like to underline the superiority of the FPQ approach by pointing out several advantages not fulfilled in other confocal microscopy-based methods for the assessment of protein adsorption:

(i) In the FPQ setup, the calibration signal and the sampled signal, both are detected simultaneously within the same field of view of the confocal image, thus ensuring identical conditions of acquisition essential for quantification.

(ii) FPQ methodology eliminates the contribution of the spherical aberration caused by the mismatch of the refractive indices.

(iii) In contrast to static measurements, FPQ enables the parallel performance of kinetic studies of protein adsorption, desorption and exchange, particularly compatible with FRAP technique.

(iv) FPQ strategy is applicable to transparent materials with nanometre- to micrometre- sized topographical features enabling the local assessment of protein immobilization on discrete micrometre-scale surface structures. The contribution of sub-resolution nanometre-scale surface features is accounted for by the normalization with the specific surface area parameter.

1.2.3. Protein-surface interaction microarrays

FPQ technique provides the quantitative assessment of the adsorbed surface density with a straightforward applicability to nanorough surfaces. A major limitation of the FPQ method is however, its low throughput. Protein adsorption on solid substrates – and the interaction between biomolecules and material surfaces in general – is affected by a multitude of variables, including the physicochemical properties of the protein molecules, the bio-interface and the surrounding medium. To probe multiple variables in a wide range of variation, high-content and high-throughput methods are required.

In biology, a break-through of large-scale studies was made possible by the microarray technology that has laid the foundations for the various –omics fields of research accelerating scientific discoveries, as well as the development of the technological aspects of microarrays, covered by numerous review articles (MacBeath; Roemer et al., 2012; Russo et al., 0000; Sobek et al., 2006; Templin et al., 2002; Vegas et al., 2008). In the field of materials science and engineering, microtiter plate (Holmes et al., 2008; Petersen et al., 2010) and microarray formats (Mant et al., 2006; Yang et al., 2010) have been proven advantageous for the high-throughput synthesis and characterization of polymer libraries, moreover, microarrays have often been used for the screening of cell interactions with polymers (Gallagher et al., 2006). Libraries of solid thin films have been created by combinatorial approach enabled through various deposition methods

(Guerin et al., 2006; Schlesinger and Bruns, 2000; Senkan, 1998). Recently, several authors have utilized the microarray format for the evaluation of thin films implemented as coatings for DNA or protein array chips (Armelao et al., 2008; Nijdam et al., 2007; Saal et al., 2006), however, the material optimization itself was not achieved by high-throughput methods. Alternatively, Bras et al. (Bras et al., 2004) have demonstrated a true high-throughput approach to the optimization of DNA microarray substrates by first, creating a stepwise gradient of thin silicon/silicon dioxide films on a single glass slide and subsequently probing the applicability of the coating by oligonucleotide hybridization.

Our group has elaborated a high-throughput approach to protein adsorption studies: the protein-surface interaction microarrays (PSIM) (Scopelliti et al., 2010). Here, the high-throughput is established by the arraying of subnanoliter droplets of fluorescently labelled protein solution onto material surfaces of interest that are subsequently scanned to detect the fluorescence of surface-bound proteins. Introducing special surface chemistry of the array slides, covalent immobilization of proteins can be carried out. Our main interest however, is the non-specific interaction of proteins with surfaces possessing topographical features on the nanometre-scale; therefore in this and in our previous studies, we have immobilized proteins by physical adsorption on nanostructured titania thin films. We intended the protein-surface interaction microarrays to be a complementary method to the FPQ technique, the former producing high-throughput semi-quantitative data, the latter measuring the adsorbed density in absolute units. Within the scope of physical adsorption, PSIM method measures only the population of fluorescently labelled proteins that is retained on the material surface after specific procedures undertaken for the treatment of array slides prior to scanning. In particular, only those protein molecules are detected, which remain on the surface after the removal of the bulk solution, i.e., after rinsing of the array slides, as well as the blocking and the drying steps. This implies that in case of reversibly adsorbed population removed by the slide treatment, the adsorbed amount obtained by PSIM method cannot be directly correlated with the FPQ method. This problem can be solved by quantitative evaluation of the adsorbed amount after the slide treatment by FPQ method and

then correlating these quantitative results data obtained by PSIM under similar conditions. Thereafter, the correlation factor can be applied for the calibration of PSIM data obtained on any samples accompanied by the calibration sample. The primary difference between the measurement setups of PSIM and FPQ is however, the requirement of bulk solution for the quantification of fluorescence in the FPQ method, as opposed to the absence of bulk solution in the PSIM method. Due to the reasons described, the calibration sample must be carefully chosen to fulfil the requirement of correlation between PSIM data and FPQ data. Our group has proposed to use fluorescently labelled bovine serum albumin adsorption on ns-TiO_x for the calibration of PSIM data, based on the findings that 80 to 90 % of the adsorbed BSA on ns-TiO_x is immobile, i.e., irreversibly immobilized, and the characteristic timescale of desorption of the mobile fraction of BSA is on the order of an hour. Additionally, the blocking step of microarrays is carried out with a 1 % solution of BSA, avoiding the introduction of more than one adsorbing species in the calibration sample and making the immobilized BSA an appropriate sample for the calibration of other protein adsorption on ns-TiO_x surfaces, provided that both, BSA and the protein under investigation are conjugated to the same fluorophore. The equation for the calibration is expressed then as:

$$\rho_i = \rho_{BSA} \cdot \frac{F_i}{F_{BSA}} \cdot \frac{MW_i}{MW_{BSA}} \cdot \frac{DOL_{BSA}}{DOL_i}$$

where ρ_i and ρ_{BSA} denote the surface density of the protein of interest and the surface density of BSA estimated by FPQ and measured in the units of mass per surface area (ng/cm^2). F_i and F_{BSA} stand for the fluorescence intensity detected by PSIM and corresponding to the surface density ρ_i and ρ_{BSA}, respectively. MW_i and MW_{BSA} are the molecular weights of the protein studied and that of BSA. DOL_i and DOL_{BSA} represent the degree of fluorescent labelling of the protein and of BSA, i.e., the number of fluorophore moieties per protein molecule, which can be estimated by spectrophotometry measurements. In the current work, however, a different calibration protocol was applied for trypsin adsorption on ns-TiO_x: we used trypsin surface density values obtained by

the FPQ method in the quasi-linear low range of adsorption isotherm, in order to quantify the whole adsorption isotherm acquired by PSIM method.

1.2.4. Extension of the PSIM method for surface-bound enzyme activity detection

Substantial part of the current work was dedicated to the further development of the PSIM method with the aim of assessment of the activity of enzymes adsorbed on nanorough surfaces. The conventional enzymatic assays are mostly not applicable to physisorbed enzymes, since they are biased by the activity originating from the enzymes desorbed from the material surface into reaction solution (Caro et al., 2010; Koutsopoulos et al., 2007). An alternative activity assay was necessary that would exclude the contribution of enzyme molecules that were no longer bound on the surface due to the leakage. We reckoned that the PSIM methodology can offer such possibility since only surface-bound molecules are detected in our microarray setup. This in turn, could be accomplished by tagging with a fluorescent label only those adsorbed enzyme molecules that are active, whereas no label would be attached to the adsorbed molecules that are inactive, e.g., denatured upon adsorption on the nanostructured surface. Enzyme labelling according to the state of their catalytic activity has been demonstrated by the usage of activity-based probes for enzymes (Campbell and Szardenings, 2003). The activity-based labelling relies on the high affinity of a synthesized molecular probe towards a specific residue of the active site of an enzyme molecule, as a result of which covalent binding of the probe molecule to the active site of the enzyme proceeds. This reaction scheme suggests that such molecular probes act as mechanism-based inhibitors or the so-called “suicide substrates” turning the enzyme molecule inactive due to irreversible binding to its active site (Evans and Cravatt, 2006). If this molecular probe bears a chemical moiety that enables its detection, e.g., a fluorophore reporter, the read-out of the probe signal correlates with the presence of active enzyme. Hence, the basic structure of an activity-based probe incorporates the reactive group, the reporter moiety and auxiliary groups, such as moieties that enhance the specificity of probe recognition by the enzyme, as well as linker groups.

Activity-based probes have been synthesized targeting either a wide range of enzymes sharing a common active site configuration, e.g., serine hydrolases (Patricelli et al., 2001), or a narrow range of enzymes when carrying a specificity determinant group, e.g., serine proteases (Fonovic and Bogyo, 2007). The main area of application of the activity probes has been the activity-based proteomics or "catalomics", aimed at high-throughput identification and characterization of enzymes, as well as fingerprinting of enzyme substrates and inhibitors (Johnson et al., 2010; Uttamchandani et al., 2009). The idea of our group was to transfer an existing technology from the studies of biological systems to the field of (nano)-material science by utilizing activity probes within the framework of PSIM method and develop a novel strategy for activity-based screening of nanostructured materials. In this respect, we reversed the goal of activity labelling from the characterization of enzyme-substrate or enzyme-inhibitor interaction to that of enzyme-biomaterial characterization.

For our studies, we selected a commercially available fluorescently labelled activity probe designed for the recognition of a wide family of enzymes – the serine hydrolases, in particular, the TAMRA-tagged ActivX Fluorophosphonate (FP) Probe produced by Pierce, Thermo Scientific. This type of probes contains a fluorophosphonate reactive group that specifically attacks the nucleophilic serine residue of the active site of a serine hydrolase and binds to it covalently in the manner of a mechanism-based inhibitor. The fluorophosphonate moiety is connected via spacer to the carboxytetramethylrhodamine (TAMRA) fluorophore providing the means for detection (Fig. 1.2.4.1.). Initially, fluorophosphonate activity probes have been used for the selective labelling of serine hydrolases within complex protein mixtures and the subsequent detection in a gel-based format of SDS-PAGE and Western blotting methods (Liu et al., 1999; Patricelli et al., 2001). Few years later, microarray-based detection of immobilized enzymes was proposed and successfully tested for the high-throughput identification and characterization of enzymes using the activity probes (Chen et al., 2003; Sieber et al., 2004).

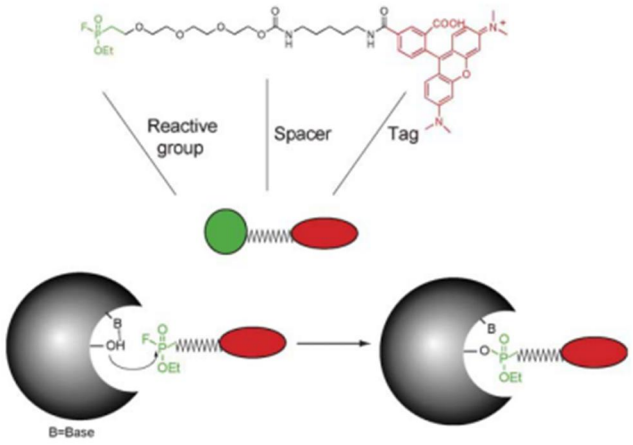

Fig. 1.2.4.1. Chemical structure and reaction mechanism of the fluorophosphonate activity probe targeting the family of serine hydrolases. Image taken from the review by Sieber and Cravatt (Sieber and Cravatt, 2006).

It must be emphasized, that in proteomics and catalomics, direct immobilization of enzymes onto microarray slides is carried out exclusively by covalent attachment (Chen et al., 2003; Funeriu et al., 2005), as opposed to the methodology of PSIM where enzymes are physisorbed on slides coated with the material of interest. The rationale behind the covalent immobilization strategy is the prevention of undesired side-effects typical of non-specific adsorption, i.e., leakage of enzymes from slide surface and cross-contamination between adjacent array spots (Sun et al., 2006). Being aware of the two mentioned issues, we set up a study to verify the feasibility of the serine hydrolase fluorophosphonate probe for the detection of physisorbed enzyme activity using the principles of PSIM method. In this proof of concept, we intended to explore the influence of the nanometre-scale roughness of titanium oxide films on the activity of an adsorbed model serine hydrolase trypsin. The established protocols are described in the “Materials and Methods” chapter, while the results of the validation study are presented in the “Results and Discussion” chapter.

1.3. Surface-bound trypsin as model enzyme

1.3.1. General characteristics of trypsin

Trypsin was chosen as model enzyme for this work, owing to its well-studied structure and properties, its availability and common use in cell culture and proteomics laboratories, as well as the ability to target trypsin with fluorophosphonate activity-based probes.

A. B.

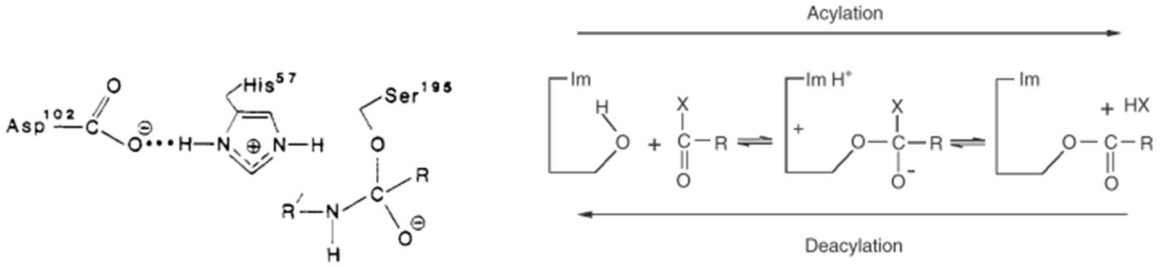

Fig. 1.3.1.1. The catalytic mechanism of serine proteases.

A) Key amino acid residues of the active site, Asp 102, His 57, as well as Ser 195 forming a tetrahedral intermediate complex with a peptide substrate. Image taken from Bachovchin (Bachovchin, 1986).

B) Catalysis described as cycles of acylation and deacylation of the enzyme. "Im" marks the imidazole ring of His 57. "X" denotes NHR or OR in acylation via the hydrolysis of peptide or ester bonds, respectively, while in deacylation "X" stands for OH of the water molecule. Scheme taken from Polgar (Polgár, 2005).

Trypsin belongs to a subgroup of the serine hydrolase family, the class of enzymes called serine proteases, indicating that, besides possessing the active site mechanism typical to serine hydrolases, with nucleophilic serine as the key residue; it cleaves proteins by catalysing the hydrolysis of peptide bonds. Trypsin is found in the digestive system of vertebrates, produced by the pancreatic tissue as its inactive precursor trypsinogen which is secreted into duodenum where the removal of an N-terminal hexapeptide by enteropeptidase, another serine protease of the

duodenum, or by already active trypsin turns trypsinogen into the active form known as β-trypsin. The physiological role of trypsin, along with other pancreatic enzymes, is the digestion of proteins and peptides releasing amino acids absorbable in the small intestine (Stroud, 1974).

Trypsin consists of a single polypeptide chain of 223 amino acids interconnected by six disulphide bridges. It is a globular protein with molecular dimensions of 4.9 × 3.9 × 3.3 nm and the molecular weight of around 24 kDa (Abbas et al., 2009). The isoelectric point of trypsin is in the range of pI 10.2 – 10.8, and the range of the optimum activity is between pH 7 – 9 (Buck et al., 1962), hence trypsin is in its highly active cationic form at physiological pH. The catalytic site of trypsin incorporates the general mechanistic structure typical to all serine proteases, named the "catalytic triad" after the three residues of the active site pocket that coordinate the catalytic reaction: serine 195, histidine 57 and aspartate 102 (numbering of residues according to chymotrypsin, the first determined protease structure) (Fig. 1.3.1.1. A.). The mechanism of serine protease action has often been described by the "charge-relay" model that explains the formation of a Ser 195 nucleophile by the proton transfer between the involved residues (Bachovchin, 1986). The catalytic reaction can be conveniently described as cycles of acylation (removal of the hydroxyl group) and deacylation of Ser 195 (Fig. 1.3.1.1. B.) (Polgár, 2005). In the acylation reaction, the hydrogen bonding between Asp 102 and His 57 enables the imidazole ring of His 57 to act as a general base in deprotonating Ser 195 and forming an imidazolium ion. The nucleophilic Ser 195 attacks the carbonyl carbon of the enzymatic substrate resulting in a tetrahedral intermediate. The imidazole group transfers the proton of the Ser 195 hydroxyl group to the amine group of the substrate, creating acyl-enzyme and the amine product. The further reaction is described by the deacylation cycle to which the reverse reaction scheme can be applied (Fig. 1.3.1.1. B.). Now, a water molecule acts as nucleophile attacking the carboxyl carbon and protonating the imidazole group of His 57. A second tetrahedral intermediate forms and breaks down by the deacylation of Ser 195 and formation of the carboxyl product. The enzymatic substrate, as noted in the reaction scheme (Fig. 1.3.1.1. B.) can be a peptide or an ester, since it was found that besides peptide bonds of proteins, trypsin can hydrolyze ester bonds and amide

bonds of amino acid derivatives opening the possibilities for the development of convenient trypsin activity assays using designed synthetic substrates (Schwert et al., 1948). It has been shown that trypsin cleaves peptide bonds exclusively at the carboxyl-side of arginine and lysine residues (Olsen et al., 2004) – these positively charged side chains are electrostatically stabilized by the aspartic acid residue Asp 189 in the substrate binding pocket of trypsin (Li et al., 1998). Bearing surface-exposed arginine and lysine residues, trypsin is prone to autoproteolysis, respectively, digestion of trypsin molecules by other trypsin molecules. Autodigestion has been demonstrated to largely depend from the concentration of trypsin in solution, as well as from a number of the solution parameters, such as temperature, pH and buffer composition (Fraser and Powell, 1950; Li et al., 1998; Sriram et al., 1996). At the bulk concentration of 0.2 µM in 20 mM $CaCl_2$, pH 8.0 and incubation at 37°C, the reported half-life of trypsin was 10.5 hours (Li et al., 1998). The presence of Ca^{2+} ions at 1 mM and higher concentrations in the solution has been shown to efficiently defend 0.5 – 0.7 µM trypsin against autoproteolysis (Green and Neurath, 1953; Sipos and Merkel, 1970), an effect attributed to the more stable conformation acquired by the binding of the calcium ion (Hehemann et al., 2008).

1.3.2. General concepts of enzyme kinetics

A general catalytic reaction where enzyme E reacts with the substrate S to form the product P proceeding to an intermediate complex ES, can be described by the scheme:

$$E + S \rightleftarrows ES \rightleftarrows P + E$$

where the forward reactions and the reverse reactions are determined by the on-rate constants (k_{1on} and k_{2on}) and the off-rate constants (k_{1off} and k_{2off}), respectively. This reaction can be described by a second order kinetic equation in respect to the formation of enzyme-substrate complex ES:

$$\frac{d[ES]}{dt} = k_{1on}[E][S] - k_{1off}[ES] - k_{2on}[ES] + k_{2off}[P][E]$$

The full kinetic equation is simplified by considering the initial states of the reaction: then, the concentration of the formed product is negligibly small, hence, the term k_{2off}[P][E] can be omitted rewriting the equation as:

$$\frac{d[ES]}{dt} = k_{1on}[E][S] - k_{1off}[ES] - k_{2on}[ES]$$

The concentration of enzyme is expressed as the difference between the total enzyme concentration and the concentration of enzyme bound to the substrate as: [E] = $[E]_0$ – [ES], thus leading to:

$$\frac{d[ES]}{dt} = k_{1on}([E]_0 - [ES])[S] - (k_{1off} + k_{2on})[ES]$$

The crucial step to the simplification of this kinetic equation was introduced by Briggs and Haldane (Briggs and Haldane, 1925), claiming that the formation rate of the enzyme-substrate complex ES is equal to its breakdown rate, i.e., the steady-state assumption:

$$k_{1on}([E]_0 - [ES])[S] = (k_{1off} + k_{2on})[ES]$$

From this expression, one can deduce:

$$[ES] = [E]_0 \frac{[S]}{[S] + \frac{(k_{1off} + k_{2on})}{k_{1on}}}$$

where a constant K_M can be introduced: $K_M \equiv (k_{1off} + k_{2on})/k_{1on}$. The constant K_M is essentially the equilibrium dissociation constant for the enzyme-substrate complex ES valid under the preassumption that the kinetic equation describes the initial stages of the reaction at a steady state. From the practical considerations, the absolute value of the concentration of the enzyme-substrate complex ES in real time is difficult to measure, the former equation can be translated into measurable entities. In order to do so, additional assumptions are made, namely:

(i) the concentration of the enzyme is significantly lower than the concentration of the substrate, the abundance of substrate implies [E] ≤ 10^{-2} · [S] at any stage of the reaction.

(ii) Provided that the rate constant k_{2off} is negligibly small and the assumption (i) is valid, the initial rate of the product formation dP/dt = k_{2on}[ES]. The product formation rate dP/dt is referred to simply as the initial velocity V_0.

(iii) Provided that the assumption (i) is valid, the maximum reaction velocity V_m is limited only by the total concentration of the enzyme, namely all of the enzyme is bound to the substrate: $V_m = k_{2on}[E]_0$.

Substituting [ES] and $[E]_0$ by the expressions of V_0 and V_m in the steady state equation, leads to the well-known Michaelis-Menten equation (Porter and Trager, 1977):

$$V_0 = V_m \frac{[S]}{[S] + K_M}$$

The relevance of Michaelis-Menten equation is that it enables the approximation of the enzyme progress curves by a simple idealized model involving quantities that are easy to determine by experiment: the initial substrate concentration [S] and the initial velocity V_0, estimated as the slope of the linear region of the product formation curve versus time. For the fitting of experiment data with the Michaelis-Menten model, linearization of the Michaelis-Menten equation is often performed (Atkins and Nimmo, 1975). The most popular linearization method is the Lineweaver-Burk plot that describes the reciprocal of the initial velocity $1/V_0$ as a function of the reciprocal of substrate concentration1/[S] in the form y = ax + b:

$$\frac{1}{V_0} = \frac{K_M}{V_{max}} \cdot \frac{1}{[S]} + \frac{1}{V_{max}}$$

Whenever it comes to the analysis of enzymatic reactions, the classical Michaelis-Menten kinetics is employed, except the single molecule studies of catalysis when the reaction cannot be described as the collective behaviour of an ensemble according to classical thermodynamics (Li and Yeung, 2008). In special cases, such as catalysis on solid surface, enzymatic reactions are often modelled as Michaelis-Menten kinetics perturbed by other factors that govern the reaction rates, such as Langmuir adsorption of the reacting species or the influence of surface diffusion (Gaspers et al., 1994; Kobayashi and Laidler, 1974; Lee et al., 2005).

1.3.3. Enzyme immobilization on solid surfaces

The usage of immobilized enzymes ranges from laboratory to industry. Generally, the choice of the immobilization platform and the attachment technique depends on the properties of the

enzyme and on the specific application of the immobilized biocatalyst system. The primary area of application of immobilized trypsin is the protein digestion into peptides for mass spectrometry analysis. A considerable number of studies have been dedicated to the optimization of tryptic digestion by improving the methods of trypsin immobilization in terms of the catalytic activity and stability of the protease, as well as the reusability of the system (Ma et al., 2009). Many successful solutions have been found by incorporation of proteases into nanostructured carrier matrices (Kim et al., 2010). Here, we will briefly focus on several commonly used immobilization methods in the context of trypsin.

Covalent attachment of enzymes to interfaces has been preferred owing to the stability of immobilization. Most often, covalent binding is accomplished benefiting from the abundance and reactivity of the primary amines of surface-exposed lysines as well as the N-termini of protein molecules with a variety of functional groups that can be fabricated on the material surface, such as aldehyde and epoxy groups (MacBeath and Schreiber, 2000; Rusmini et al., 2007). One of the most frequently used approaches is the usage of aldehyde groups as linkers between amine groups of the solid surface and the amines of the enzyme surface, whereby the reaction proceeds via Schiff chemistry. In particular, glutaraldehyde has been utilized to cross-link trypsin molecules on top of porous glass (Migneault et al., 2004) and polypyrrole (Biloivan et al., 2007), as well as to bind trypsin covalently to a number of various solid supports, including silane-modified glass and silica (Liu et al., 2009; Migneault et al., 2004; Zhao et al., 2006), plasma polymerized allylamine films (Abbas et al., 2009) and poly(ethylene imine) films on stainless steel (Caro et al., 2010). Glutaraldehyde cross-linking has been proven efficient as an additional method accompanying the covalent attachment, in order to boost the amount of immobilized trypsin beyond the limit given by the available surface area – an approach that has been demonstrated by trypsin binding on polymer nanofibers (Kim et al., 2009). In most of the cases studied, glutaraldehyde immobilization has partially diminished the catalytic activity of trypsin; on the other hand, a remarkable stabilization has been achieved, which is an essential parameter for proteolytic enzymes prone to autodigestion.

Several authors have taken advantage of the combination of the large effective surface area, reactive surface chemistry and porosity by immobilizing trypsin on glycidyl methacrylate beads functionalized with carboxyl groups or coated with dextran (Kang et al., 2006; Malmsten and Larsson, 2000). Besides the covalent binding, porous materials offer opportunities for alternative immobilization techniques: physical adsorption is facilitated by the large surface area presented by the micrometre to sub-micrometre sized pores, as demonstrated by trypsin adsorption on silica gels, as well as ordered mesoporous silica (Díaz and Balkus Jr, 1996; Gómez et al., 2009; Yiu et al., 2001a). Here, besides the surface chemistry and electrostatic properties, the diameter and volume of the pores play a crucial role in the total loading capacity and the leakage of the adsorbed enzymes. Furthermore, the resulting reaction rate is limited by the diffusion of reaction substrates to the surface-bound enzymes within the porous network. Undesired effects include the adsorption and retention of the reaction products inside the pores. Enhanced catalytic activity observed for enzymes immobilized on nanoporous materials has been linked to the confinement and increased local concentrations of the reactants inside the nanoscale structures (Qiao et al., 2008).

Another approach is the encapsulation of enzymes within the porous matrix, particularly used with sol-gel synthesis techniques , enabling a well-defined confinement of the enclosed enzymes – indispensable for the high-throughput on-chip tryptic digestion and enzymatic activity assays (Gill and Ballesteros, 1998; Park and Clark, 2002; Sakai-Kato et al., 2003; Yang et al., 2006).

Entrapment in layered polyelectrolyte structures has been demonstrated as an attractive approach for trypsin immobilization due to the formation of electrostatic bonding between trypsin molecules and the charged polymer network and the hydrophilic environment supporting the native conformation of trypsin (Garbers et al., 2007; Liu et al., 2007).

1.3.4. Trypsin activity assays

The methods for enzymatic activity estimation depend on the mechanism of enzyme action and on the nature of reaction products determining the mode of read-out of the reaction

outcome. For trypsin, the established activity assays have initially been developed for the measurement of the activity of free trypsin in solution. These standard activity assays have then been adapted for the assessment of the activity of surface-bound trypsin. The multitude of methods can be classified in three general groups: (i) assays that use chromogenic or fluorogenic enzymatic substrates; (ii) analysis of tryptic digestion products by mass spectrometry; (iii) activity-based probes.

The principle of the first group of assays is the analysis of the composition of the reaction solution, in order to estimate the amount of the product by detecting changes in the intensity or spectral distribution of absorbance or fluorescence. To assure a facile and linear correlation between the measured optical parameters and the enzyme activity without the need to separate the reaction products, enzymatic substrates have been synthesized that incorporate either amide or ester bonds and, upon cleavage by trypsin, release a chromophore or a fluorophore with distinct spectral characteristics. Substrates that include a short peptide sequence with the amino acid arginine determining the cleavage site, are by far the most frequently used for the activity assessment of free trypsin in solution, as well as surface-bound trypsin. By continuous or steady-state read-out of the absorbance (or fluorescence) change with time, kinetic assays can be performed. Enzymatic activity is defined as the amount of product generated per time, expressed in units of moles per second and estimated, according to the classical Michaelis-Menten kinetics (Briggs and Haldane, 1925), as the initial slope of the product versus time curve. By probing the reaction rate in a range of chromogenic (fluorogenic) substrate concentrations, the kinetic constants (Michaelis-Menten constant K_M, the maximum velocity and the turnover number k_{cat}) can be determined by various linearization methods of the Michaelis-Menten equation (Atkins and Nimmo, 1975). The chromogenic and fluorogenic assays are facile to perform, the drawbacks are however, the limited sensitivity and the failure to discriminate between the activity originating from the adsorbed trypsin and the trypsin in solution, e.g., in case of leakage often present upon physical adsorption. Despite of the limitations, colorimetric substrates have been applied for the determination of physisorbed trypsin activity. Johnson and Whateley (Johnson and

Whateley, 1981) used activity assays with colorimetric substrates to characterize the autolysis of trypsin and chymotrypsin caused by physical adsorption on colloidal silica and glass. They measured the total enzymatic activity in the reaction solution containing the particles and compared it to the autolysis observed for enzyme solution inside a vessel of the corresponding material. First-order rates of autolysis were found in both cases, as opposed to inert vessels where second-order autolysis kinetics was observed, suggesting a conformational destabilization of protease upon adsorption to glass and silica surfaces. Koutsopoulos et al. (Koutsopoulos et al., 2007) studied the adsorption of trypsin on hydrophilic silica versus hydrophobic polystyrene surfaces. While the adsorbed amount was determined by reflectometry, the activity was assessed by a colorimetric method. Adsorption affinity was higher on the hydrophobic polystyrene compared to the hydrophilic silica, the saturation plateau values were however similar on both surfaces. Furthermore, the adsorption stability was strikingly different on the two probed materials, as reflected by desorption of trypsin from the surfaces observed during the incubation of the activity assay. In particular, the activity of trypsin adsorbed on polystyrene did not substantially change if rinsing of the surface was carried out before the activity assay. In contrast, after rinsing of silica surface with the adsorbed trypsin, the detected activity decreased by 80 %, indicating leakage of trypsin from the hydrophilic surface confirmed by reflectometry. In this work, reflectometry and colorimetric assay were used in combination to reveal the characteristics of trypsin adsorption and its influence on the resulting enzymatic activity.

In the studies aimed at the optimization of reactors for on-line tryptic digestion, the evaluation of trypsin activity has been carried out in terms of digestion efficiency by methods compatible with proteomic analysis, e.g., high performance liquid chromatography (HPLC) or capillary electrophoresis (CE) that can further be linked to mass spectrometry. In some cases, colorimetric assays have been carried out with HPLC detection to derive the kinetic constants of enzyme activity (Jiang et al., 2000), mostly however, the activity is described by the detection of the peptide fragments of established protein standards, such as insulin chain B (Bonneil and Waldron, 2000; Migneault et al., 2004; Stigter et al., 2007).

The third class of methods for the determination of enzyme activity implies the usage of synthesized activity-based probes that covalently bind to the target enzyme, thus facilitating the identification and characterization of immobilized enzymes. The principles of this methodology have already been described in the section 1.2.4., introducing the methods used in this PhD work.

It is important to note here that the enzymatic activity signal reported by a fluorescent activity-based probe bears a different information content compared to the activity signal detected by a fluorogenic substrate assay. In the latter case, the fluorescent signal is generated as a result of the two-step catalysis (in the simplest approach ignoring any intermediate states), including both: i) the formation of the enzyme-substrate complex via a binding reaction and ii) the collapse of the enzyme-substrate complex via product formation and release of the free enzyme. The catalysis detected by fluorogenic substrate assays can therefore be described in terms of Michaelis-Menten kinetics applying the two basic kinetic parameters, K_M, the Michaelis constant, k_{cat}, the turnover number, as well as the ratio of the two parameters, k_{cat}/K_M that characterizes the catalytic efficiency of an enzyme in binding the particular substrate and transforming it into the product. By contrast, the activity-based probes function as substrates that bind the enzyme active site irreversibly, i.e., the enzymatic reaction involves only the first step of enzyme-substrate binding without the subsequent dissociation step. In this respect, the activity signal reported by activity-based probes is not strictly equivalent to the catalytic activity according to Michaelis-Menten concepts. Nevertheless, Funeriu et al. (Funeriu et al., 2005) have shown that the binding of an activity-based probe to the enzymes belonging to the class that the probe is targeting, can be described by modified Michaelis-Menten kinetics. Funeriu et al. have circumvented the absence of the catalytic step by treating the activity-based probe binding to enzyme as a two-step reaction: the first step corresponding to the formation of the enzyme-activity-based-probe complex, the conversion of which into an irreversible product proceeds in the second step. Accordingly, this binding model was approximated with the classical Michaelis-Menten kinetics modified by the absence of the release of the free enzyme in the second step of the reaction and thus perturbing the value of the turnover number k_{cat}. Consistent with these considerations

however, the signal detected by the activity-based probe bound to an enzyme does not reflect a catalytic reaction, instead, it accounts for the affinity and reactivity of the enzyme active site towards the particular activity-based probe.

Further, we would like to point out the advantages of the activity-based probes for the activity assessment of surface-bound enzymes. The principal relevance of the activity-based probe approach is related to the potentialities of high-throughput screening, including on-chip enzyme activity assays, enabling the transition from the microtiter plate format to the microarray format. Alternative approaches to achieve high-throughput detection of immobilized enzymes include the confinement of the enzymes inside microwells fabricated by soft lithography techniques or sol-gel encapsulation (Rondelez et al., 2005; Sakai-Kato et al., 2006), these methods are however directed at the elaboration of on-chip microreactors rather than the screening of enzymes. On the other hand, protease profiling is usually carried out by applying protease treatment to specific substrates immobilized on the microarray slides, rather than immobilizing the proteases – in this way, on-chip activity read-out is accomplished via the detection of spot fluorescence upon the cleavage of fluorogenic substrates by protease (Salisbury et al., 2002; Uttamchandani et al., 2005). Similarly, Angenendt et al. demonstrated that the activity of horseradish peroxidase and alkaline phosphatase can be detected in microarray format using standard fluorogenic substrates pre-spotted on polystyrene slides, on top of which the corresponding enzymes were spotted (Angenendt et al., 2005). In contrast, activity based probes can be employed for the activity screening of enzymes immobilized directly on the microarray slides (Chen et al., 2003; Funeriu et al., 2005).

1.4. Cluster-assembled nanostructured titanium oxide films fabricated by SCBD method

1.4.1. Supersonic cluster beam deposition method

The remarkable stochastically rough nanometre-scale surface topography in the spotlight of this PhD study is attained by vacuum deposition of titanium clusters delivered by a supersonic beam of an inert carrier gas produced in a pulsed microplasma cluster source (PMCS) according to the principles of supersonic cluster beam deposition (SCBD). Pulsed microplasma cluster source (Fig. 1.4.1.1. A.) represents a cavity where a cathode of the target material is sputtered by pulsed plasma discharge in vacuum creating a high pressure gradient that quenches the ablated species promoting condensation of clusters (Wegner et al., 2006). The pressure gradient is further coupled to the vacuum expansion chamber to form a supersonic cluster beam which is collimated by aerodynamic lenses and guided to the deposition chamber where nanostructured films are grown under high vacuum on a substrate positioned in the plane transverse to the beam axis (Fig. 1.4.1.1. B.).

A. B.

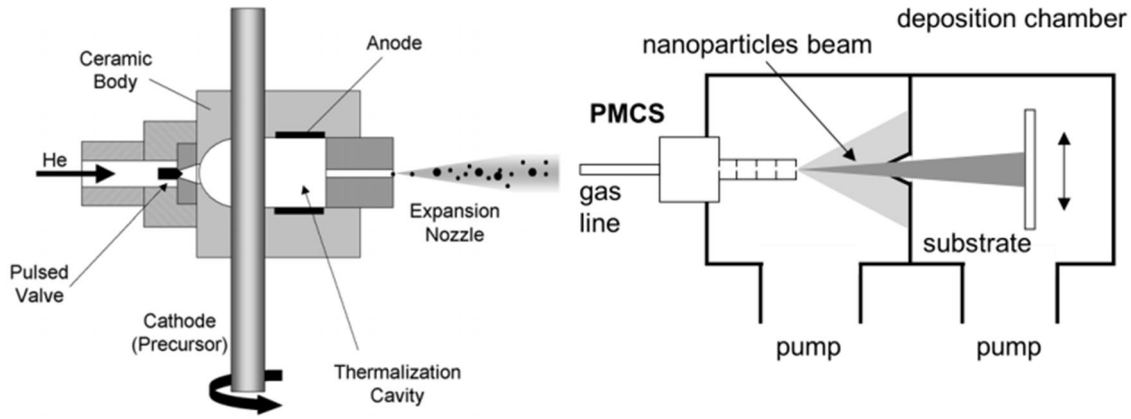

Fig. 1.4.1.1. Schematic representation of the pulsed microplasma cluster source (PMCS) (A), Image taken from Wegner et al. (Wegner et al., 2006) and the apparatus for the supersonic cluster beam deposition combined with PMCS (B). For more details on the working principle, please, see the text.

The mass distribution of the initial cluster precursors is directly related to the gas pressure in the ablation region and inversely related to the cluster residence time inside the PMCS cavity (Barborini et al., 1999); in our system, the two parameters were adjusted to give the typical aggregate size in the range of several hundreds of atoms per cluster with the average diameter of 1 – 3 nm (Vyas et al., 2011). Furthermore, supersonic cluster beam deposition (SCBD) method allows the control of cluster energy enabling a low energy deposition regime (< 0.5 eV per atom) preventing the fragmentation of clusters impinging on the substrate surface. The combination of the SCBD method with the pulsed microplasma cluster source produces stable high intensity beams providing high deposition rates (tens of nanometres per minute). By beam collimation and aerodynamic separation, additional tuning of the cluster size distribution and deposited film thickness is achieved (Kholmanov et al., 2003). Large surface areas can be deposited by raster scanning of the source, whereby patterning is possible by placing masks in front of the substrate. As a bottom-up method, supersonic cluster beam deposition offers the possibility of the controlled variation of surface topography while retaining a constant surface chemistry – an important aspect for the evaluation of phenomena caused by geometrical and morphological constraints of the material interface.

1.4.2. Physicochemical properties of the nanostructured titanium oxide films

Nanostructured films are grown as a uniform assembly of clusters on the substrate surface under high vacuum. The nanometre-range thin films of pure titanium are rapidly oxidized upon exposure to air, resulting in a titanium oxide layer with a slight substoichiometry, (hence, the index x instead of 2), related to the abundance of defects at the surface and boundaries of clusters (Podesta et al., 2009), such as oxygen vacancies and undercoordinated titanium atoms (Sanjines et al., 1994), confirmed by the presence of Ti 3d states in the band gap (Barborini et al., 2005). These defect states are known to promote dissociative adsorption of water (Lindan et al., 1998; Pan et al., 1992; Schaub et al., 2001), as well as adsorption of various inorganic and organic species (de la Garza et al., 2005; Diebold, 2003; Wahlström et al., 2003), including volatile

contaminants from air witnessed as elevated background in the UV photoelectron spectra (Giorgetti et al., 2008).

The thickness of the deposited films is regulated by the deposition rate and duration. The specifics of the film synthesis define a stochastically rough surface composed of the nanometre-sized clusters. The density of the cluster-assembled titanium oxide thin films is by a factor of 1.6 lower than that of bulk titanium dioxide, i.e., 2.5 – 2.7 g/cm^3 (Barborini et al., 2005), as opposed to the bulk density of TiO_2 in the range of 3.9 – 4.3 g/cm^3, indicating a porous morphology. XRD studies have shown that the deposited ns-TiO_x films consist primarily of amorphous phase with occasional nanocrystalline insertions (Kholmanov et al., 2003).

The overall film morphology on the micrometre-scale is characterized by globular features of various sizes dependent on film thickness, which represent the coalesced aggregates of clusters. In contrast, the nanometre-scale structures consist of grains of size on the order of magnitude of tens of nanometres and independent of film thickness, whereas other surface morphology parameters change in concert with thickness (Kholmanov et al., 2003). In particular, the nanometre-scale porosity and granularity can be partially accounted for by two quantifiable parameters: the root-mean-square roughness and the specific area, that grow as functions of film thickness. If the deposition rate is constant, roughness and specific area are linearly correlated with thickness (Podesta et al., 2009), whereby a thickness increase from 25 to 300 nm corresponds to approximately 20 nm difference in the deposited film roughness.

After the deposition, ns-TiO_x films are subjected to thermal treatment to ensure a complete oxidation of the films and to remove contaminants readily adsorbed on the surface upon exposure to air. The structural and physicochemical evolution of ns-TiO_x films upon annealing at temperatures in the interval from 400°C to 800°C in ambient atmosphere has been deeply studied in the earlier work of our group (Kholmanov et al., 2003), revealing temperature-dependent phase transitions and structure transformations. In particular, annealing at 400°C induces the amorphous-to-anatase transition evidenced by the growth of nanocrystalline grains and peaks in the XRD spectra typical to anatase phase. The anatase-to-rutile transition occurs at

temperature below 600°C, whereas higher annealing temperatures increase the fraction of the rutile phase until, at around 800°C, anatase phase is mostly replaced by the rutile phase. Importantly, it was shown that annealing at temperatures up to 400°C does not affect the thickness and roughness of the films, whereas annealing at 1000°C resulted in increased roughness while still retaining morphology on nanometre scale (Barborini et al., 2005; Podesta et al., 2009).

The impact of mild thermal annealing treatment is demonstrated by the changes in wettability of the ns-TiO_x films. Films that have been exposed to air after the deposition without any further treatment ("as-deposited films") are hydrophobic, whereas annealing in air at 200°C and 400°C renders the ns-TiO_x films mildly hydrophilic and super-hydrophilic, respectively. Instead of structural changes, these wettability effects have been explained by the changes in surface chemistry upon mild annealing, i.e., the variations in the composition of chemisorbed species. Immediately after taking the deposited films out of the vacuum deposition chamber, the surface of films is highly reactive due to the large specific surface area provided by the nanometre-sized clusters. Furthermore, the rapidly oxidized superficial layer is rich of defects that act as adsorption sites therefore it is rapidly populated by chemisorbed species present in the air under ambient conditions. The hydrophobicity of the as-deposited ns-TiO_x films is attributed to organic contaminants that are replaced by dissociated water molecules upon mild thermal annealing in air, turning the surfaces hydrophilic. The effects of mild annealing up to 400°C are entirely reversible within the time-scale of days/months, since the surface is re-populated by organic contaminants when exposed to air. Noteworthy, the hydrophobic as well as the hydrophilic character is expressed more with increasing surface roughness – this implies that the thermal annealing acts as reversible switching between two distinct wettability regimes, while the control over film morphology allows the fine-tuning of the degree of wettability (Podesta et al., 2009).

1.4.3. Interaction of nanostructured titanium oxide with proteins and cells

Titanium dioxide has been long proven as a biocompatible material in medicine (Brunette et al., 2001), approximately two decades ago however, an avalanche of studies on the detailed interaction between titanium surface and biomolecules was initiated, focusing on physically relevant questions in the biological context of titanium application as implant material both, in terms of protein adsorption mechanisms (Ellingsen, 1991; Imamura et al., 2008; Klinger et al., 1997), as well as the optimization of material performance (Harris et al., 2004; Lausmaa et al., 1985; Linderbäck et al., 2010). Micro- and nanofabricated titanium has attracted attention due to the potentialities of combining bio-friendly interfaces with microelectronics technologies for the development of biosensing devices (Garipcan et al., 2008; Mathur et al., 2009).

Nanostructured titanium oxide films synthesized by the supersonic cluster beam deposition method coupled with pulsed microplasma cluster source have been verified as biocompatible platforms for cell-based assays, supporting the adhesion and growth of primary and tumour cells (Carbone et al., 2006). Recently, ns-TiO_x was reported to serve as substrate for the in vitro expansion and differentiation of myogenic stem cells (Belicchi et al., 2010). The optically transparent thin ns-TiO_x films with tuneable wettability properties have been tested as promising candidates for microarray slide coatings. In another study, live cell microarrays were created on ns-TiO_x films in a multi-step process, involving the printing of streptavidin arrays, followed by the second printing of biotinylated retroviruses and subsequent infection of cells for the overexpression or downregulation of genes in a lab-on-chip format (Carbone et al., 2007). Feasibility of ns-TiO_x films as platforms for protein microarrays was investigated by non-contact spotting of protein solutions directly on ns-TiO_x-coated slides (Carbone et al., 2009; Giorgetti et al., 2008). Protein binding on ns-TiO_x was based solely on the physisorption without the need of further functionalization of the surfaces. The reproducibility and signal-to-noise ratio of the protein arrays on ns-TiO_x were comparable to conventionally used commercial slide coatings. Significant efforts have been made to dissect the mechanisms of protein adsorption on ns-TiO_x films and thus identify the factors that determine the biocompatibility characteristics of these

surfaces, highlighting the role of nanometre-scale surface morphology. The chemical nature of protein binding to ns-TiO_x has been interpreted by the formation of coordinated covalent bond between carboxylic acid residues and undercoordinated titanium atoms (Giorgetti et al., 2008). Atomic force spectroscopy studies involving silicon nitride AFM tips functionalized with silanol and silylamine groups have confirmed the putative interaction mechanism between hydrophilic functional groups typically displayed on protein surface and the hydrated nanostructured titanium oxide surface (Vyas et al., 2011). According to the suggested model, undercoordinated superficial titanium atoms are attacked by the nucleophiles of the functional groups, resulting in the formation of coordinate dative covalent bonding, possibly accompanied by hydrogen bonding between the protons of the incoming chemical moieties and the oxygen atoms of the ns-TiO_x surface.

Extensive AFM investigation was carried out to decipher the role of the nanometre-scale morphology in protein adsorption. The depth and width distributions of the nanometre-sized pores were assessed by scanning of the stochastically rough surface before and after adsorption of proteins. It was clarified that the key parameter that governed protein adsorption was the aspect ratio of the nanopores: adsorption occurred as the preferential filling of pores with higher aspect ratios, rather than homogenous coverage of the surface. Experiment data obtained with three different proteins on a series of ns-TiO_x samples were accounted for by the proposed model (Scopelliti et al., 2010).

1.4.4. Surface characterization by atomic force microscopy

Atomic force microscopy (AFM) was developed as an important extension to the general methodology of scanning probe microscopy applicable to non-conducting samples, as opposed to the scanning tunnelling microscopy (STM) (Binnig et al., 1986). The working principle of AFM can be roughly described as stylus profilometry on atomic scale: the sample surface is scanned in three dimensions by a tip, the movement of which is regulated by a feedback circuit that enables to keep constant either the force between the tip and the sample, or the tip-sample distance. The

changes in the forces are read out as the deflection of a laser beam reflected from the cantilever at the end of which the AFM tip is attached, while the movement of the tip is carried out by piezoelectric actuators. The forces detected by AFM method can originate from diverse interactions between the atoms of the tip apex and the atoms of the sample surface, such as electrostatic, van der Waals interactions and capillary forces. AFM imaging can be performed in two basic regimes, i.e., the static or the dynamic mode, that are further classified into sub-groups according to the specifics of the detection. In the static mode, the static deflection of the cantilever is measured and translated into units of force: in the contact mode, the value of the interaction force during the sample scan is maintained constant, whereas in the force spectroscopy mode, the change of the interaction force is measured as a function of the tip-surface distance (Bowen et al., 1998). On the other hand, in the dynamic mode, the shift in the amplitude (amplitude modulation or the tapping mode) or the shift in the resonance frequency (frequency modulation) of the vibrating tip is measured. Due to the reduction of the tip-sample interaction achieved by the amplitude modulation, tapping mode is the most commonly applied AFM technique for the imaging of soft surfaces or molecules that are weakly attached to the sample surface, typical for biological samples (Möller et al., 1999; Sit and Marchant, 2001). AFM methodology, that was initially used as high resolution (on the order of Å to nm, depending on the sample) imaging technique to reveal the structure, surface defects and adsorbate molecules on crystalline surfaces, has been further developed to measure the strength of atomic and molecular bonds on single molecule level (Dufrene, 2008; Lee et al., 1994; Merkel et al., 1999) as well as to allow manipulations of single molecules and surface patterning on nanometre-scale (Garipcan et al., 2008; Takeda et al., 2003). In the field of protein adsorption, numerous reports have been published on the AFM investigation of the structure of protein layers adsorbed on atomically flat surfaces, such as silicon, graphite or mica, where AFM has often been accompanied by complementary surface-sensitive techniques for probing the adlayers, including ellipsometry, XPS and QCM (Dufrêne et al., 1999; Lubarsky et al., 2007; Wälivaara et al., 1997).

In this PhD work, the usage of AFM method has been limited to the tapping-mode characterization of the stochastically-rough nanometre-scale surface morphology of the nanostructured titanium oxide films produced by supersonic cluster beam deposition method that were applied for the studies of enzyme-biomaterial interactions performed by other (fluorescence-based) methods. Surface morphology was described by two quantitative parameters – the root-mean-square roughness and the specific area, as explained in details in the "Materials and Methods" chapter. The insights from the previous works by our group using force spectroscopy in combination with functionalized AFM tips to model protein adsorption on nanostructured titanium oxide (Giorgetti et al., 2008; Vyas et al., 2011), as well as the AFM characterization of individual surface nanopores (Scopelliti et al., 2010), were used for the interpretation of the findings on trypsin adsorption in the current study.

2. MATERIALS AND METHODS

2.1. Preparation of nanostructured titanium oxide films

2.1.1. Fabrication of nanostructured titanium oxide films

Ns-TiO_x films used in this work, were deposited onto standard round microscopy cover glasses (thickness number 1.5, diameter 13 mm) and onto standard microarray slides (250 × 750 mm) to apply them either for microscopy-based methods (AFM, FRAP, FPQ) or for microarray-based methods (PSIM). Ns-TiO_x films were fabricated onto standard microarray slides creating a stepwise thickness gradient with either four or six steps (depending on the designated application of the particular samples), corresponding to four or six different nanoscale morphologies, respectively. The two types of gradients had the following nominal thickness values: 1) 50nm; 100nm; 200nm; 300nm and 2) 25nm; 50nm; 100nm; 150nm; 200nm; 300nm. On the microscopy cover glasses, homogenous films of each nominal thickness value were deposited. In order to remove any possible weakly adsorbed surface contaminants, prior to further usage samples were thermally treated at 250°C for 2 hours in a muffle oven under dry air flow, and subsequently sealed under vacuum to be preserved for 24 hours until the planned measurements. Within 32 hours after annealing, the samples were applied for nanoscale surface morphology characterization, as well as trypsin adsorption and activity studies.

2.1.2. AFM characterization of surface morphology

Surface morphology of the deposited films was probed by Multimode AFM equipped with a Nanoscope IV controller (Veeco Instruments). Surface scanning was carried in air using the Tapping Mode. Single crystal silicon tips were utilized with the nominal radius of curvature 5 – 10 nm and cantilever resonance frequency in the range of 200 – 300 kHz, scan rates were 1.5 – 2 Hz. Sampling resolution was 2048 × 512 corresponding to dimensions of the scanned areas of 2μm ×

1µm. The root-mean-square roughness was defined as the root-mean-square deviation of surface height from its average value:

$$\sigma = \sqrt{\frac{1}{N}\sum_{i,j}\left(h_{ij} - \bar{h}\right)^2}$$

where h_{ij} is the height value found in row "i" and column "j"; N is the total number of measured height values and $\bar{h}$ is the average value of height. The specific area was determined as the ratio of the calculated three-dimensional surface area versus its projected two-dimensional area according to:

$$A = \frac{1}{N}\sum_{ij}\sqrt{1 + \left|\nabla h_{ij}\right|^2}$$

where ∇h_{ij} is the surface gradient vector.

2.2. Protein adsorption characterization

2.2.1. Fluorescent labelling of trypsin

Trypsin (porcine trypsin powder T0303, Sigma-Aldrich, Saint Louis, MO, USA) was resuspended in 2 mg/ml in 0.5 ml 0.67 M borate buffer containing 0.02 M Ca^{2+}, pH 8.1, to which the amine-reactive dye Alexa Fluor 555 (alternatively Alexa Fluor 647) succinimidyl ester (Molecular Probes, Eugene, OR, USA) was added, according to producers instructions. Initially, the amine-reactive FITC dye (fluorescein isothiocyanate) was used, however it was substituted by Alexa dyes due to occurrence of photobleaching during the confocal measurements. Labelling reaction was incubated for one hour at room temperature, after that the separation of conjugate from the free dye and simultaneous buffer exchange was carried out by gel filtration in spin columns (ZebaTM Desalt Spin Columns, 10 kDa MWCO, Thermo Fisher Scientific Inc., IL, USA) equilibrated with Milli-Q water (Milli-Q water system Millipore, MA, USA). After the purification, conjugate solution was pipetted as 10 µl aliquots in 50 µl PCR tubes and frozen rapidly either on dry ice or in liquid nitrogen. The final product of freeze drying was rehydrated in modified Tris

Buffered Saline (TBS-Ca^{2+}) – 25 mM Tris base, 100 mM NaCl, 20 mM $CaCl_2$, pH8. Initial batches of labelled trypsin were subjected to freeze-drying, however, after encountering trypsin aggregates in the prepared aliquots after rehydration, freeze-drying was omitted using aliquots of trypsin frozen in modified Tris Buffered Saline buffer and stored on dry ice. Concentration of the conjugate after labelling and the degree of labelling was assessed by spectrophotometry at 280 and 555 nm, using molar extinction coefficients 35100 $M^{-1} \cdot cm^{-1}$ for trypsin (280 nm) and 150000 $M^{-1} \cdot cm^{-1}$ for Alexa Fluor 555 (at 555 nm) and 237000 $M^{-1} \cdot cm^{-1}$ for Alexa Fluor 647 (at 650 nm). After estimation of the concentration of the labelled aliquot, the working solution of trypsin was prepared by diluting the labelled aliquot with freshly prepared non-labelled trypsin so that the ratio of labelled-to-non-labelled trypsin was set between 0.04 and 0.1. During the preparation steps of all the experiments, trypsin solutions were always kept on ice, in order to minimize the impact of autoproteolysis.

2.2.2. Confocal microscopy based methods: Fluorescence Photobleaching Quantification and Fluorescence Recovery after Photobleaching

For the quantitative estimation of adsorption, a novel specially adapted FRAP-based confocal microscopy approach was applied that has been recently developed by our group and termed *Fluorescence Photobleaching Quantification* (FPQ) (Scopelliti et al., 2010). In the FPQ setup, protein adsorption is monitored in the transverse XZ plane displaying both, the adsorbed protein layer and the protein solution above it. The principle of this new robust method is based on the usage of the protein solution at known nominal protein concentration above the layer, as the calibration standard for the fluorescence signal of the adsorbed protein layer itself. In this way, a calibration standard is present within each FPQ measurement without the need of an external signal calibration. The term `*Photobleaching*` is used in the name of the method due to the bleaching step of a region of the adsorbed protein layer in order to derive the signal of protein solution without the contribution of the layer at the material surface – the position within the

field of view that is minimally perturbed by spherical aberrations of the confocal system (Diaspro et al., 2002; Hell et al., 1993).

The details of both, FPQ and FRAP measurements, were, as follows: the assessment of protein adsorption was accomplished by imaging the solution of fluorescently labelled proteins applied as a 200 µl drop on top of ns-TiO_x coated glass coverslip (13 mm diameter, #1.5) fixed inside a home-built microscope chamber equipped with a poly (tetrafluoroethylene) gasket (10 mm inner diameter). All studies were performed with the TCS SP2 AOBS inverted laser scanning microscope (Leica Microsystems Heidelberg GmbH, Germany) using 514 nm argon ion laser line for the excitation of Alexa Fluor 555 dye; 514 nm argon emission and 561 nm diode-pumped solid state laser emission were used for the photobleaching of Alexa Fluor 555 dye (alternatively, 633 nm He-Ne laser line for Alexa Fluor 647 dye). HCX PL APO lbd.BL 63× NA=1.40 oil immersion objective and a 3.0 zoom were used for all acquisitions. Image resolution was always 256 × 256 corresponding to pixel dimension of 210 nm.

Fluorescence recovery after photobleaching (FRAP) monitoring was performed in parallel with the FPQ measurements benefiting from the similarity of the two setups. In both, FPQ and FRAP experiments, 15 µm × 15 µm region of interest was bleached in the centre of the 79.4 µm × 79.4 µm large field of view in XY plane. Bleaching was performed in XY plane due to a more homogenous bleached region with well-defined borders in XY plane compared to XZ plane. Then, the acquisition was switched to XZ plane, obtaining the signal of the adsorbed protein layer and the signal of the bulk solution above the layer, both within the same image. Moreover, within the 80 µm × 80 µm large field of view in the XZ plane, both, the bleached and the non-bleached regions of layer were captured, as well as the signal of the bulk solution adjacent to the bleached region and hence, not perturbed by the aberrations, important for the FPQ-calibration of the adsorption signal. The acquisition and switching from XY to XZ imaging modes was carried out automatically by using pre-recorded macro sequences available in the Leica TCS SP2 software. The automatic acquisition enabled temporal resolution of 1.5 seconds when switching between different imaging modes. Each field of view was acquired in three channels: fluorescence,

reflectance and transmission. Reflectance and transmission were detected as reference signals at the laser wavelength in use, to account for variations in laser output. The dynamic range of the FPQ method in terms of usable protein concentrations depends on the layer signal versus solution signal ratio which determines the imaging contrast, therefore it depends on the adsorption characteristics of the particular protein. Here, fluorescent trypsin was probed in the concentration range of 1 – 10 μM that provided optimal imaging contrast.

For the fluorescence recovery monitoring of the adsorbed protein layer, automatic time-resolved image acquisition was carried out. After switching from XY to XZ mode, the recovery of the layer signal was recorded with the acquisition rate of 0.033 s^{-1} (one scan every 30 seconds) for the first five minutes and the subsequent acquisition rate of 0.0083 s^{-1} (one scan every 120 seconds) for the remaining 30 to 60 minutes. After the recovery monitoring, automatic switching from XZ to XY plane was performed, in order to control the end position of the image centre relatively to the centre of the bleached region. Control of the position was necessary to ensure that the XZ recovery signal was acquired from the bleached region and not from the adjacent non-bleached region, since a deviation might occur due to focal drift in the XY plane during the long monitoring time.

Quantitative image analysis was performed by ImageJ software (http://rsb.info.nih.gov/ij/).

FRAP data were analysed, as follows: fluorescence recovery curves measured by FRAP method were fitted with monoexponents and the respective recovery kinetic parameters were derived from the reaction-dominant model (Sprague et al., 2004), as follows:

$$y = M\left(1 - e^{-\frac{x}{t}}\right)$$

M denotes the mobile fraction and the index of the exponent t is related to the recovery halftime τ as $\tau = t \cdot ln(2)$. The bleached signal of the recovery curves was set to 0 and the initial signal normalized to 1. The usage of the reaction dominant model was appropriate since the estimated recovery halftime values were by a factor of 60 lower than the theoretical diffusion

time of trypsin molecule calculated from the Stokes-Einstein relation, as described in the "Introduction" chapter.

Quantitative determination of the adsorbed density of proteins per resolution area was accomplished by FPQ method according to the equation:

$$\rho = \frac{L}{B}\frac{V_{res}}{S_{res}} C$$

where ρ stands for the adsorbed protein density of the layer; L and B denote the fluorescence signal of the layer and of the bulk solution (Background), respectively. V_{res} is the resolution volume, defined as box with the sides equal to the full width at half maximum (FWHM) of the point spread function along the corresponding axis. S_{res} is the respective resolution surface or the base area of the V_{res} box, equivalent to the squared lateral FWHM of the point spread function.

C signifies the bulk concentration of the protein at the beginning of the FPQ experiment, which has to be measured with a complementary method. We measured trypsin concentration prior to adsorption on ns-TiO_x via spectrophotometry, as described in the section 2.2.1., on the fluorescent labelling of trypsin. We assumed the bulk concentration as constant, since no significant changes were detectable in the fluorescence of the bulk solution during the whole experiment, thus the depletion of trypsin molecules from the bulk was negligible.

The values of V_{res} and S_{res} depend on the optical system and the fluorescence emission wavelength. Since the ratio of V_{res} to S_{res} reduces to the axial resolution, we estimated the axial FWHM experimentally as $(FWHM)_z = 1.32 \pm 0.06$ µm and plugged this value for the calculation of adsorbed protein surface density. The measured fluorescence intensity distribution along Z axis of the adsorbed protein layer in the absence of bulk solution is demonstrated in Fig. 2.2.2.1.

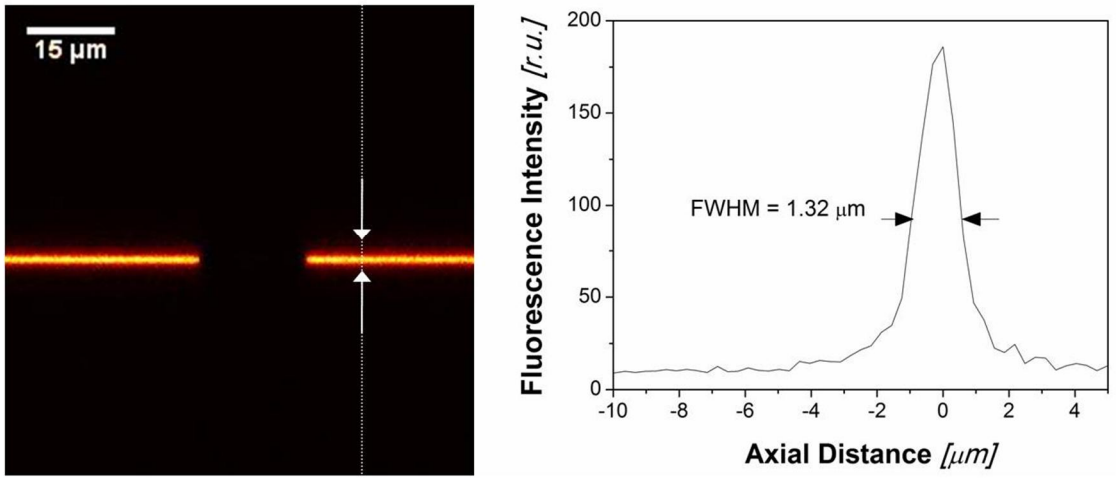

Fig. 2.2.2.1. Estimation of the axial resolution equivalent to the full width at half maximum of the fluorescence intensity distribution of the sub-resolution protein layer in the absence of bulk solution.

The values of trypsin surface density were normalized by the specific surface area estimated by AFM, in order to account for the nanoscale morphology of ns-TiO_x. Trypsin surface density values, expressed in mass of adsorbed trypsin per unit area (µg/cm^2), were then translated into monolayer units to define the relative coverage of ns-TiO_x surface upon trypsin adsorption. The theoretical monolayer units of trypsin coverage were calculated taking into account the approximate dimensions of trypsin molecule given by crystallography (4.9 × 3.9 × 3.3 nm) (Abbas et al., 2009). The maximum relative coverage (the so called, jamming limit θ) was determined by the Random Sequential Adsorption model for unoriented hard rotation ellipsoids according to the equation obtained by interpolating the numerical results and given by Adamczyk et al. (Adamczyk et al., 2002):

$$\theta = 0.304 - 0.123 \cdot A + \frac{0.365}{A}$$

where A is the ratio of the axis of the rotation ellipsoid. The weighted mean jamming limit for all three trypsin orientations was estimated as θ ≈ 0.69 and taken for the calculation of monolayer coverage.

2.2.3. Protein-Surface-Interaction microarrays

For high-throughput studies of protein interaction with biomaterial surfaces, our group has established a new microarray-based methodology that allows the screening of protein-material interactions versus an ensemble of biomaterial parameters with a panel of proteins in a single experiment (Scopelliti et al., 2010). In order to calibrate the semi-quantitative high-throughput data, Protein-Surface-Interaction-Microarrays were used in combination with the Fluorescence Photobleaching Quantification method.

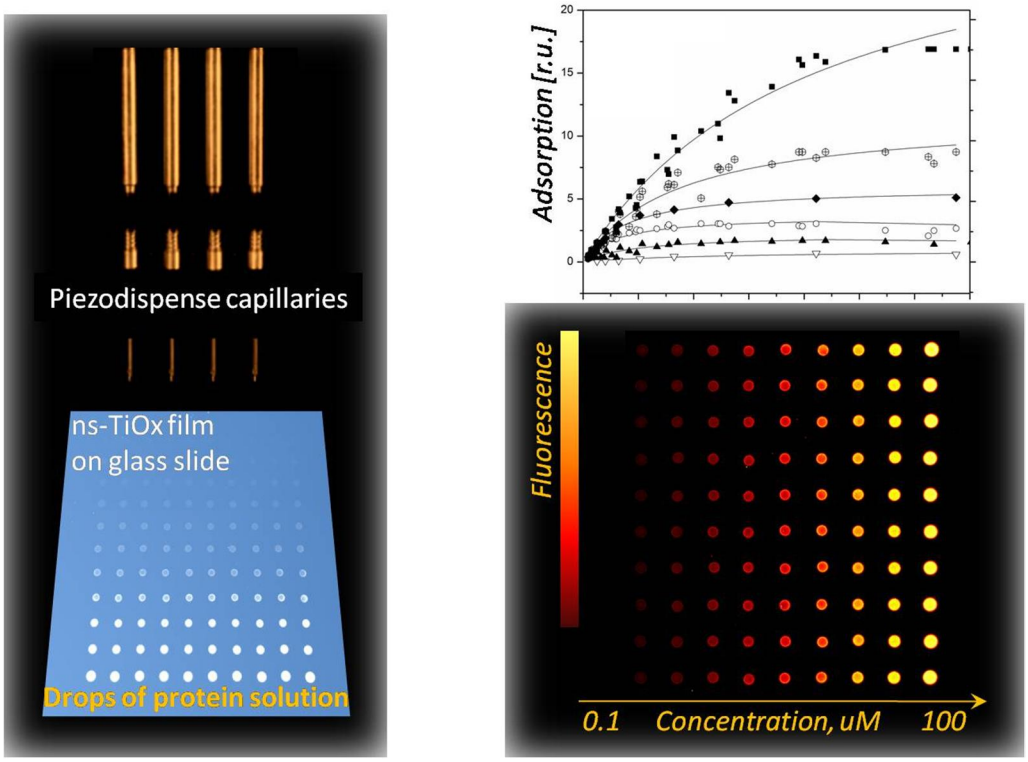

Fig. 2.2.3.1. Principle of the PSIM method. Left panel: Fluorescently labelled protein gradients are physisorbed by means of arraying on the material surface of interest. Right panel: After blocking and washing off of the unbound proteins, slides are dried and scanned, obtaining protein adsorption isotherms in the concentration range covering three orders of magnitude on a panel of biomaterials within a single experiment.

Here, Alexa Fluor 555-trypsin (or Alexa Fluor 647-trypsin) was used in TBS-Ca^{2+} buffer, pH 8, in the concentration range of 0.5 – 175 µM. Trypsin solution was arrayed (200 – 400 picoliters

per spot) using non-contact piezo dispenser sciFLEX ARRAYER S3 (Scienion AG, Germany) in a 10 × 10 pattern corresponding to ten replicates of ten serial dilutions arranged as spots with 550 µm pitch and approximate spot diameter of 250 µm on ns-TiO_x coated standard microarray slides (Nexterion, Glass B (Schott)) (Fig. 2.2.3.1). After 1 hour incubation in the dark, at room temperature and 60 % humidity, slides were blocked for 10 minutes with 1 % bovine serum albumin solution in Phosphate Buffered Saline (PBS), pH 7.4, and washed two times with PBS and one time with Milli-Q water. Thereafter, slides were dried with a flux of dry air and scanned with the 532 nm and 635 diode laser lines of Power Scanner (Tecan Trading AG, Switzerland) using the emission filter sets designed for CY3 and CY5 dyes (579 nm and 676 nm central wavelengths with 30 nm bandwidth). Images were analyzed with ScanArray Express software (Perkin Elmer Inc, MA, USA).

Adsorption isotherms were approximated with the Langmuir model which relates the surface coverage Γ of adsorbent occupied by adsorbate molecules with the bulk concentration of the adsorbate, C:

$$\Gamma = \frac{SU_L}{1 + \frac{k_{DL}}{C}}$$

where SU and k_D are the saturation uptake and the equilibrium dissociation constant, respectively (letter "L" in lowercase denotes the Langmuir model). Approximation with Hill model was used to account for the cooperativity of adsorption characterized by Hill coefficient n:

$$\Gamma = \frac{SU_H}{1 + \frac{k_{DH}}{C^n}}$$

where letter "H" in lowercase stands for Hill model. Value of the Hill coefficient $n > 1$ indicates cooperative adsorption related to more than one binding sites to the surface or binding between the adsorbate molecules. Value of Hill coefficient $n < 1$ signifies non-cooperative adsorption, i.e., the presence of repulsive protein-protein or protein-surface interactions. In case n=1, Hill plot is reduced to Langmuir model.

For the desorption studies, ns-TiO_x slides with arrayed trypsin gradients were prepared according to the described PSIM protocol. Thereafter, slides were mounted inside a 16-well chamber ensuring the localization of a single 10 × 10 pattern sealed within each well. Drops of 100 µl of the TBS-Ca^{2+} buffer solution pH 8, were applied to the wells, which were subsequently incubated with the buffer solution for various time intervals, namely: 0; 5; 15; 20; 30; 45; 60; 90 minutes. After the incubation, buffer solution was removed; slides were washed with Milli-Q water, dried with a flux of dry air and scanned. Trypsin isotherms were plotted corresponding to every incubation time interval in order to track the desorption at various initial coverage values of trypsin. Desorption curves were approximated with a monoexponential function:

$$y = (y_0 - y_\infty) \cdot e^{-\frac{x}{t}} + y_\infty$$

$(y_0 - y_\infty) = y_d$ denotes the total desorbed (reversibly adsorbed) amount, where y_0 is the initial coverage and y_∞ is the irreversibly adsorbed amount. The exponent index t is proportional to the desorption halftime $\tau_d = t \cdot ln(2)$.

2.3. Activity assessment of physisorbed trypsin

2.3.1. Activity probe binding assay in solution

We intended to develop a high-throughput approach for the estimation of the activity of physisorbed enzymes on nanostructured randomly-rough surfaces. The fluorescent activity-based small molecules probes available on the market offered a potential to reach our goal. Prior to the usage of the activity probe for trypsin in microarray format, we performed several experiments to test the binding of the activity probe to trypsin versus bovine serum albumin (BSA) in solution, as well as the binding of the activity probe to physisorbed trypsin versus physisorbed BSA on slide surfaces homogenously incubated with these proteins.

The test of activity probe binding to proteins in solution was accomplished, as follows: first, equimolar (50 µM) trypsin and BSA (Sigma-Aldrich) solutions in TBS-Ca^{2+} buffer were incubated with 10 µM carboxytetramethylrhodamine (TAMRA) labelled activity probe (Cat #

88318 ActivX TAMRA-FP Serine Hydrolase Probe (Pierce/Thermo Scientific), shortly termed "activity probe") for 30 minutes. Immediately after incubation, the reaction solutions were filtered for the removal of unreacted probe using centrifugal filters (NMWL 10kDa, Amicon Ultra-0.5 ml (Millipore)). After centrifugation, the concentration of activity probe and the concentrations of proteins were determined in the filtrate and retentate solutions by spectrophotometry, using molar extinction coefficients 35100 $M^{-1} \cdot cm^{-1}$ for trypsin (280 nm) and 80000 $M^{-1} \cdot cm^{-1}$ for tetramethylrhodamine (558 nm), with the correction factor 0.34 for TAMRA at 280 nm.

2.3.2. On-slide activity assay without arraying

Standard microarray slides coated with ns-TiO_x gradients consisting of four steps of increasing film thickness and roughness were prepared as described in section 2.1.1. Slides were mounted in a slide chamber (Nexterion IC-16 (Schott)) divided in 16 square-shaped wells by tightly sealed hydrophobic walls, resulting in four wells per one ns-TiO_x gradient zone. The ns-TiO_x surface inside each well was subjected to various treatments: a) 1 hour long incubation with 100 µl of 150 µM non-labelled trypsin and subsequent blocking with 1 % (150 µM) BSA for 10 minutes; b) 10 minutes long incubation with 1 % (150 µM) BSA and c) no treatment. The prepared surfaces a), b) and c), were washed two times with TBS-Ca^{2+} buffer and one time with Milli-Q water without removing the slides from the incubation chamber. Then, the TAMRA-labelled serine hydrolase activity probe was resuspended in TBS-Ca^{2+} buffer to a final concentration of 1 µM, applied to each well and incubated for 30 minutes. Immediately after reaching the end of the incubation time, the contents of the wells were removed and the surfaces were subjected to several washing steps. Half of the wells were washed two times with 1 % SDS solution in TBS buffer, the other half (control wells) were washed twice with TBS buffer (no detergent addition), after that, all wells were washed twice with TBS buffer and once with Milli-Q water. Then, the slides were removed from the chamber, immersed in Milli-Q water, sonicated for two minutes, dried with a flux of dry air and scanned. Fluorescence intensity was quantified by drawing a region of interest

corresponding to the area of ns-TiO_x surface of each well using the analysis options of ImageJ software.

2.3.3. Microarray-based enzyme activity assay

The principle of the enzyme activity assay in microarray format is shown in Fig. 2.3.3.1.

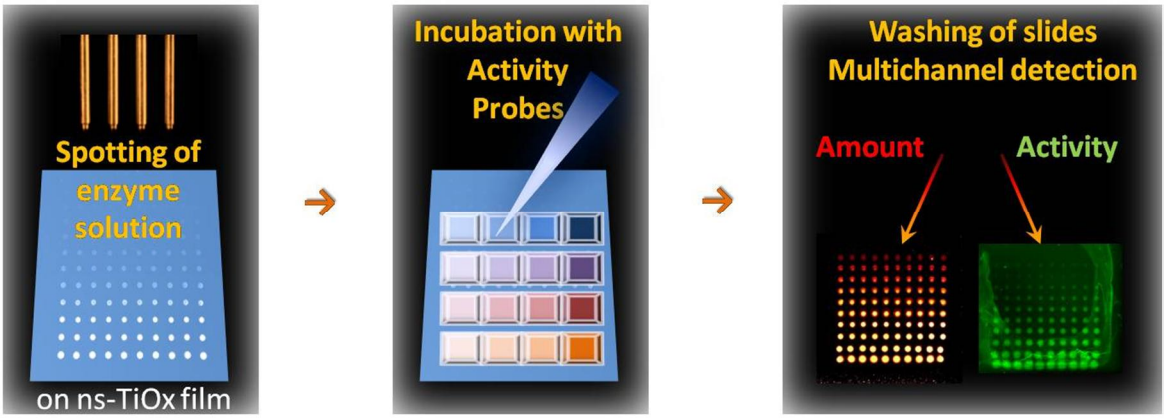

Fig. 2.3.3.1. Scheme of the microarray-based assay for high-throughput assessment of the activity of physisorbed enzymes. Left panel: Fluorescently labeled enzymes are physisorbed by means of arraying on the material surface of interest. Middle panel: The immobilized enzyme arrays are incubated with various concentrations of fluorescent activity probes for a range of time intervals. Right panel: Slides with arrays are blocked, washed and scanned to detect the adsorbed amount, as well as the activity in separate fluorescence channels.

Slides coated with four-step ns-TiO_x gradients were prepared as described in section 2.1.1. Alexa-647-trypsin was arrayed according to the protocols presented in section 2.2.3. After blocking, washing and drying, slides were mounted in the 16-well slide chamber in such a manner that each well enclosed one 10 × 10 array. TAMRA-labelled serine hydrolase activity probe was resuspended in TBS-Ca^{2+} buffer and diluted to five final working concentrations between 0.5 and 5 µM. The activity probe was then applied to the chamber wells and incubated for various time intervals, depending on the goal of experiment. Immediately after reaching the end point of

incubation, the contents of the wells were removed, and the wells were washed twice with 1 % SDS solution in TBS buffer, twice with TBS buffer and once with Milli-Q water. Then, the slides were removed from the chamber, immersed in Milli-Q water and sonicated for two minutes, followed by drying with dry air flux. Fluorescence was detected simultaneously in CY3 and CY5 channels, using the excitation of 532 nm and 635 diode laser lines combined with the corresponding emission filter sets (579 nm and 676 nm central wavelengths with 30 nm bandwidth) of the Power Scanner (Tecan). Images were analyzed with ScanArray Express software (Perkin Elmer).

2.3.4. Activity assay with chromogenic substrate

In parallel to the newly developed activity assay in microarray format, the activity of physisorbed trypsin was measured using a standard method involving the chromogenic substrate Nα-Benzoyl- DL -arginine 4-nitroanilide hydrochloride (BAPNA, B4875, Sigma-Aldrich) that enables the estimation of esterase activity of trypsin.

In order to obtain the kinetic parameters of enzyme activity, the following steps were undertaken: 1) a set of ns-TiO_x –coated cover slips were incubated with trypsin solution of known concentration for 2 h at 4°C; 2) the amount of the adsorbed enzyme was estimated using the Fluorescence Photobleaching Quantification method; 3) the fluorescent trypsin solution was removed and three washing steps with the TBS-Ca^{2+} buffer, pH8 were performed; 4) ns-TiO_x – coated cover slips with adsorbed trypsin were positioned inside a 24-well plate (1 cover slip per well); 5) reaction solution containing various concentrations (100 – 500 µM) of BAPNA was added to the single wells (2.5 ml per well); 6) 400 µl of the reaction solution was pipetted inside plastic cuvettes for spectrophotometry measurements at regular time intervals (6 cuvettes of reaction solution and 1 blank cuvette containing only BAPNA at the corresponding concentration); 7) after each measurement, the dispensed reaction solution was returned to the respective wells with ns-TiO_x coverslips; 8) reaction rate was measured versus time as the increase in absorbance at 410 nm resulting from the liberation of absorbing dye p-nitroaniline, using the molar extinction

coefficient 8800 $M^{-1} \cdot cm^{-1}$; 9) after 150 minutes of absorbance measurement, reaction solutions were left inside the cuvettes for a continuous 60 minutes monitoring of the absorbance in order to test if desorbed trypsin was present in the solutions.

Kinetic parameters V_{max}, K_M and k_{cat} were estimated according to the Lineweaver-Burk linearization of Michaelis-Menten equation:

$$\frac{1}{V_0} = \frac{K_M}{V_{max}} \cdot \frac{1}{[S]} + \frac{1}{V_{max}}$$

where [S] is the initial concentration of the substrate BAPNA and V_0 is the initial reaction velocity expressed as the slope of the linear region of the absorbance versus time curves and translated into units of μmol of formed product per minute. The turnover number k_{cat} is calculated from V_{max} and $[E]_{tot}$, the total concentration of the enzyme estimated by the FPQ method, as:

$$k_{cat} = \frac{V_{max}}{[E]_{tot}}$$

Specific activity was expressed as the maximum velocity in versus the total mass of adsorbed enzyme in $\mu mol \cdot min^{-1} \cdot mg^{-1}$.

3. RESULTS AND DISCUSSION

The catalytic activity of surface-bound enzymes is intimately linked to the chosen immobilization method and the physicochemical conditions of immobilization, including i) the forces that constitute the bonds, i.e., covalent, ionic, van der Waals or other interactions, ii) the properties of the interface, such as temperature, solvent, pH and buffer ionic strength, as well as iii) the physical, chemical and topographical features of the solid surface. Additionally, whenever enzymes are immobilized by means of physisorption as it is in this case, the timescale of binding has to be taken into account based on the dynamic equilibrium between the adsorption and desorption processes. Another time-dependent parameter is the conformation of surface-bound enzyme molecules that can be subjected to changes until an equilibrium state is reached and therefore might differ from the native catalytically active conformation of the enzyme. Furthermore, certain intrinsic properties of enzyme molecules can contribute to the loss of their native conformation, hence, the catalytic activity, upon immobilization; among the latter, autoproteolytic activity has to be regarded in the case of protease, i.e., trypsin, immobilization. Following the considerations listed, we initially focused on exploring the physisorption behaviour of trypsin on cluster-assembled nanostructured titanium oxide (ns-TiO_x) surfaces to gain understanding of the effect of trypsin-ns-TiO_x interaction on the enzymatic activity of surface-bound trypsin and to associate it with particular nanoscale properties of the ns-TiO_x surfaces. To do so, we firstly synthesized ns-TiO_x thin films by supersonic cluster beam deposition method (SCBD) and determined their typical nanoscale features by atomic force microscopy (AFM). Secondly, we studied trypsin adsorption on ns-TiO_x surfaces with various nanoscale parameters using the methodological approach developed in our laboratory, as elucidated in the "Materials and Methods" chapter, namely, the protein-surface interaction microarrays (PSIM) combined with the fluorescence photobleaching quantification (FPQ). We then applied fluorescence recovery after photobleaching (FRAP) for the assessment of the adsorption kinetics that served as an estimate of trypsin binding stability on ns-TiO_x and enabled us to draw conclusions about its role

in the enzymatic activity of immobilized trypsin. In the course of the study, the protein-surface interaction microarrays (PSIM) method was further developed to function as a high-throughput activity assay for adsorbed enzymes in parallel with its feasibility of adsorption assessment. In this manner, the enzymatic activity of trypsin was measured simultaneously with the amount of adsorbed trypsin on a panel of ns-TiO_x within a single experiment, thus, allowing for a direct linkage between the activity and the adsorption of the immobilized enzyme.

In this chapter of "Results and Discussion", we represent:

1) the analysis of trypsin adsorption that will be referred to particular nanoscale parameters of the ns-TiO_x surfaces;

2) the findings on the activity of physisorbed trypsin which will be interpreted in the light of trypsin adsorption phenomena.

3.1. Trypsin physisorption characteristics on ns-TiO_x

3.1.1. Nanostructured titania films as supports for trypsin adsorption

The supersonic cluster beam deposition method (SCBD) was used for the growth of nanostructured (ns) films benefiting from its outstanding feasibility of controlled variation of nanoscale topography retaining constant the chemical properties of the surface. Titanium oxide films were chosen based on the earlier findings of our group demonstrating their excellent biocompatibility and high protein loading capabilities solely by physisorption process (Carbone et al., 2007; Giorgetti et al., 2008). Another important criterion for selecting ns-TiO_x films was their outstanding performance as coatings for protein microarrays resulting from the high protein adsorption and functionality of the adsorbed proteins, as well as from the good reproducibility of the array spots determined by the optimized surface wettability of ns-TiO_x films (Carbone et al., 2009; Giorgetti et al., 2008).

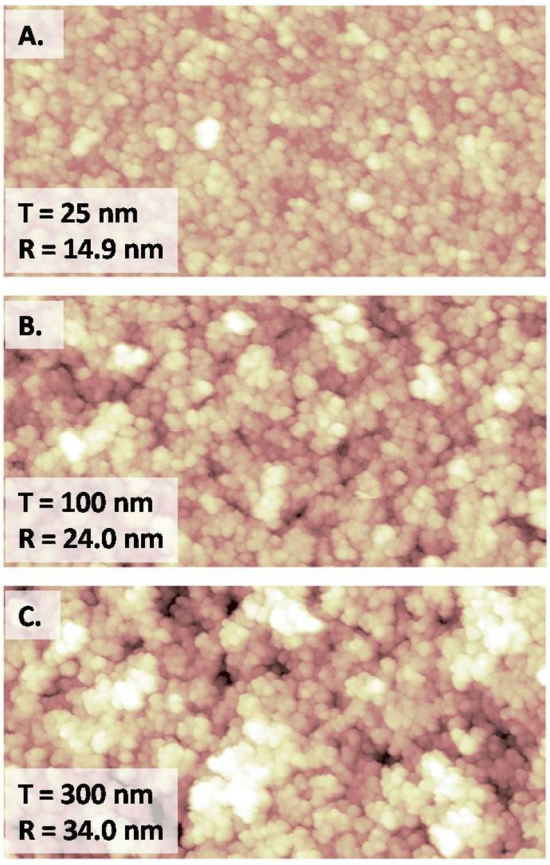

Fig. 3.1.1.1. Representative images of ns-TiO_x surface morphology corresponding to different nominal film thickness in the range from 25 to 300 nm and root-mean-square roughness from 14.9 to 34.0 nm, as determined by AFM: A) thickness 25 nm and roughness of 14.9 nm; B) thickness 100 nm and roughness 24.0 nm; C) thickness 300 nm and roughness 34.0 nm. Image dimensions from (A) to (C) are: 2000 nm × 1000 nm × 160 nm.

With our methodology, wettability was tailored by the deposition procedure on one hand, which enabled the fine-tuning of the water contact angle and by the post-deposition thermal treatment on the other hand, which switched between hydrophilic and hydrophobic regimes (Podesta et al., 2009).

As explained in details in the "Introduction" chapter, ns-TiO_x films possess randomly-rough nanostructured surfaces whereby such film parameters as thickness, roughness and specific area can be arbitrarily varied and are uniquely linked with each other. The results of ns-TiO_x surface morphology evaluation obtained by AFM are displayed in Fig. 3.1.1.1. and Fig. 3.1.1.2., showing representative images of ns-TiO_x films with three different nanoscale topographies (Fig. 3.1.1.1.), as well as the relation between the nanometre-scale morphology parameters – root-mean-square roughness, specific area and the nominal film thickness. As seen from the graph in Fig. 3.1.1.2., roughness and specific area obey the same trend as functions of the nominal thickness with a slight variation at low thickness values. These results were further used for the analysis of trypsin adsorption dependence on ns-TiO_x nanometre-scale morphology.

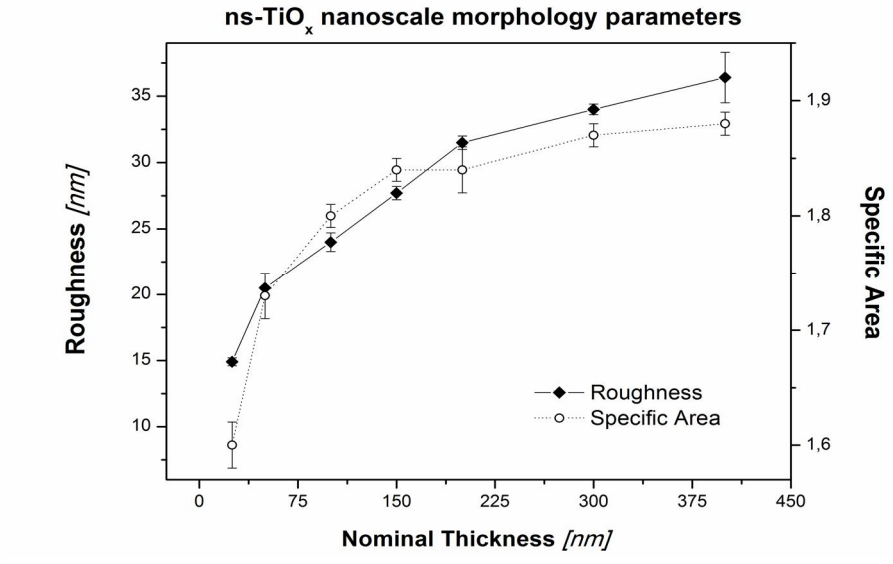

Fig. 3.1.1.2. Relation between the three key-parameters of ns-TiO_x nanoscale morphology. Root-mean-square roughness (filled diamonds) and the specific area (empty circles) versus the nominal thickness of the deposited films. Symbols represent data points± standard deviation bars of three samples.

3.1.2. Optimization of the fluorescent labelling of trypsin

The main three methods chosen in this work - FRAP, FPQ and PSIM – are based on the detection of fluorescence signals and hence, involve the usage of fluorescently labelled molecules. Thus, fluorophores were covalently linked to trypsin prior to its use for the adsorption and activity studies, following general protocols for primary amine-reactive dyes adapted for trypsin (see chapter "Materials and Methods"). In the initial attempts, fluorescein isothiocyanate (FITC) was used to label trypsin giving FITC trypsin conjugates with the excitation peak centred around 495 nm and emission peak around 521 nm. The FITC-trypsin conjugates however, exhibited a remarkable acquisition photobleaching in the course of FRAP measurements with a high acquisition rate (one image every 3 to 15 seconds). Fig. 3.1.2.1. illustrates the photobleaching of the adsorbed FITC-trypsin layer caused purely by the laser exposure during acquisition raster scanning with an acquisition rate of one image every 3 seconds. In this example, as early as 5 minutes of acquisition that corresponds to 100 images yielded 74 % signal impairment of the layer fluorescence and 7 % reduction in the solution fluorescence, whereby the contrast between the layer and solution was diminished by a factor of 3.5 (the detected solution fluorescence was less affected by photobleaching thanks to the molecule mobility in the solution). FRAP settings were varied to minimize the acquisition photobleaching by decreasing the laser power and acquisition rate while maximizing the contrast between the layer and solution fluorescence by increasing the detector gain. However, the imaging conditions that were required for a reasonable recovery curve (minimum initial acquisition rate of one image every 30 seconds) and the laser and detector settings that provided a satisfying contrast still resulted in detectable photobleaching of the layer during acquisition.

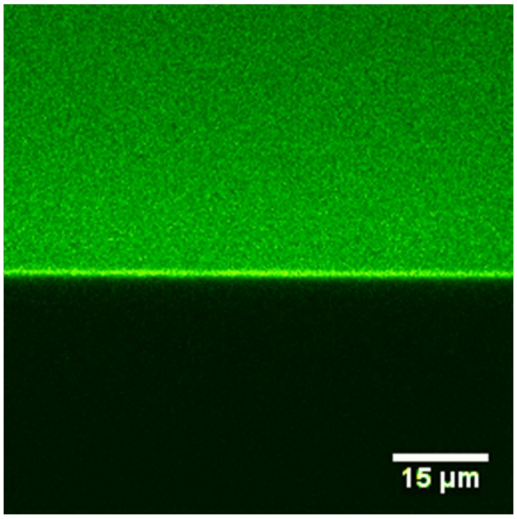

A.
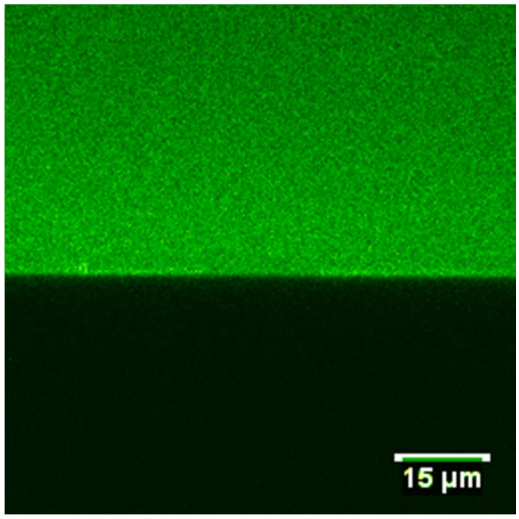

B.

Fig. 3.1.2.1. Acquisition photobleaching of FITC-trypsin conjugate fluorescence: XZ-plane is demonstrated with 5 µM solution of FITC-trypsin in PBS with 20 mM $CaCl_2$, pH8 above 21 nm rough ns-TiO_x surface, and the adsorbed FITC-trypsin layer (A) before bleaching and (B) the adsorbed layer has been remarkably photobleached already after 5 minutes of acquisition with a rate of one image every 3 seconds during a FRAP measurement. Scale bars 15 µm.

Therefore two other amine-reactive dyes were tested which showed no detectable acquisition photobleaching: Alexa Fluor 555 (555nm excitation; 565nm emission) and Alexa Fluor 647 (650nm excitation; 665nm emission). These more photostable dyes were selected to match the CY3 and CY5 excitation and emission channels conventionally used in microarray reading, including our setup for the PSIM method. We introduced a routine protocol for trypsin labelling with the Alexa dyes, described in the "Materials and Methods" chapter.

After fluorescent labelling of trypsin, we tested whether the label had any influence on the adsorption behaviour of trypsin. In order to ascertain that, we performed series of FPQ measurements quantifying the adsorbed amount of trypsin onto ns-TiO_x surface, thereby equal initial concentration of trypsin solution (10 µM) was used in each series of measurements, whereas the ratio of labelled versus non-labelled trypsin in the solution was varied, as follows: 100 %, i.e., only labelled trypsin, as well as solutions of 80 %, 60 %, 40 % and 20 % proportion of labelled to non-labelled trypsin.

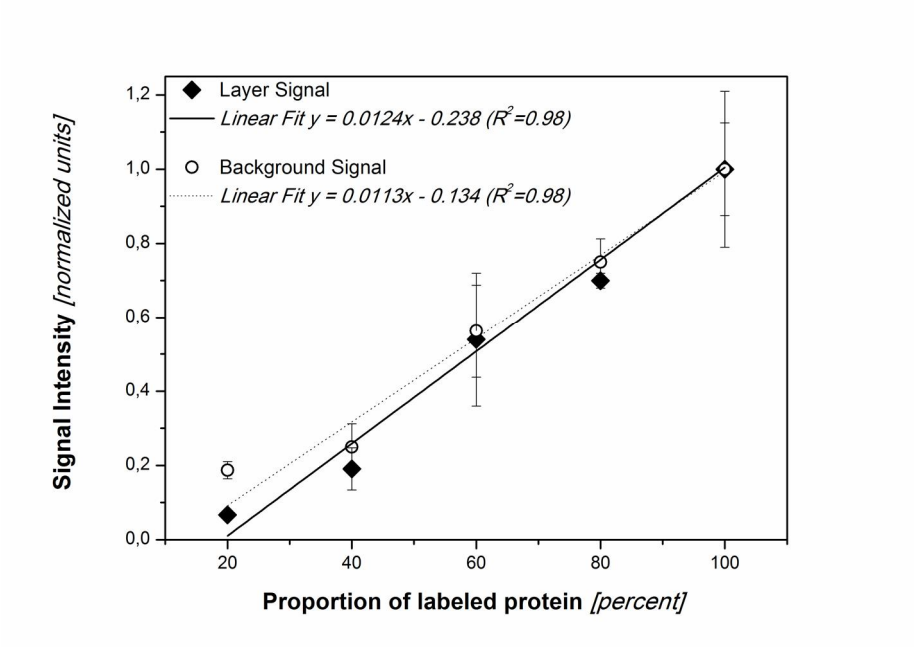

Fig. 3.1.2.2. Fluorophore influence on trypsin adsorption. Both, the fluorescence signal of the adsorbed trypsin layer and fluorescence signal from free trypsin in solution, showed a linear dependence on the percentage of the labelled trypsin, confirming that the fluorescent labelling does not perturb the adsorption behaviour of trypsin. Linearity test was performed on 21 nm rough ns-TiO_x samples with the initial bulk concentration 10 µM; error bars show the standard error (n=3).

The measured fluorescence signals of both, the adsorbed trypsin layer and the trypsin solution (termed "Background") were normalized against the transmission signal of the corresponding image for the correction of possible variations in laser power; the obtained results were then plotted versus the percentage of labelled trypsin, setting the values to 1 at 100 % (Fig. 3.1.2.2.).

Both, layer and background signals grew linearly with the percentage of labelled trypsin within the margins of the standard deviation, as expected in the case if the influence of the fluorescent label on trypsin adsorption can be neglected. It was noticed that the standard variation of the three replicates reached relatively high values in some cases, i.e., relative error reached from 8 to 33 %; the validity of the linear trends was however not doubted, since the results were always reproducible during the course of further experiments with varying ratios of

labelled versus non-labelled trypsin.

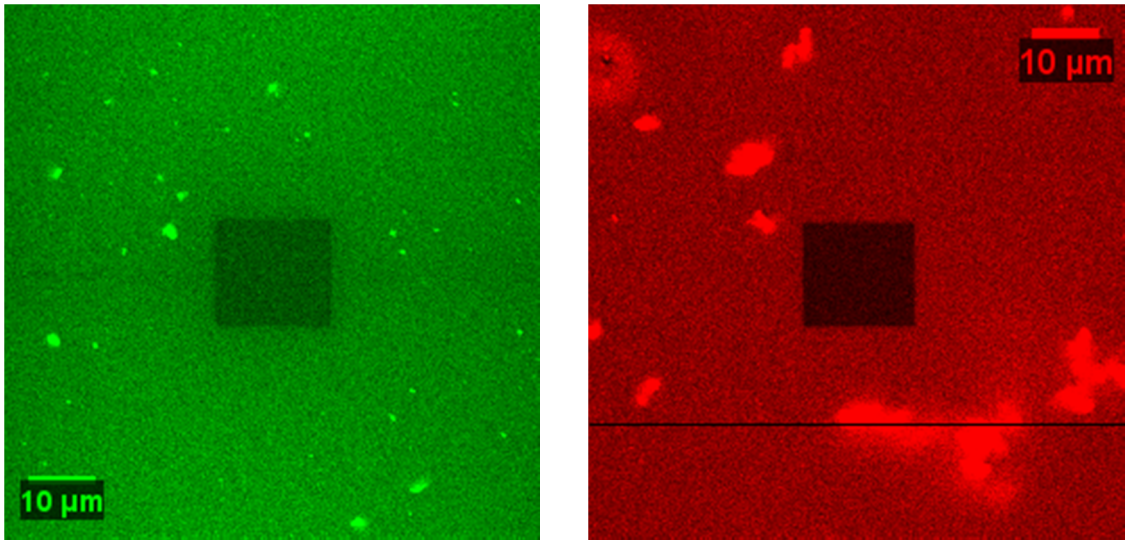

A. B.

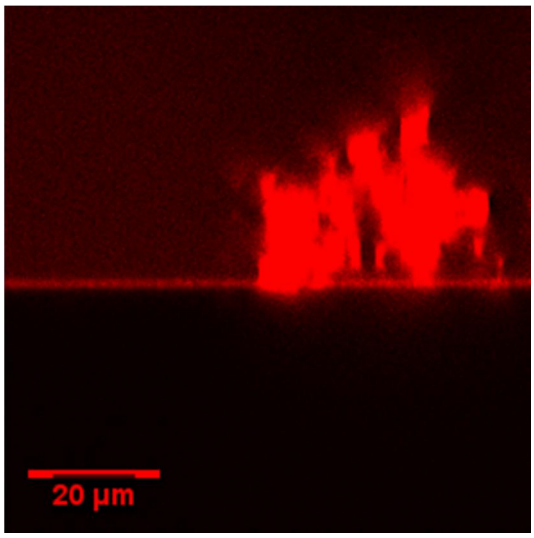

C.

Fig. 3.1.2.3. Aggregation of fluorescent trypsin conjugates: protein clusters of various sizes were observed on a part of samples which underwent a prolonged incubation at room temperature. The aggregates are shown in the vicinity of the square-shaped 15 µm x 15 µm bleached regions. Scale bars correspond to 10 µm. A) 5 µM solution of FITC-trypsin in PBS with 20 mM $CaCl_2$, pH8 after 60 min incubation on 50 nm ns-TiO_x surface at room temperature. B) 5 µM solution of Alexa555-trypsin in TBS-$CaCl_2$ buffer, pH8 after 165 min incubation on 21 nm rough ns-TiO_x surface at room temperature. C) Cross-section of the field of view of image B) along the black line at 190 min incubation time (scale bar 20 µm).

In the course of the confocal studies, we encountered a phenomenon linked to the preparation of fluorescently-labelled trypsin aliquots. As soon as during the first tests with the FPQ method, clusters of irregular micron-sized fluorescent particles were observed on ns-TiO_x surface after 1 to 3 hours incubation time of trypsin solution on ns-TiO_x, as evident from the images in (Fig. 3.1.2.3.). The examples displayed in Fig. 3.1.2.3. are representatives of the timescale and dimensions of cluster formation, however they do not account for any possible differences between trypsin conjugated either with FITC or Alexa555 dye. The aggregates of FITC-trypsin, visible in Fig. 3.1.2.3. A., appeared approximately after one hour of sample imaging at room temperature, whereas Alexa555-trypsin clusters in Fig. 3.1.2.3. B. and C. were first observed after two hours of sample incubation at room temperature. After their first appearance, the size of the clusters grew rapidly reaching tens of microns within 30 minutes.

After a careful control of the ns-TiO_x specimens, it was excluded that the particles would originate from contaminants on the ns-TiO_x surfaces, moreover it was clarified that the particles are of trypsin origin since they exhibited fluorescence excitation and emission peaks matching those of the fluorophores used for trypsin labelling; no autofluorescence was detected as it would be in the case of dust particles. Furthermore, we excluded the possibility that the aggregation was initiated by the nanostructured surface itself, since in two cases the aggregates were observed in the bulk of trypsin solution immediately after the deposition of the solution on top of ns-TiO_x surface. Hence, ns-TiOx surface could not cause the appearance of large detached trypsin aggregates within a minute in few cases, while not inducing aggregation in other cases. A more systematic and detailed analysis of trypsin aggregate formation was not possible since the results were irreproducible with our set of methods, namely, the clusters appeared at various timescales within the range of 1.5 to 3 hours incubation time, while at other times, no cluster formation occurred even after 3 hours of incubation at room temperature. Thus, we assumed that the aggregate formation was triggered by certain factors which were difficult or impossible to control

in our experimental setup, i.e., variations in temperature and pH during trypsin sample preparation and labelling, variability in the handling times of the trypsin samples, variations in freezing and thawing rates of the labelled trypsin aliquots, etc. Despite of the irreproducibility, we intended to determine which step of trypsin preparation could have initiated the aggregation.

First, we reasoned that, most probably, the aggregates could have formed as a consequence of trypsin denaturation during the preparation of trypsin aliquots. The growth of the size and the number of the aggregates with time, could be explained with the presence of single denatured molecules or even small clusters (i.e., not detectable by confocal microscopy) of denatured trypsin that formed bigger (detectable) clusters in the course of the confocal measurements due to protein-protein interactions, presumably, hydrophobic interactions resulting from the exposure of hydrophobic residues of the denatured molecules. Ns-TiO_x surface could play a role in promoting the growth of the clusters either by further denaturation of trypsin upon adsorption and/or by the proximity of adsorbed molecules that were denatured prior to adsorption.

Further, we wanted to clarify the reasons underlying trypsin denaturation before adsorption on ns-TiO_x. In particular, three handling steps could have facilitated the denaturation of a detectable fraction of trypsin: i) the labelling reaction, ii) and iii) the freeze-drying and the rehydration of the labelled aliquots.

One particular property to be taken into account was the autoproteolytic activity of trypsin, which results in a fraction of “self-digested” molecules having a non-native or even denatured conformation and consequently entering a non-active state. In any conditions when trypsin molecules are in an active state and close proximity to neighbour trypsin molecules – the magnitude of this deactivated molecule fraction rises as a function of time, the exact shape of the function being influenced by multiple factors, such as trypsin concentration, buffer contents, pH and temperature (Dallas Johnson et al., 2002; Sriram et al., 1996) and therefore turning it difficult to control the absolute amount of the deactivated molecules within a probe solution. The

autoproteolytic activity of trypsin during the labelling reaction could have created a population of denatured molecules owing to the one hour long incubation time of the reaction solution at pH 8 and room temperature – conditions that ensure an optimal catalytic activity of trypsin and as a side effect – the self-digestion.

The freeze-drying or the rehydration of the labelled aliquots could have denatured a fraction of the labelled trypsin even without the contribution of autoproteolysis due to local jumps of pH and temperature. Another possibility of trypsin aggregate formation was during the freeze-drying process during which small aliquots of labelled trypsin were freeze-dried inside 50 µl PCR tubes. Trypsin molecules located at the liquid-air interfaces could have formed aggregates due to protein-protein interactions upon the expansion of the freezing water at the interface, a phenomenon that has been reported previously in the context of aggregation of proteins adsorbed on hydrophobic surfaces in the course of lyophilisation (Wälivaara et al., 1995).

We were not able to estimate the quantitative amount of the denatured population that could have resulted from trypsin self-digestion. However, we tested a batch of labelled trypsin produced without the freeze-drying step, but instead using a rapid freezing of 10 µl aliquots in liquid nitrogen in order to minimize the denaturation caused by freezing process, as suggested in literature (Deng et al., 2004). Aggregate formation was encountered in few cases during the confocal measurements using the mentioned batch of trypsin. The freeze-drying procedure was omitted from our protocols; however we decided to apply the rapid freezing in nitrogen, primarily aimed at long-term storage of the prepared aliquots. Moreover, due to the irreproducibility of the results related to trypsin aggregation, all data measured on the specimens where cluster formation occurred, were discarded. Taking into account the possibility of self-digestion during the labelling reaction, we decided to use a solution consisting of a minor fraction (4 - 10 %) of labelled trypsin mixed with a high fraction of freshly prepared non-labelled trypsin of known proportions, with the goal to minimize the contribution of the non-quantifiable denatured population of trypsin. Subsequently, the adsorption behaviour was attributed solely to the native

non-denatured population of trypsin, since the results of the FPQ, FRAP and PSIM experiments where no aggregation was observed, demonstrated a reasonable reproducibility. The usage of a mixture of labelled and non-labelled trypsin at an arbitrary ratio gave also the possibility of using a broader trypsin concentration range by adjusting the ratio of labelled molecules to match the optimal dynamic range of the FPQ method, which was limited by the contrast between the trypsin layer and the solution signals in the bleached image (more details in the section 2.2.2. on Fluorescence Photobleaching Quantification in the "Materials and Methods" chapter).

3.1.3. Assessment of trypsin adsorption by Langmuir and Hill models

PSIM data obtained at a wide range of trypsin bulk concentrations applied onto ns-TiO_x surfaces with six different nanoscale topographies were plugged in the Langmuir adsorption model which relates the surface coverage Γ of adsorbent occupied by adsorbate molecules with the bulk concentration of the adsorbate, C:

$$\Gamma = \frac{SU_L}{1 + \frac{k_{DL}}{C}}$$

where SU and k_D are the two parameters of a typical Langmuir adsorption isotherm, while letter "L" in lowercase denotes the Langmuir model. The saturation uptake SU signifies the maximum loading capacity of the adsorbent surface with the adsorbate molecules, while the equilibrium dissociation constant k_D is inversely proportional to the effective affinity between the adsorbate and the adsorbent surface, both parameters in this case being influenced by the physiochemical properties of trypsin and ns-TiO_x but additionally, by the topographical properties of the nanostructured surfaces. Besides the geometrical restrictions of a flat surface, the Langmuir model considers only one interaction between the adsorbate and the adsorbent. In order not to exclude the probability of more than one type of interaction between trypsin molecules and ns-TiO_x surface and/or interaction between trypsin molecules, Hill plot was used to model the adsorption isotherms in comparison with Langmuir approximation. Hill model introduces the Hill coefficient n to account for additional interactions:

$$\Gamma = \frac{SU_H}{1 + \frac{k_{DH}}{C^n}}$$

where letter "H" in lowercase stands for Hill model as opposed to Langmuir model. In case the Hill coefficient n >1, adsorption is described as cooperative indicating the presence of extra attractive interactions, namely attractive protein-protein interactions. Instead, n < 1 signifies non-cooperative adsorption via the presence of repulsive potential either between the adsorbent and protein molecules in case of multiple binding sites, or repulsive protein-protein interaction. In case n = 1, Hill plot is reduced to Langmuir model accounting for only one type of interaction between proteins and the adsorbent surface.

We compared the fitting of experiment data with Hill model versus Langmuir model as a special case of Hill model with the coefficient n set to 1. The results were summarized in Table 3.1.3.1., where each ns-TiO_x film surface was marked by its nominal thickness and root-mean-square roughness (rms), and listed with the corresponding Hill coefficients n and goodness of fit values R^2. Interestingly, both, Langmuir model and Hill model yielded fairly good approximations with minor differences: the R^2 values of Langmuir fit slightly exceeded the respective R^2 values of Hill fit at the two lowest roughness ns-TiO_x samples, whereas on all other ns-TiO_x samples, Hill model gave a slightly higher goodness of fit. Furthermore, for the two lowest roughness values, i.e., 14.9 and 20.5 nm, the value of Hill coefficient was n=0.9±0.2 and n=1.1±0.2, respectively, thus including the special case of Langmuir model within the boundaries of the standard error. For all the roughness values above 20.5 nm however, the value of Hill coefficient was significantly higher than the Langmuir case n=1, a finding to which we will return in the chapter 1.5. Due to the close matching of the goodness of fits for both models, it was decided to include both cases in the further analysis, also considering the interpretation of the values of Hill coefficient. The ns-TiO_x samples of 20.5 nm roughness (50 nm nominal thickness) demonstrated an equally good agreement with Hill and Langmuir models and were chosen for the quantification of the microarray experiments. In the further work, samples will be labelled according to their rounded roughness values, as 15 nm ns-TiO_x; 21 nm ns-TiO_x and so on.

Morphology			Langmuir $n_L=1$	Hill	
Nominal Thickness nm	Specific Area	Roughness nm	R_L^2	n_H	R_H^2
25	1.60 ± 0.02	14.9 ± 0.3	0.908*	0.9 ± 0.2	0.907
50	1.73 ± 0.02	20.5 ± 0.1	0.858*	1.1 ± 0.2	0.853
100	1.80 ± 0.01	24.0 ± 0.7	0.964	1.53 ± 0.08	0.987*
150	1.84 ± 0.01	27.7 ± 0.5	0.984	1.39 ± 0.07	0.997*
200	1.84 ± 0.02	31.5 ± 0.5	0.954	1.4 ± 0.1	0.964*
300	1.87 ± 0.01	34.0 ± 0.4	0.980	1.35 ± 0.08	0.987*

Table 3.1.3.1. Comparison of Langmuir versus Hill approximations of trypsin adsorption isotherms on ns-TiO_x surfaces. Ns-TiO_x morphology parameters were characterized by AFM giving the root-mean-sqare roughness values ± standard deviations at each nominal film thickness, as well as the calculated specific area. Hill coefficient n_H was estimated by fitting PSIM data with Hill model, whereas n was set to n=1 for fitting with the Langmuir adsorption model. Standard errors for n_H, as well as the goodness of fit R^2 values were listed for the evaluation of the two models.

3.1.4. Quantification of surface-bound trypsin

In order to understand the physisorption behaviour of trypsin onto ns-TiO_x surfaces, the amount of adsorbed trypsin was assessed quantitatively using Fluorescence photobleaching quantification (FPQ) approach developed in our laboratory (see chapter "Materials and Methods").

Systematic FPQ measurements were performed in the low concentration range corresponding to the initial quasi-linear part of Langmuir adsorption isotherm on ns-TiO_x samples of 20.5 nm roughness – this FPQ data set was used for the calibration of the high-throughput semi-quantitative adsorption data obtained by PSIM methodology that yielded the whole isotherm up to the saturation plateau. The calibration procedure was based upon the fact that the initial portion of the adsorption isotherm was in good agreement with a linear function giving the slope of the isotherm. Fig. 3.1.4.1. illustrates the steps of calibration using Langmuir approximation of PSIM experiment, an equivalent procedure was applied using Hill approximation. However, the slope of isotherm obtained from Langmuir fit was selected for the

calibration of all the other samples, due to the fact that Langmuir model gave more relevant values at the isotherm plateau where the Hill plot continued to grow at a higher rate (Fig. 3.1.4.1. A.). In the following way, PSIM experiment data were fitted with a standard Langmuir (or Hill) adsorption curve where each isotherm was obtained from the results of five independent experiments (Fig. 3.1.4.1. A.). The low range (up to 5.5 µM concentration) of trypsin adsorption curve on rms = 20.5 ns-TiO_x surface was then approximated with a linear function (Fig. 3.1.4.1. B.) having its slope and intercept expressed in relative fluorescence units versus concentration. Correspondingly, FPQ experiments obtained at five trypsin solution concentrations: 1.6; 4; 6; 8 and 10 µM, were plotted against concentration and approximated with a linear function up to the 6 µM concentration margin. The initial slope of the whole adsorption isotherm determined by PSIM was then directly translated into the absolute density units and the relative coverage units known from the slope of FPQ experiment. The experiment data of both, PSIM and FPQ were plotted in absolute units along with the corresponding fitted functions, as displayed in the graph (Fig. 3.1.4.1. C.). This calibration curve was subsequently adapted for the quantification of all the microarray-based experiment data on all the sampled ns-TiO_x surfaces. In Fig. 3.1.4.1. D., the isotherm is calibrated according to Langmuir fit, as well as Hill fit, revealing that the higher the concentration, the more significant is the discrepancy between both models. It was then concluded that the chosen calibration method, i.e., usage of the initial slope, is prone to errors at the isotherm plateau, thus impairing the accuracy of the quantitative estimate of protein density. More accurate approach of calibration would have been the usage of ratio of isotherm plateau values of two different ns-TiO_x samples, as suggested already by Scopelliti et al. (Scopelliti et al., 2010), hence avoiding the isotherm fitting step and the need to rely on mathematical approximations. Unfortunately, the suggested approach was not applied within the current study, limiting its quantitative validity to the boundaries of the standard errors of mathematical fitting. Instead, the further analysis was focused rather on the comparison of both, Langmuir and Hill models and their consequences for trypsin adsorption on ns-TiO_x surfaces.

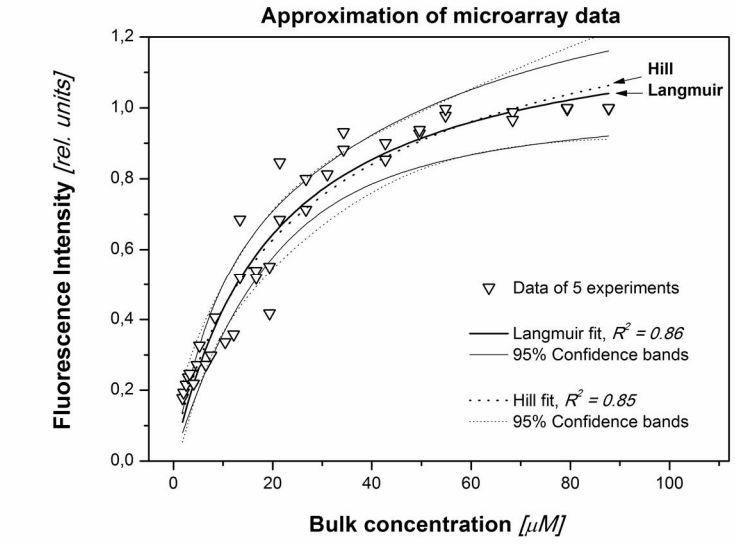
Approximation of microarray data
Fluorescence Intensity [rel. units]
Bulk concentration [μM]
Hill
Langmuir
Data of 5 experiments
Langmuir fit, R² = 0.86
95% Confidence bands
Hill fit, R² = 0.85
95% Confidence bands

A.

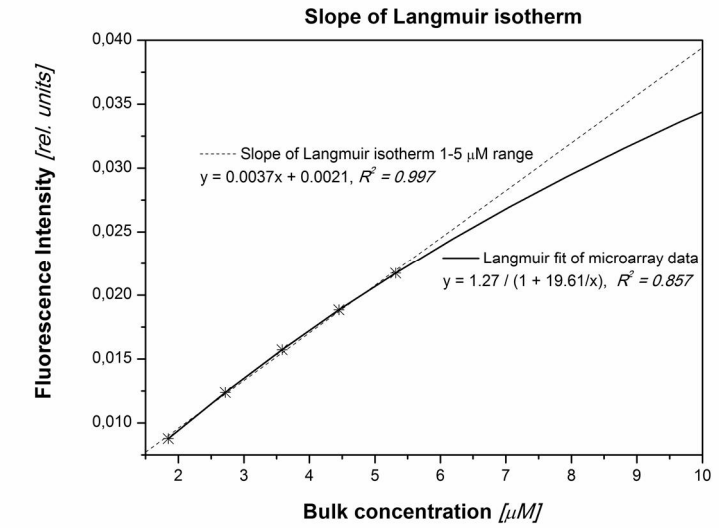
Slope of Langmuir isotherm
Fluorescence Intensity [rel. units]
Bulk concentration [μM]
Slope of Langmuir isotherm 1-5 μM range
y = 0.0037x + 0.0021, R² = 0.997
Langmuir fit of microarray data
y = 1.27 / (1 + 19.61/x), R² = 0.857

B.

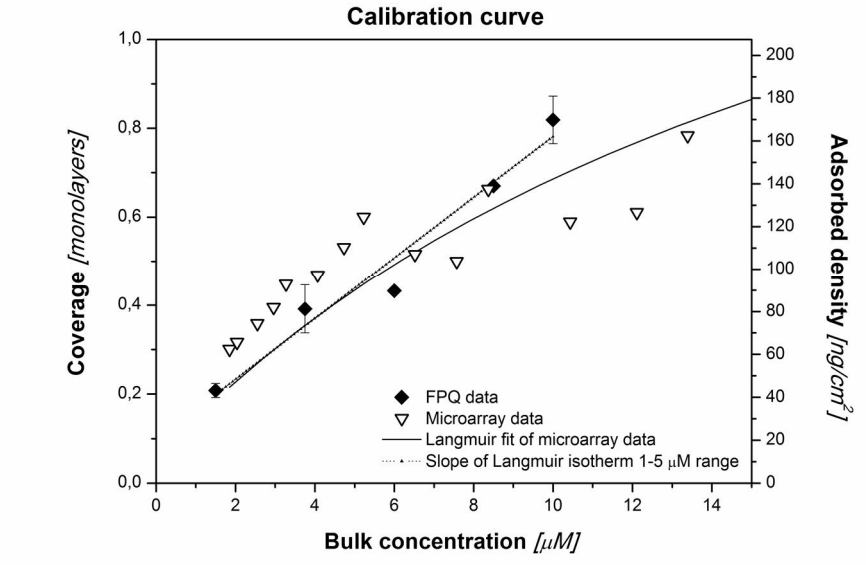
Calibration curve
Coverage [monolayers]
Adsorbed density [ng/cm²]
Bulk concentration [μM]
FPQ data
Microarray data
Langmuir fit of microarray data
Slope of Langmuir isotherm 1-5 μM range

C.

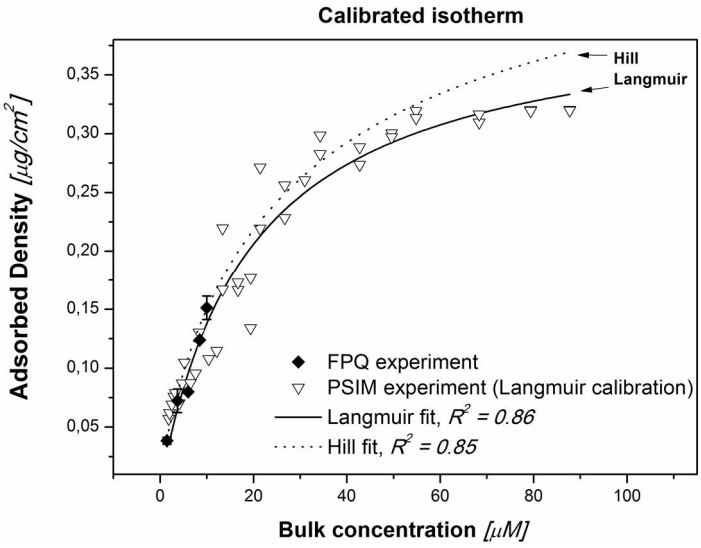

D.

Fig. 3.1.4.1. Langmuir and Hill approximation of microarray data

A) Langmuir and Hill approximations of microarray data obtained in five independent PSIM experiments performed on 21 nm rough ns-TiO_x surfaces. Experiment data (empty triangles) were plotted in relative fluorescence units and fitted with the Langmuir curve (solid line) in the form $y = SU / (1+k_D/x)$, as well as with the Hill curve (dotted line) $y = SU / (1 + k_D/ x^n)$ with the resulting R^2 values 0.857 and 0.854, respectively. 95 % confidence bands were shown as thin lines.

B) Slope of Langmuir isotherm in relative units was determined by fitting the isotherm with a linear function in the range of 1 to 5.5 µM. Langmuir curve (solid line) displayed with its linear approximation (dotted line) $y = 0.0037x + 0.0021$ ($R^2 = 0.997$). The five data points used for fitting were marked with stars.

C) Calibration curve of the Protein-Surface Interaction Microarray method by Fluorescence Photobleaching Quantification: the values of three FPQ experiments up to 6 µM concentration were fitted with a linear function giving the initial slope of the adsorption isotherm in absolute surface density units [ng/cm^2], thus endowing a quantitative meaning to the PSIM measurements. In the graph, FPQ (filled diamonds) and PSIM (empty triangles) experiment data shown with the Langmuir isotherm (solid line) and its initial slope (dotted line).

D) Isotherm calibration using Langmuir versus Hill fitting. FPQ experiment data ± standard error bars (filled diamonds) shown with data of five PSIM experiments (empty triangles) which were calibrated against the Langmuir isotherm (solid line), the Hill isotherm (dotted line) was plotted to demonstrate the difference in calibration between the two models.

3.1.5. High-throughput assessment of trypsin adsorption by PSIM

The high-throughput approach of PSIM method enabled us to sample our ns-TiO_x library obtaining complete trypsin adsorption isotherms up to the plateau within a single experiment. Films of ns-TiO_x were deposited on glass slides in a pattern of six adjacent zones with six different stochastically rough morphologies and identical surface chemistry. Nanostructured morphology gradient was probed with 10 × 10 patterns of trypsin concentration gradients in the range from 0.5 to 175 μM (Fig. 3.1.5.1.). The entire data set was then calibrated as described in the previous chapter, to provide a quantitative estimate of adsorption and thus explore the impact of nanometre-scale roughness on trypsin interaction with ns-TiOx.

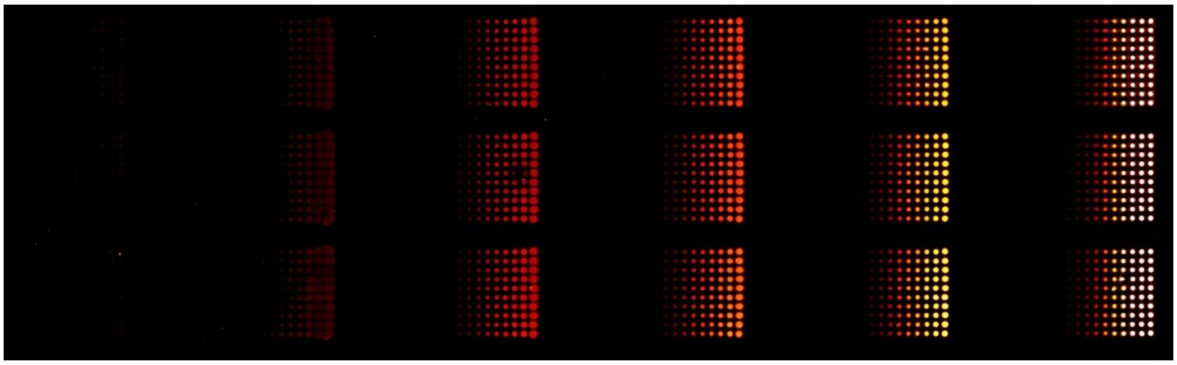

Fig. 3.1.5.1. High-throughput characterization of trypsin adsorption on a panel of nanostructured titanium oxide films. Scanned image of a typical microarray slide with the ns-TiO_x deposited in a step-wise gradient of increasing film thickness and roughness (from left to right), probed with trypsin gradients of increasing arrayed concentration (from left to right).

PSIM experiment results corresponding to all six different ns-TiO_x surfaces were plotted in the same graph with the fitted adsorption isotherms (Fig. 3.1.5.2.) to facilitate the comparison of trypsin density and relative coverage on various ns-TiO_x specimens. For the sake of clarity, only Langmuir fits were shown in Fig. 3.1.5.2., including the cases when Hill fits yielded higher R^2 values. First of all, from the PSIM experiment it was evident that within the nearly three orders of magnitude wide concentration range of trypsin, the adsorbed amount grew rapidly, the growth

rate notably increasing with the roughness of ns-TiO_x films. This qualitative trend was further inspected by isotherm approximation, the results of which were summarized in Table 3.1.5.1.

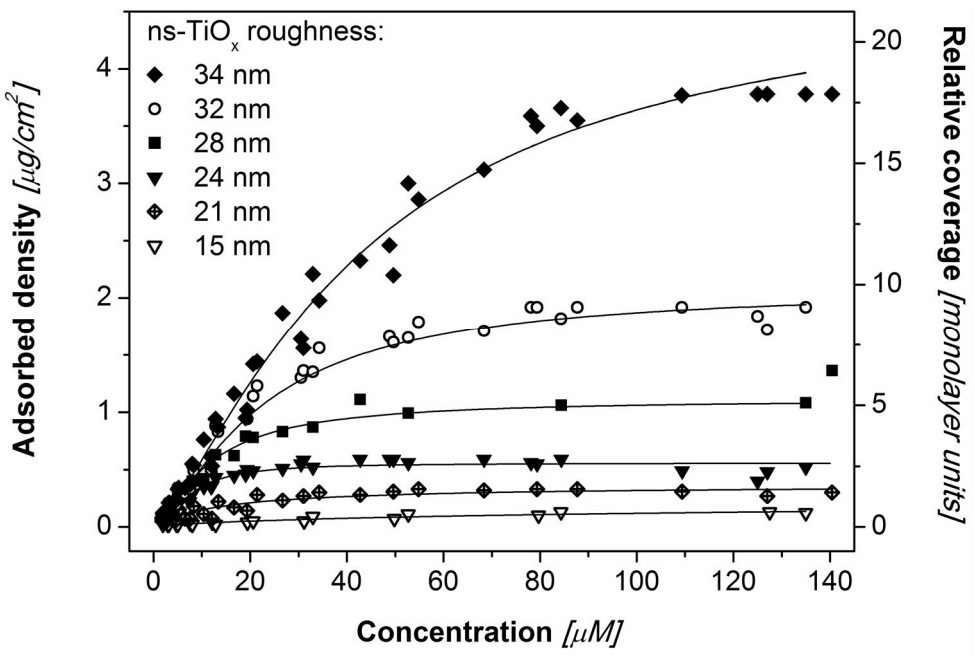

Fig. 3.1.5.2. Trypsin adsorption isotherms on ns-TiO_x surfaces of various roughness. Within each single PSIM experiment, trypsin adsorption was assessed on ns-TiO_x of six different nanotopographies and with the trypsin concentration range covering more than two orders of magnitude. Data points of PSIM experiments were marked with symbols (given in brackets), while the corresponding Langmuir fits were drawn as solid lines. The sampled ns-TiO_x roughness values were: 15 nm (empty triangles); 21 nm (crossed diamonds); 24 nm (filled triangles); 28 nm (filled squares); 32 nm (empty circles) and 34 nm (filled diamonds). All data were calibrated in both, surface density units [μg/cm^2] and coverage units [monolayers], and normalized by the specific area typical for each ns-TiO_x surface.

A rise of the saturation uptake by a factor of twenty corresponded to a minor two-fold increase in roughness, while the specific area increased only 1.2 times, as concluded from the comparison of ns-TiO_x samples with the highest and the lowest morphology parameters in Table 3.1.5.1. Furthermore, the upper limit of the relative coverage by far exceeded the monolayer adsorption regime for the rougher and thicker ns-TiO_x films having a roughness of more than 24 nm (SA > 1.8 and thickness > 100 nm), as seen from Fig. 3.1.5.2. The relative coverage was

calculated to give a rough idea of the "grade of exceeding" the monolayer regime. Protein density of one full monolayer was estimated by applying a RSA model for non-interacting prolate spheroids which for trypsin gives the weighted mean jamming limit of 0.69. Noteworthy, even applying the jamming limit of a hexagonal close packed monolayer, namely 0.91, the relative coverage values reach up to 13 monolayers on the highest roughness ns-TiO_x surface. Moreover, this total number of monolayers describes the adsorbed protein density normalized by the specific area, thus taking into consideration the additional geometric area typical of the nanostructured surfaces.

Much controversy can be found in literature regarding the influence of surface nanotopography on the amount of adsorbed proteins: in some studies, no differences have been found comparing smooth and nanorough surfaces (Cai et al., 2006; Denis et al., 2002; Han et al., 2003), in most cases however, augmentation of protein adsorption induced by nanostructures has been reported (Blanco et al., 2008; Dolatshahi-Pirouz et al., 2009; Khang et al., 2007; Muller et al., 2001; Rechendorff et al., 2006; Riedel et al., 2001; Salakhutdinov et al., 2008; Sousa et al., 2007). Moreover, a trend of increasing protein adsorption versus roughness has been verified for the root-mean-square roughness value range of approximately 0.5 to 25 nm (Khang et al., 2007; Muller et al., 2001; Riedel et al., 2001; Sousa et al., 2007). This adsorption enhancement has often been ascribed to the additional surface area allocated by the nanostructures and further explained either by the availability of additional adsorption sites (Muller et al., 2001), or by the increase in the total surface energy (Khang et al., 2007). Several authors have found that the increment in protein adsorption substantially outruns the respective increase in the surface area (Dolatshahi-Pirouz et al., 2009; Rechendorff et al., 2006). This observation has been explained by the change of protein conformation induced by surface nanostructures which for particular protein and material combinations can benefit a more tight protein packing and a higher adsorbed amount (Rechendorff et al., 2006), whereas with other proteins, resp., materials, a reverse effect can be achieved (Hovgaard et al., 2008).

Morphology			Langmuir n_L=1			Hill			
Nominal Thickness nm	Specific Area	Roughness nm	SU_L [μg/cm²]	k_{DL} [μM]	R_L^2	SU_H [μg/cm²]	k_{DH} [μM]	n_H	R_H^2
25	1.60 ± 0.02	14.9 ± 0.3	0.18 ± 0.02	56 ± 11	0.908*	0.27 ± 0.21	47 ± 12	0.9 ± 0.2	0.907
50	1.73 ± 0.02	20.5 ± 0.1	0.40 ± 0.04	15 ± 3	0.858*	0.5 ± 0.2	17 ± 7	1.1 ± 0.2	0.853
100	1.80 ± 0.01	24.0 ± 0.7	0.68 ± 0.02	12 ± 1	0.964	0.58 ± 0.01	26 ± 4	1.53 ± 0.08	0.987*
150	1.84 ± 0.01	27.7 ± 0.5	1.20 ± 0.05	15 ± 2	0.984	1.07 ± 0.02	30 ± 4	1.39 ± 0.07	0.997*
200	1.84 ± 0.02	31.5 ± 0.5	2.46 ± 0.12	35 ± 4	0.954	2.01 ± 0.10	76 ± 23	1.4 ± 0.1	0.964*
300	1.87 ± 0.01	34.0 ± 0.4	6.39 ± 0.35	83 ± 8	0.980	4.6 ± 0.2	160 ± 33	1.35 ± 0.08	0.987*

Table 3.1.5.1. Summary of ns-TiO_x morphology parameters and fitting parameters derived from trypsin adsorption isotherms on the respective ns-TiO_x surfaces. ns-TiO_x surface topography was characterized by AFM giving the roughness values ± standard deviations (n=3) at each nominal film thickness, as well as the calculated specific area. Saturation uptake SU, equilibrium dissociation constant k_D and Hill coefficient n, were all determined by the approximation of PSIM experiment data with Langmuir (n set to 1) and Hill adsorption models. Parameters referring to Langmuir fit were labelled with lowercase "L", while those referring to Hill plot – with lowercase "H". Standard errors, as well as the adjacent R-Square values were taken from the fitting results.

It was known from our earlier work that the ns-TiO_x films grown by SCBD method and subjected to post-deposition thermal treatment at 250°C, are hydrophilic (Podesta et al., 2009) therefore assuming an additional surface area available to the proteins in the solution above the surface. In the current study however, the contribution of the surface specific area had already been cancelled out by normalizing the density and coverage units with the specific area of each ns-TiO_x sample. Hence, factors other than the simple increase in the geometric surface area associated with surface nanotopography had to be accounted for. We therefore highlighted the role of root-mean-square roughness in trypsin adsorption by inspecting its effect on the saturation uptake and k_D.

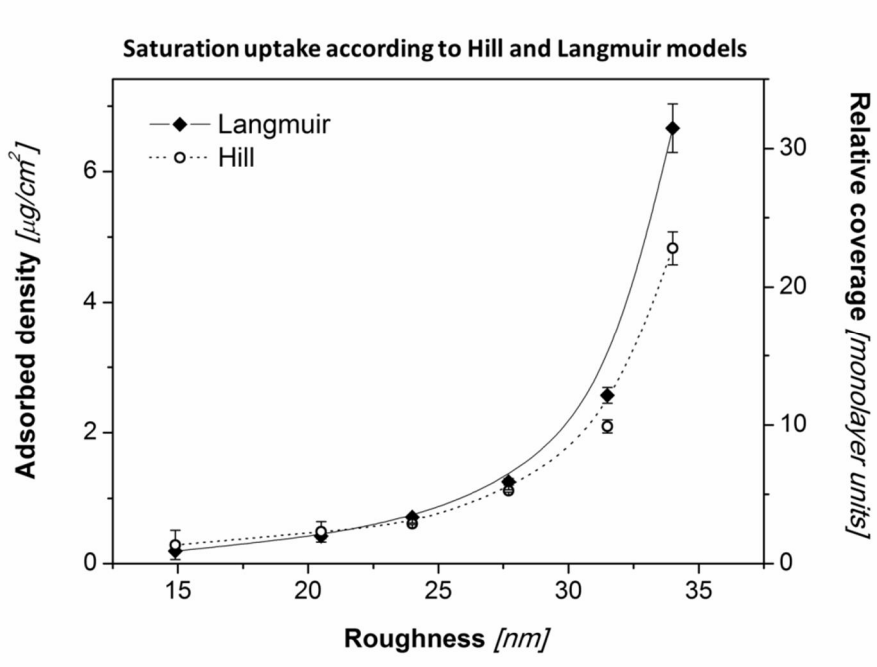

A.

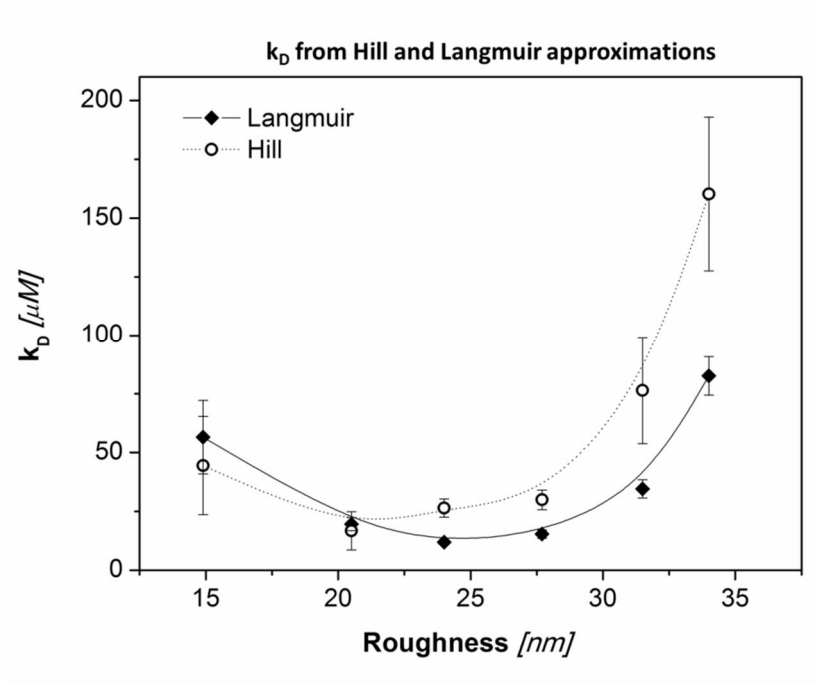

B.

Fig. 3.1.5.3. Dependence of saturation uptake and k_D from ns-TiO_x roughness

A) Dependence of saturation uptake from ns-TiO_x roughness. Values of SU derived from Langmuir (diamonds) and Hill (circles) approximations were calibrated and normalized by the specific area factor of each ns-TiO_x sample. Error bars mark the standard errors obtained by fitting of the data of at least three experiments, lines represent the trends.

B) k_D versus ns-TiO_x roughness. k_D values with standard errors were obtained from Langmuir (diamonds) and Hill (circles) approximations. Lines are drawn for better visualization.

Both, the saturation uptake and the k_D dependence from roughness, demonstrated a close match between Langmuir and Hill models, as evident from the graphs in Fig. 3.1.5.3. For saturation uptake SU, the deviation between the two models exceeded the boundaries of the standard error only for the two highest roughness samples where the Langmuir model tended to overestimate the values of SU (Fig. 3.1.5.3. A.). Both models however, converged in a common trend of saturation uptake growth with roughness. In the sampled roughness range, the following relation was observed: the higher was the ns-TiO_x roughness, the more rapid was the growth of the saturation uptake.

For k_D, both models yielded a function from roughness with a minimum k_D value coinciding with the roughness region from 20 to 25 nm (Fig. 3.1.5.3. B.). The minima of k_D concurred with 21 and 24 nm roughness values according to Hill and Langmuir models, respectively. The appearance of a minimum k_D indicates the corresponding maximum of the equilibrium binding constant k, that qualitatively can be defined as roughness region where the effective trypsin affinity towards ns-TiO_x reaches its peak.

As noted in section 3.1.3., better agreement with the Langmuir model was observed for 15 and 21 nm rough samples, while the Hill model generated higher goodness-of-fit values for all the samples with roughness between 21 and 34 nm. Although both models produced similar qualitative trends of saturation uptake and k_D, we intended to clarify the reasons behind the differences in the quantitative values of SU and k_D estimated by the two models. The key parameter distinguishing the two models is the Hill coefficient n which identifies the Langmuir model as a special case of the Hill plot when n equals 1.

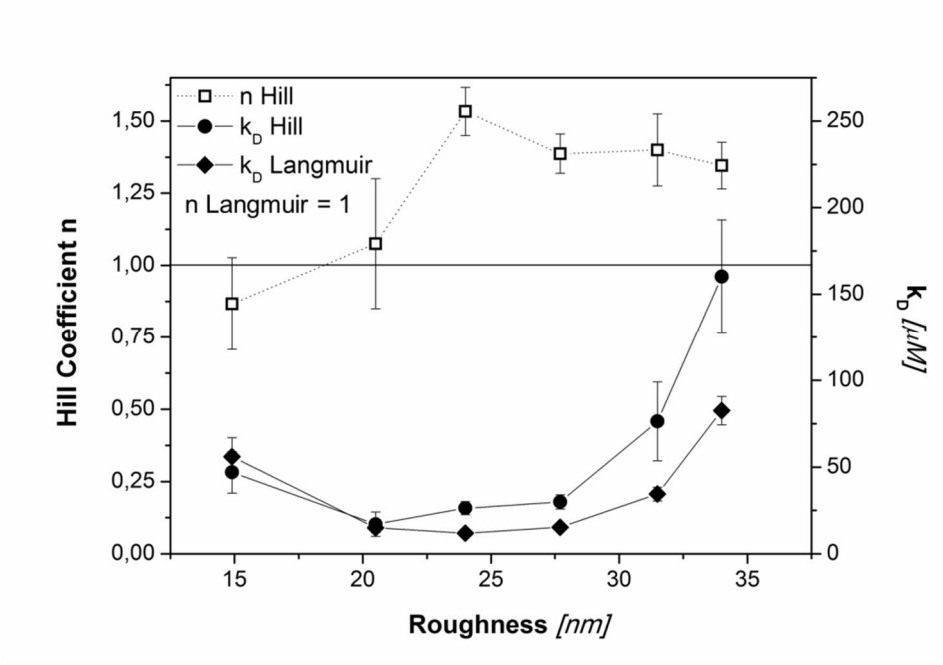

Fig. 3.1.5.4. Dependence of Hill coefficient n from ns-TiO_x roughness. Hill model parameters, Hill coefficient n (empty symbols, squares) and equilibrium dissociation constant k_D (filled symbols, circles and diamonds), were plotted on the primary and on the secondary Y-axis respectively, versus roughness. Hill parameters were determined by fitting trypsin adsorption isotherms to the Hill plot. Langmuir model was represented as the line n = 1.

Accordingly, the situation when n = 1 can be reduced to one type of interaction between protein molecules and the adsorbent surface, whereas n ≠ 1 describes either positive (n > 1) or negative (n < 1) cooperative adsorption requiring a further interpretation of more than one type of interactions present. We followed the evolution of Hill coefficient with roughness in order to determine the influence of roughness on the interactions between trypsin and ns-TiO_x surfaces (Fig. 3.1.5.4.).

Hill coefficient n was plotted versus roughness along with the second parameter of the Hill model – the equilibrium dissociation constant k_D (Fig. 3.1.5.4.), where the values of k_D were marked against the secondary Y-axis. The following relation was found: Hill coefficient was significantly higher than 1 for the samples where Hill fitting resulted in higher R^2 values; on the contrary, Hill coefficient was lower and coincided with Langmuir model for the samples where the Hill plot gave poorer R^2 values compared to Langmuir fit. For the two lowest roughness values, 15

and 21 nm, Hill plot conformed to Langmuir model within the boundaries of the standard errors, also seen from the close matching of k_D values at low roughness. The deviation of Hill coefficient from its Langmuir value n = 1 (horizontal line in the graph of Fig. 3.1.5.4.) was accompanied by a corresponding divergence in the k_D values given by Hill and Langmuir models. Within the sampled roughness range, the Hill coefficient increased with the decrease of k_D and slightly decreased with the rise observed for k_D, although the variation in Hill coefficient was not directly proportional to the variation in k_D, as it would be expected due to the close interlinkage of these two parameters in protein adsorption. In particular, the steep rise of k_D, i.e., a remarkable drop in the adsorption affinity in the 28 – 34 nm roughness region could indicate a corresponding decrement in cooperative adsorption, i.e., the Hill coefficient. The observed decrease in Hill coefficient however, was not significant, hence it did not account for the drop in the adsorption affinity, i.e., rise of k_D.

It is known that at the pH 8 used in this study, the surface of ns-TiO_x is hydroxylated bearing a negative charge, since it has been shown that the isoelectric point of ns-TiO_x films produced by SCBD lies below pH 5 – 6 (Vyas et al., 2011), while trypsin molecules acquire an overall positive charge having the isoelectric point at around pH 10.2 – 10.8 (Buck et al., 1962; Walsh et al., 1970). This implies the occurrence of attractive electrostatic interactions that could lead to hydrogen bonding between trypsin molecules and ns-TiO_x. Additionally, in the previous studies of the interaction between ns-TiO_x and proteins, our group has shown that the non-specific adsorption of streptavidin on ns-TiO_x proceeded via formation of coordinated molecular bond between the exposed residues of carboxylic acids (glutamic or aspartic acid) that are deprotonated at pH 8, and undercoordinated titanium atoms of the surface (Giorgetti et al., 2008). In a more recent report by our group, the interaction of hydrated ns-TiO_x with –OH and -NH_2 groups was investigated by means of the Force Spectroscopy mode of AFM; it was demonstrated that the nucleophiles of these functional groups can displace already adsorbed hydroxyl ions and water molecules, forming coordinate bonds with undercoordinated titanium atoms, while the hydrogen atoms of these functional groups can be involved in hydrogen bonding

with the oxygen atoms of ns-TiO_x surface (Vyas et al., 2011). Considering that trypsin consists of a single chain polypeptide of 223 amino acid residues with the hydrophilic side chains exposed on the surface, there are numerous candidates for the bonding to ns-TiO_x, including 12 aspartic acids and 10 glutamic acids with $–CO_2^-$ groups, as well as the positively charged 6 arginine and 11 lysine residues with $–NH_3^+$ groups (NCBI Reference Sequence: XP_002687122.1). Consequently, the attractive electrostatic interactions and the molecular bonds between carboxylic trypsin residues and superficial titanium atoms can account for the non-specific binding of trypsin to ns-TiO_x surfaces. In this study however, we propose that the adsorption induced by the physicochemical affinity between trypsin and ns-TiO_x surface is further enhanced by the nanometre-scale surface morphology.

The thin films produced by the SCBD method consist of stochastically assembled nanometre-sized clusters (hence, termed “cluster-assembled”) forming a granular nanoporous structure with the general character of a self-affine fractal surface (Milani et al., 2001). Owing to the ballistic deposition regime, the two nanoscale parameters, roughness and specific area, are unequivocally determined by the nominal film thickness (Podesta et al., 2009). Furthermore, roughness of the ns-TiO_x films correlates with the average depth of surface pores, as estimated by the statistical evaluation of AFM images (Scopelliti et al., 2010). Considering the abovementioned characteristics of cluster-assembled ns-TiO_x films, solely from the size distribution of their surface pores on the order of magnitude of protein molecules, confinement of proteins within these pores can be anticipated according to theoretical models reported in literature (Benesch et al., 2003). In addition to the mean pore size, the roughness of pore walls can be expected to enhance the entrapment effect, since roughness has been linked to impaired self-diffusion and increased residence time of particles inside pores (Malek and Coppens, 2001). As a result of trapping of proteins inside surface pores, an elevated local density can, in turn, give rise to supersaturation spikes triggering either heterogeneous protein nucleation or disordered clustering at randomly rough surfaces, an effect described theoretically (Chayen et al., 2006) and observed

experimentally for a range of disordered mesoporous materials (Chayen et al., 2001; Liu et al., 2007).

In our previous study of the adsorption of three model proteins bovine serum albumin, fibrinogen and streptavidin on ns-TiO_x films (Scopelliti et al., 2010), we performed a detailed AFM analysis of the surface morphology obtaining the mean width and depth distributions of surface nanopores before and after protein adsorption. The adsorption occurred via a pore filling mechanism whereby increasing the bulk concentration of proteins or the roughness of the sample surface, nanopores with higher depth-to-width aspect ratio were filled first. The increase in depth-to-width ratio of nanopores was accompanied by a shift of the pore depth distribution towards deeper pores, while the pore width distribution remained relatively constant, as a result of which the roughness of samples was directly correlated with the mean depth of the surface pores (Scopelliti et al., 2010). Therefore we interpreted the observed behaviour as roughness-induced protein clustering arguing that deeper nanopores, i.e., higher roughness, support a higher protein density but require a higher bulk concentration to reach the local supersaturation condition. The latter two effects are clearly reflected by the roughness dependence of the two parameters of trypsin adsorption, the saturation uptake and the equilibrium dissociation constant k_D (See Fig. 3.1.5.3. A., B.). All in all, the key-parameter governing the adsorption of trypsin on ns-TiO_x films is the nanometre-scale roughness closely interlinked with the depth-to-width (aspect) ratio of surface pores, a hallmark of nanopore shape.

However, the interaction of trypsin with ns-TiO_x is perturbed by an additional factor, namely, the cooperativity characterized by the Hill coefficient. On ns-TiO_x surface, cooperative trypsin adsorption is evident from the values of the Hill coefficient significantly higher than 1 at high sample roughness (See Fig. 3.1.5.4.). We reason that trypsin adsorption cooperativity indicated by Hill coefficient could be related to the proposed adsorption mechanism of proteins on cluster-assembled ns-TiO_x, namely, the formation of adsorbed clusters of proteins rather than individual adsorbed protein molecules, respectively, aggregation of proteins in the nanopores. It must be noted however, that trypsin molecules have been shown to form clusters upon

adsorption on flat hydrophilic silica surface (Koutsopoulos et al., 2007) – an indication that cooperative protein-protein interactions are typical for trypsin in the absence of nanometre-scale topography. In contrast to this notion, we detected low cooperativity (Hill coefficient n = 1.1 ± 0.2), or no adsorption cooperativity (n = 0.9 ± 0.2) at the two lowest roughness values, 15 nm and 21 nm, respectively. The reason for this result is unclear; we can speculate however, that the cluster formation occurs above a certain adsorbed protein surface density that might not be reached on the lowest roughness samples. The main conclusion is that the nanostructured surface morphology promotes a roughness-dependent generation of clusters, as we have demonstrated it with trypsin in this study and with a set of other proteins in our previous work.

3.1.6. FRAP studies of adsorption stability

Fluorescence Recovery After Photobleaching (FRAP) approach was aimed at investigating the temporal stability of trypsin adsorbed on ns-TiOx surfaces. In parallel to the confocal microscopy-based FPQ setup, FRAP experiments were performed on the samples of 21 nm roughness within the low range of trypsin bulk concentration from 1 to 10 μM. In the FRAP setup, ns-TiOx films were initially incubated with trypsin solutions of various bulk concentrations until the adsorption reached equilibrium (1 hour), then the adsorbed protein layer was bleached and the recovery of the layer fluorescence was monitored, as explained in details in the "Materials and Methods" chapter (Fig. 3.1.6.1.). The acquired recovery curves were approximated with monoexponential functions with two fitted parameters:

$$y = M\left(1 - e^{-\frac{x}{t}}\right)$$

M denotes the mobile fraction and the index of the exponent t is related to the recovery halftime τ as $\tau = t \cdot ln(2)$. The usage of the monoexponential approximation according to the reaction dominant model was justified, since the characteristic diffusion time, calculated from the Stokes-Einstein relation for trypsin under the experiment conditions, was by a factor of 60 lower than the typical recovery halftimes, i.e., diffusion time of 2 – 3 seconds versus recovery halftime

values between 2 and 3 minutes, indicating that the recovery occurred at a desorption- limited rate (for more details, please, see the sections 1.2.1. and 2.2.2. on FRAP method in the "Introduction" and "Materials and Methods" chapters, respectively). The surface diffusion, in turn, was ruled out based on the observation that the recovery occurred homogenously across the bleached area without decreasing the size of the bleached region which would be evident in case of exchange of bleached trypsin with the non-bleached trypsin on ns-TiO_x surface at the borders of the bleached region.

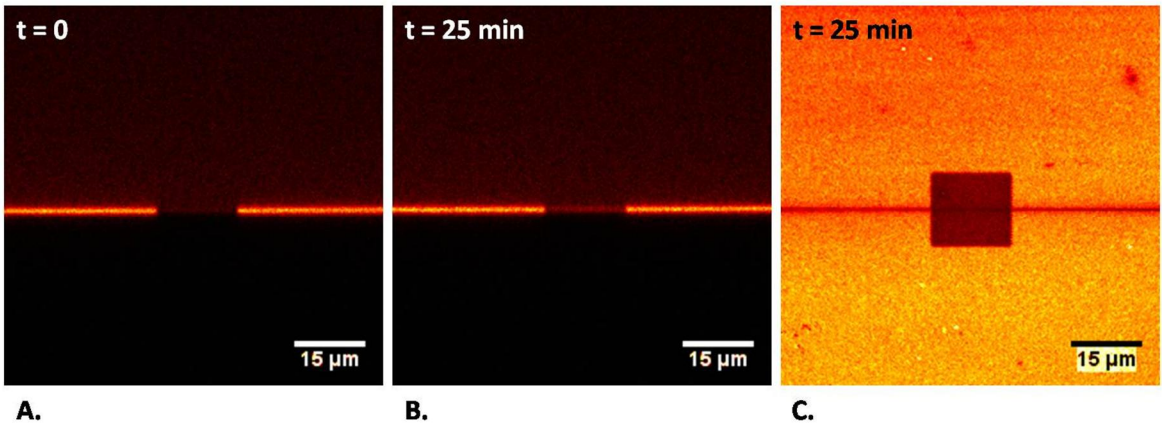

Fig. 3.1.6.1. Recovery monitoring after photobleaching of the adsorbed trypsin layer. Rectangular region of the protein layer was bleached in the XY-plane, the recovery of the fluorescence signal was monitored in the transverse XZ-plane, including the signal of the bulk solution as calibration control within the field of view. The bleached region is shown at the instant of the bleaching event t = 0 (A) and after 25 minutes of acquisition (B). The corresponding field of view in the XY-plane is demonstrated after 25 minutes of recovery monitoring, where the horizontal line that transects the image was created by bleaching of the layer in XZ-plane with the aim to verify that the focal position was within the bleached region not perturbed by focal drifts. Scale bar: 15 µm in all images.

Recovery curves with the bleached signal set to 0 and the initial signal normalized to 1, are shown in Fig. 3.1.6.2., demonstrating the exchange of trypsin molecules at two bulk concentrations: 1.6 µM and 10 µM. According to the used approach, the mobile fraction here reflects the percentage of adsorbed proteins prone to desorption in the presence of protein

solution of a certain bulk concentration. The recovery halftime, on the other hand, is inversely proportional to the exchange rate of adsorbed proteins with the proteins in bulk solution. It was found that the recovery within the probed concentration range could be fairly well ($R^2 \geq 0.95$) described by single exponents (Fig. 3.1.6.2.) indicating two basic populations of trypsin adsorbed on ns-TiO_x surfaces: an irreversibly immobilized population and a reversibly bound population exchanging with trypsin molecules in solution.

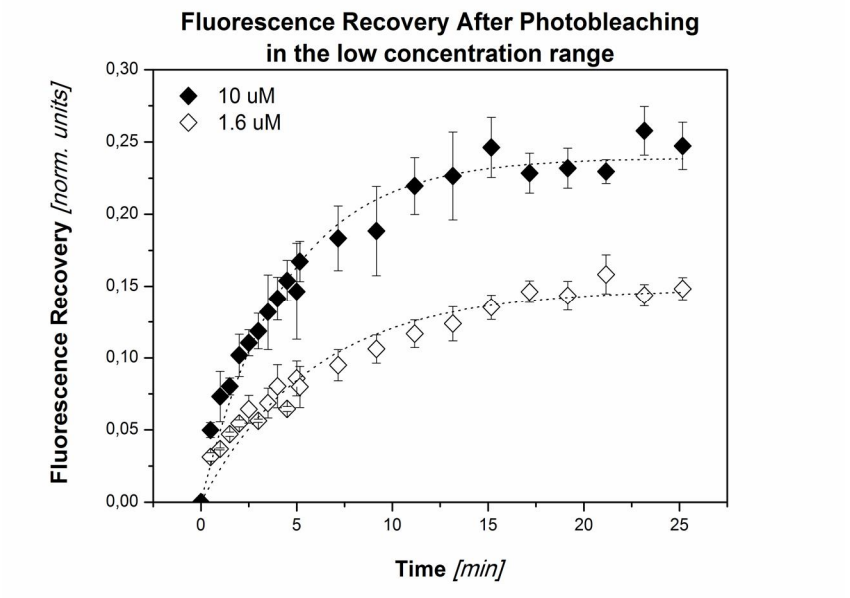

Fig. 3.1.6.2. Monoexponential exchange of adsorbed trypsin with bulk solution in the low concentration range. The two curves represent the lowest and the highest concentrations probed with the FRAP setup. Symbols mark the data with standard errors of three experiments; dotted lines correspond to the fitted functions with adjacent-R^2 values of 0.95 and 0.97, at 1.6 μM and 10 μM bulk concentrations, respectively.

The two parameters characterizing the reversibly adsorbed trypsin exchange kinetics, namely, the mobile fraction and the recovery halftime, were plotted versus the bulk concentration of trypsin in solution (Fig. 3.1.6.3. A.). An increment of about 40 % was determined for the mobile fraction with its value reaching from 0.14 ± 0.02 to 0.24 ± 0.03 within the sampled range of trypsin bulk concentrations. Since the surface coverage grows quasi-linearly with bulk concentration in the low concentration range, a very similar trend of mobile fraction dependence from the relative surface coverage was detected (Fig. 3.1.6.3. B.). Namely, mobile fraction

increased with the surface coverage in the probed sub-monolayer coverage span. The observed dependence of the mobile fraction both, from the bulk concentration and from the surface coverage is consistent with the results reported in the homologous exchange studies of IgG on Titanium particles (Ball et al., 1996). Growth of mobile fraction with bulk concentration could be attributed to the higher adsorption flux present at higher bulk concentrations.

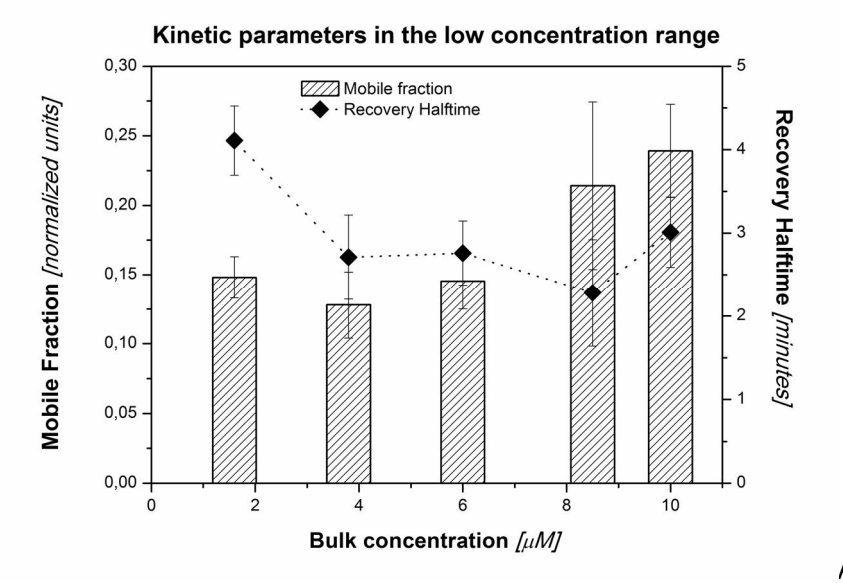

A.

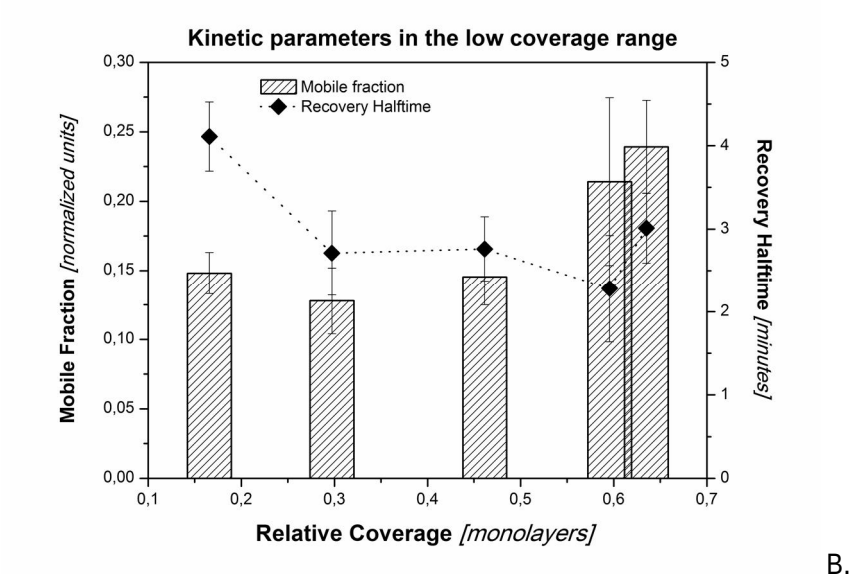

B.

Fig. 3.1.6.3. Kinetic parameters of adsorbed trypsin exchange in the low range of adsorption isotherm. Mobile fraction (bar graph) and recovery halftime (dotted line with symbols) are plotted against the bulk concentration (A) and the corresponding surface coverage (B). Increase of the mobile fraction was observed, while the recovery halftime did not exhibit a clear dependence nor from the bulk concentration, nor the surface coverage.

On the other hand, the rise of the mobile fraction with surface coverage could be interpreted by the corresponding decrease of protein footprint and, as a consequence, restricted spreading on the adsorbent surface that could lead to fewer interaction sites with the surface per molecule (Hovgaard et al., 2008), resulting in enhanced desorption of adsorbed molecules and exchange with the molecules in solution. Alternatively, repulsive interactions between adsorbed neighbour molecules can gain importance at higher coverage; this was however not the case for trypsin, as it was emphasized in the section 3.1.5., owing to the positively cooperative adsorption identified via Hill plot. Similarly, the recovery halftime was treated as a function of the bulk concentration and the surface coverage. Unlike the mobile fraction, recovery halftime did not obey a particular trend versus concentration or surface coverage (Fig. 3.1.6.3.). The value of recovery halftime dropped from 4.1 ± 0.4 minutes at the lowest bulk concentration to 2.7 ± 0.5 minutes at 3.8 mM and retained the average value of 2.7 ± 0.3 without statistically significant differences up to the highest concentration of 10 μM ($p \geq 0.19$, as determined by Student's t-test). The value of the total kinetic rate constant k inversely proportional to the estimated average recovery halftime is: $k = ln(2) \cdot \tau^{-1}$, i.e., $k = (4.3 \pm 0.5) \times 10^{-3}\ s^{-1}$. The kinetic rate constant can be ascribed to a superposition of both, the exchange rate constant k_e and the desorption rate constant k_d as: $k = k_e \cdot C + k_d$. Consequently, a decrease of the recovery halftime would correspond to an increase of the kinetic rate constant with the bulk concentration that would in turn suggest an exchange process with the trypsin molecules in the bulk solution. Within the sampled concentration domain, however, recovery halftime tends to stabilize around the average value, a behaviour that indicates that the recovery process here is limited by the desorption rate constant k_d, rather than the exchange rate constant (Bentaleb et al., 1998).

3.1.7. Desorption studies

Adsorption stability in a wider spectrum of bulk concentrations was explored by desorption studies implementing the high-throughput PSIM approach. According to the specifics

of PSIM method, trypsin was arrayed on a panel of ns-TiO_x films of varying nanoscale roughness, thereafter the temporal stability of adsorption was tested by subjecting the immobilized protein arrays to incubation in buffer solution for series of time intervals. Subsequently, the fluorescence signal of the remaining surface-bound trypsin was detected, thus estimating trypsin desorption in the whole isotherm region up to the saturation plateau. The shape of the adsorption isotherms was significantly changed upon prolonged exposure to pure buffer solution, indicating dependence of desorption on the initially adsorbed amount of trypsin. The temporal evolution of an isotherm during desorption series is demonstrated in Fig. 3.1.7.1. A., where the fluorescence signal from the immobilized protein drops with the incubation time, whereby this decrease is different at different initial bulk concentrations, respectively, different initial surface coverage values. To track the desorption dependence on coverage, we followed the change of fluorescence with time from separate initial coverage values, as shown in Fig. 3.1.7.1. B.

Assuming the simplest model of desorption with two populations, one irreversibly bound and the other, reversibly bound desorbing molecules, we approximated the calibrated desorption curves with a monoexponential function:

$$y = (y_0 - y_\infty) \cdot e^{-\frac{x}{t}} + y_\infty$$

(y_0 - y_∞) = y_d denotes the total desorbed (reversibly adsorbed) amount, where y_0 is the initial coverage and y_∞ is the irreversibly adsorbed amount. The exponent index t is proportional to the desorption halftime $\tau_d = t \cdot ln(2)$.

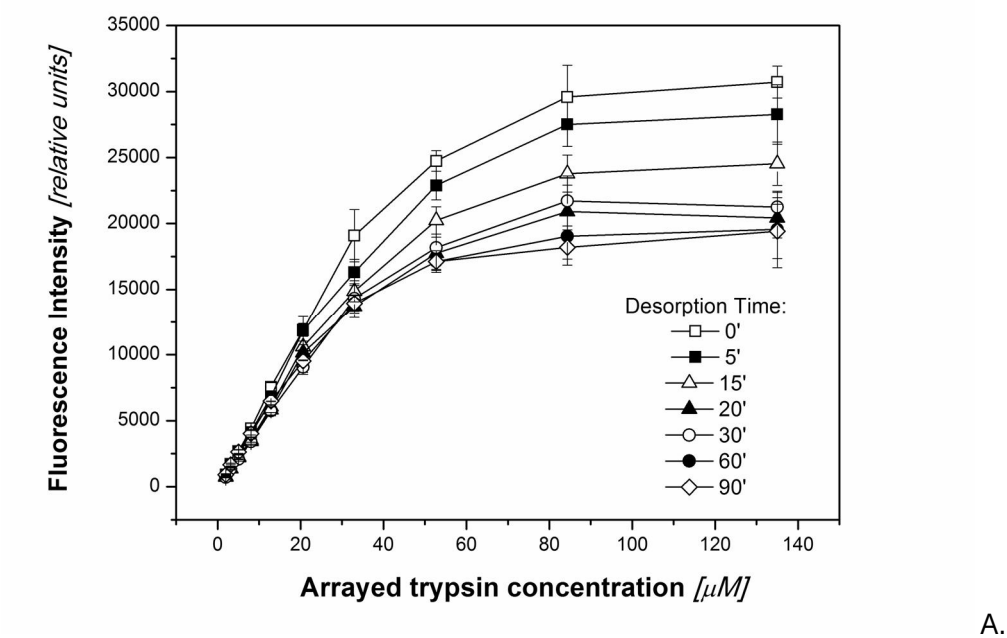

A.

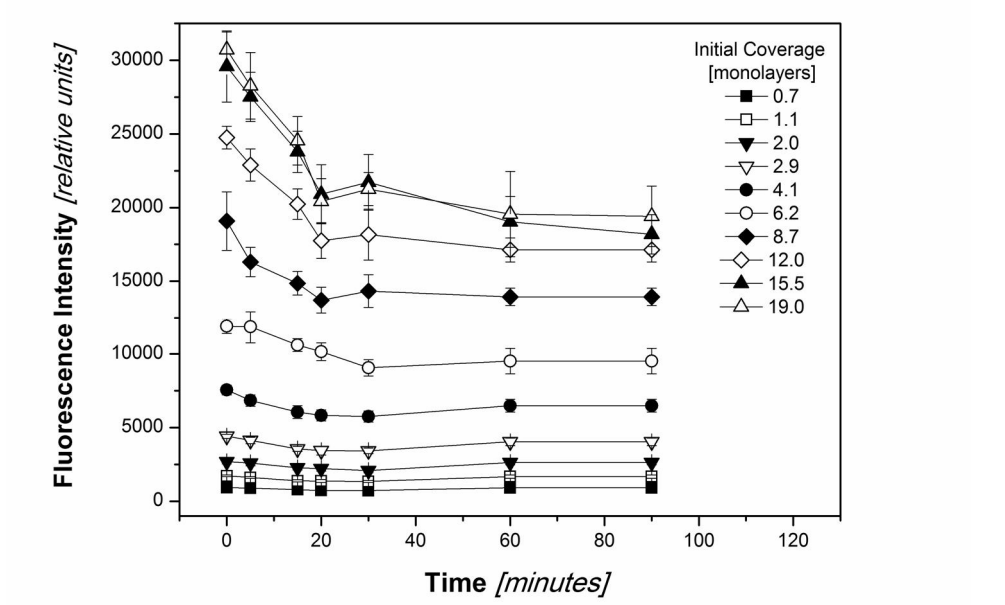

B.

Fig. 3.1.7.1. Desorption studies of adsorbed trypsin. Fluorescence signal of adsorbed trypsin was detected on a panel of ns-TiO_x after series of incubation intervals in the presence of buffer solution. (A) Typical trypsin adsorption isotherm evolution with desorption time. PSIM data points with standard deviation bars acquired at 0; 5; 15; 20; 30; 60 and 90 minutes of incubation are shown for ns-TiO_x sample of 34 nm roughness. (B) Desorption of adsorbed trypsin into buffer solution at different initial coverage values. Data points ± standard deviation are plotted for the ns-TiO_x surface of 34 nm roughness.

Results of the experiment data approximation with a monoexponential function with two fitted parameters, the exponent index t and the asymptote y_∞, are displayed in Table 3.1.7.1., where the case of the ns-TiO_x surface of 34 nm roughness is demonstrated. The desorbed amount y_d, in turn, was defined as the difference of the initial coverage y_0 given by the experiment and the irreversibly adsorbed amount y_∞ given by the fitting of experiment curves and expressed in monolayers.

Initial coverage *[monolayers]*	**Exponent Index t** *×ln(2) [min]*	**t relative error** *%*	**Asymptote y_∞** *$\times 10^2$ [r.u.]*	**y_∞ relative error** *%*
0,7	12,2	52	6,7	21
1,1	8,8	38	12,9	13
2,9	7,9	37	33,0	12
4,1	7,0	13	56,18	4
8,7	4,8	22	139,43	6
12,0	9,8	19	170,18	6
15,5	13,7	20	182,50	9
19,0	10,0	31	194,2	14

Table 3.1.7.1. Results of the monoexponential fitting of desorption curves. The relative errors of fitting demonstrate the accuracy achieved for the two fitted parameters – exponent index t and asymptote y_∞. Asymptote values were used for the characterization of trypsin desorption on ns-TiO_x surfaces with different nanoscale roughness. The example of 34 nm roughness sample is given in this table.

From the high errors of fitting however, it was concluded that the sampling frequency of the experiment was not high enough to determine the value of the exponent index with sufficient accuracy, since the exponential decay model is sensitive to the density of the experiment data at the beginning of the time course. Despite of this fact, the values obtained by fitting of the desorbed and irreversibly adsorbed populations y_d and y_∞, were considered as valid and conclusive for the relative comparison of surfaces with various roughness, since the asymptotic value y_∞ of the exponential decay curves was much less prone to fitting error caused by the low sampling frequency.

In order to compare desorption on ns-TiO_x films of different roughness, the magnitude of the desorbed amount was normalized against the initially adsorbed amount to gain the desorbed

fraction. We assessed the dependence of the desorbed fraction from the initial coverage of the various ns-TiO_x surfaces, illustrated in Fig. 3.1.7.2. As evident from the graphs in Fig. 3.1.7.2., equal surface coverage resulted in different desorbed fraction on samples with different roughness. Similarly as before, surface coverage was expressed in monolayer units, moreover it was normalized by the specific area factor. Despite of the relatively high standard errors of the desorbed fraction, two general rules were found, namely: (i) the desorbed fraction was growing with surface coverage on every ns-TiO_x sample and (ii) the desorbed fraction was diminishing with increasing sample roughness.

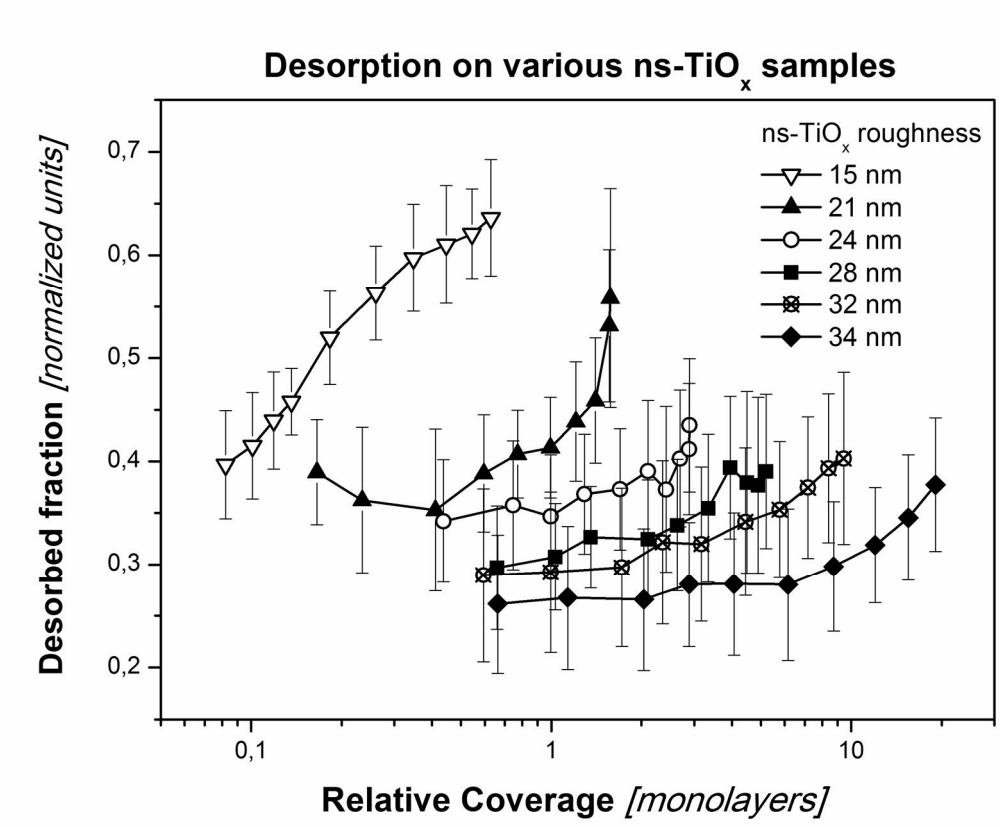

Fig. 3.1.7.2. Desorbed fraction dependence on relative surface coverage reveals the differences between surfaces of various roughness. Data points with standard error bars correspond to ns-TiO_x samples, as follows: 15 nm (empty triangles); 21 nm (filled triangles); 24 nm (empty circles); 28 nm (filled squares); 32 nm (crossed circles) and 34 nm (filled diamonds).

Notably, the desorbed fraction was rising smoothly with coverage: surpassing the theoretical limit of one full monolayer coverage did not result in a detectable change of desorption behaviour. The observation that the one monolayer coverage did not act as a threshold value can be linked to the fact that the precise meaning of the term “monolayer” can be applied only speaking about surfaces that are flat on the scale of adsorbate dimension, i.e., on the nanometre-scale in case of protein adsorption. As it was reasoned in the section 3.1.5., although the adsorption isotherms were approximated with Langmuir model, the mechanism of protein adsorption on ns-TiO_x surfaces is that of nanoporous volume filling, rather than the homogenous coverage of adsorbent surface. Therefore, in case of nanometre-scale topography, the coverage expressed in monolayer units serves primarily for the relative comparison of various surfaces.

In our previous study, we have found that the adsorption behaviour of bovine serum albumin, streptavidin and fibrinogen can be interpreted by protein clustering in the ns-TiO_x surface nanopores (Scopelliti et al., 2010); our studies of trypsin adsorption suggest the same underlying mechanism. Here, we propose that the augmentation of the desorbed fraction with coverage can be likewise attributed to the phenomenon of protein clustering. Increasing the coverage, the number of available binding sites with the adsorbent surface per protein molecule is decreasing, thus decreasing the fraction of irreversibly adsorbed protein molecules. The latter effect is even more pronounced if clustering of adsorbed proteins occurs: the number of binding sites with the adsorbent surface per protein molecule within a cluster is dropping more rapidly than for single adsorbed molecules, since a percentage of molecules within a cluster are bound by protein-protein interactions.

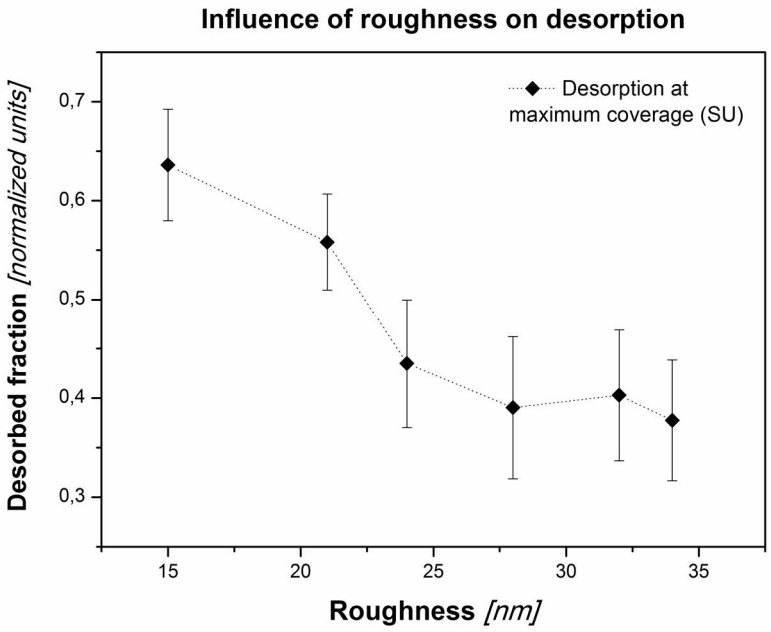

Fig. 3.1.7.3. Desorbed fraction dependence on nanometre-scale roughness. Desorption was assessed at the maximum coverage, i.e., the saturation uptake coverage of each ns-TiOx sample. Data points were plotted with standard error bars.

The finding that the desorbed fraction decreases with the roughness of the adsorbent surface was highlighted by plotting the desorbed fraction at the saturation uptake coverage versus sample roughness (Fig. 3.1.7.3.). The observed dependence can be similarly explained by the clustering of proteins inside the nanopores. We have verified earlier that the density of clustering sites rises with ns-TiO_x roughness (Scopelliti et al., 2010), hence, we conclude that – given the same relative coverage – there are more binding sites with ns-TiO_x surface per protein molecule on samples with higher roughness. Hence, lower desorbed fraction can be associated with higher roughness. Another factor playing role in the adsorption stability of trypsin on ns-TiO_x is the cooperativity between adsorbing trypsin molecules. As it was demonstrated by the Hill coefficient, attractive protein-protein interactions are evident above the threshold value of sample roughness equal to 24 nm – that is, in the roughness region where the desorbed fraction rapidly drops of around 20 % compared to lower roughness samples (Fig. 3.1.7.3.). Presumably, the attractive interactions between trypsin molecules contribute to adsorbed cluster stabilization.

3.2. Catalytic activity of trypsin adsorbed on ns-TiO_x surfaces

3.2.1. Development of a new microarray-based high-throughput surface-bound enzyme activity assay

We intended to establish a new approach for the detection of immobilized enzyme activity: in particular, none of the numerous existing enzyme activity assays could meet the demands set by our group and find application in the screening of nanostructured biomaterials. Our main aim was the high-throughput characterization of the randomly-rough nanostructured interfaces synthesized in our laboratory, from the aspect of functionality of enzymes after physisorption on these surfaces. Therefore we attempted to develop a new technique using already existing tools, namely, the protein-surface-interaction-microarrays (PSIM) in combination with activity-based small-molecule probes for serine proteases recently available on the market (further shortened to "activity probe"). We selected the serine protease trypsin for the proof of the principle of our approach. Concurrently with the implementation of trypsin in the development of the new methodology, we scrutinized its adsorption characteristics on ns-TiO_x, as reported in the sections 3.1.1 – 3.1.7. In this section, we mainly concentrate on the optimization of the microarray-based activity detection of the physisorbed trypsin.

The information on trypsin activity was retrieved benefiting from the double-channel fluorescence detection setup used in the PSIM method. Simultaneously with the fluorescence signal of the labelled adsorbed trypsin, the signal of the fluorescent activity probe bound to trypsin in the whole isotherm region was detected in the second channel. The scanned images obtained from a single slide in both fluorescence channels are shown in Fig. 3.2.1.1. Concentration gradients of Alexa-647-trypsin conjugate were spotted as 10×10 arrays on glass slides with four zones of deposited ns-TiO_x corresponding to four different roughness values. To a half of the identical trypsin arrays on each ns-TiO_x zone, activity probe labelled with carboxy-tetramethylrhodamine (TAMRA) was applied, while the other half served as control fields for the compensation of fluorescence channel cross-talk, as well as the partial desorption of the

physisorbed trypsin resulting from the incubation with the activity probe and from the washing of slides.

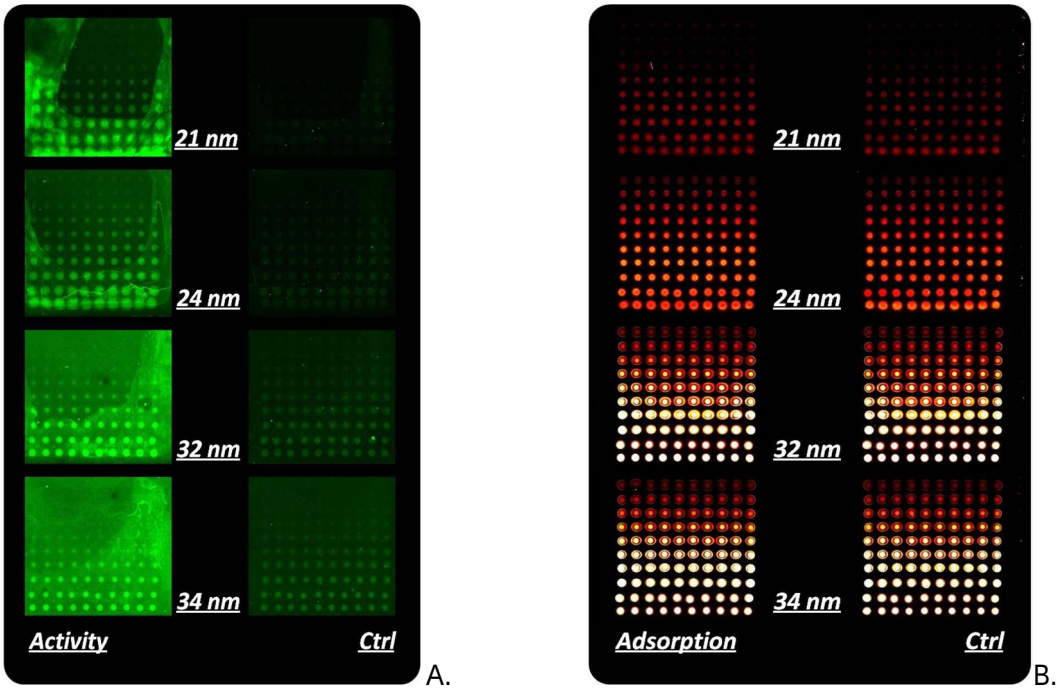

Fig. 3.2.1.1. Scanned images of a single slide acquired in two fluorescence channels depicting:

A) The fluorescence of TAMRA-tagged activity probe applied to the arrays in the left column and detected in the CY3 channel. The signal of the right column (no probe incubation) arose exclusively from the excitation of Alexa-647 by the 532 nm laser line designated to the CY3 channel and was therefore used for the estimation of channel cross-talk.

B) The signal of adsorbed Alexa-647-labelled trypsin detected in CY5 channel. The arrays of the right column not incubated with the activity probe, functioned as control to account for desorption.

Ns-TiO_x films were deposited as four adjacent zones of increasing nominal thickness and nanoscale morphology parameters. Film roughness values were indicated next to every ns-TiO_x zone. Each 10×10 pattern corresponds to a gradient of increasing trypsin concentration in the Y-direction (top to bottom) with 10 replicates in the X-direction (left to right). False colours were applied via ImageJ software using the predefined Lookup Tables “Green Hot” and “Red Hot” for the CY3 and CY5 channels, respectively. The contrast of the CY5 channel was set above the saturation (evident as white spots) by the ImageJ program with the aim to visualize the lower intensity values. The original scanner settings were however, adjusted well below the upper saturation limit of the scanner detectors.

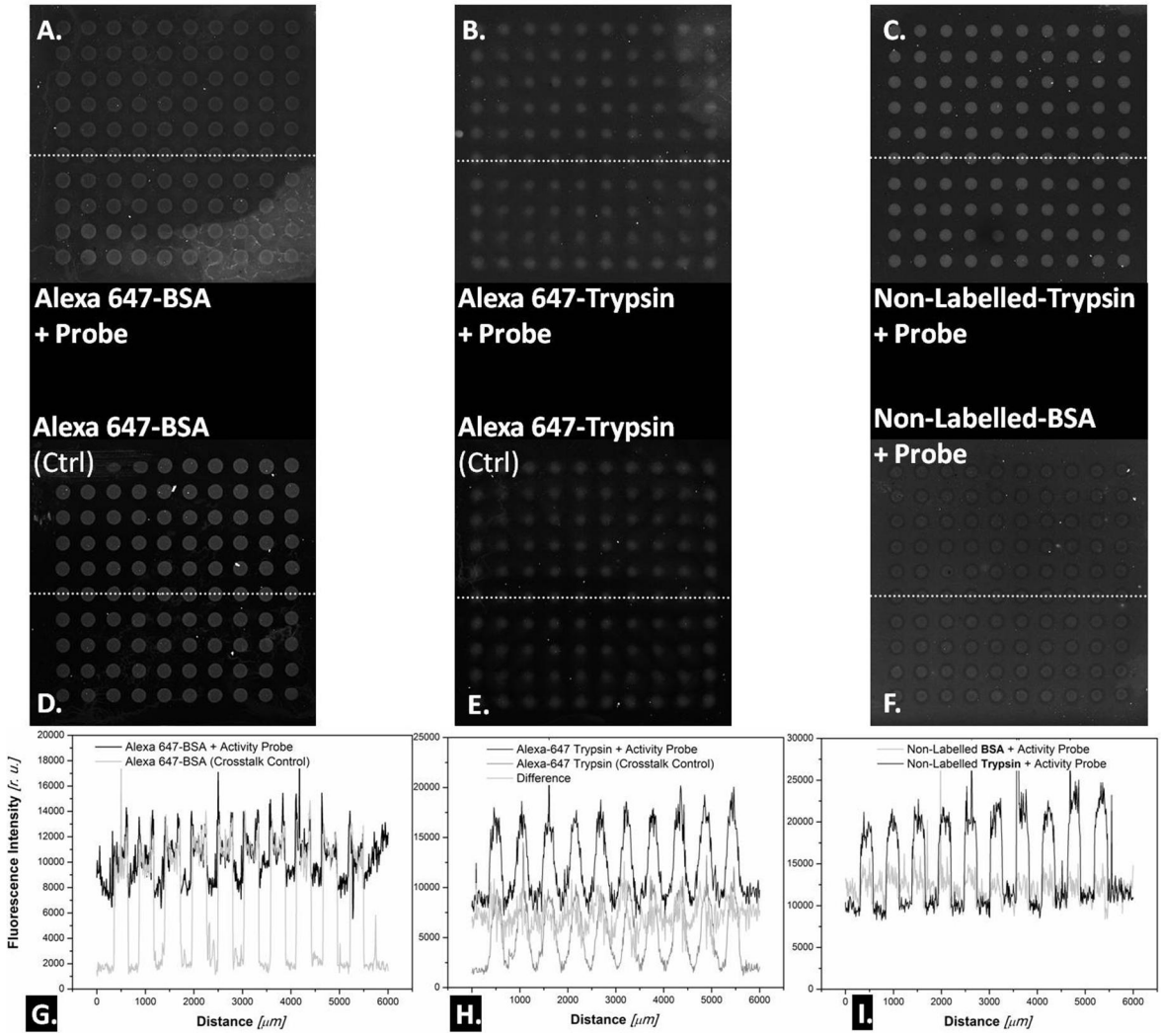

Fig. 3.2.1.2. Analysis of spot signal and background after incubation with the activity probe.

A) – F) Images of equimolar (150 µM) 10×10 arrays and G) – I) graphical representation of fluorescence intensity along the dotted white lines marked in the images.

A) Alexa-647-BSA incubated with the TAMRA-tagged activity probe;

B) Alexa-647-trypsin incubated with the activity probe;

C) non-labelled trypsin incubated with the activity probe;

D) Alexa-647-BSA control without the activity probe;

E) Alexa-647-trypsin control without the activity probe;

F) non-labelled BSA incubated with the activity probe;

G) Intensity profiles of Alexa-647-BSA after probe treatment and its control, corresponding to the dotted white lines in A) and D).

H) Alexa-647-trypsin fluorescence intensity profiles along the dotted lines in B) and E) (control).

I) Intensity profiles of non-labelled trypsin (dotted line in C)) and BSA (dotted line in F)).

The increase of trypsin adsorption with concentration and ns-TiO_x roughness can be appreciated already by the visual judgement of the CY5 channel images (Fig. 3.2.1.1. B.). On the other hand, the differences in trypsin activity on the various ns-TiO_x zones were not apparent from the images of the CY3 channel fluorescence (Fig. 3.2.1.1. A.), primarily due to the increase of the background fluorescence with ns-TiO_x roughness. It was deduced that even after washing of the slides, the activity probe was present on the background between spots of trypsin. Moreover, the background intensity was relatively high and non-homogeneous along the area of a single 10×10 array.

We attempted to identify the origin of the high background fluorescence. Equimolar (150 µM) concentrations of both, labelled and non-labelled trypsin and BSA were arrayed in parallel as 10×10 patterns, thereafter all of the slides were blocked with 1 % BSA (150 µM) (Fig. 3.2.1.2.).We investigated the binding of the TAMRA-labelled serine hydrolase activity probe to trypsin versus BSA by the quantitative comparison of the fluorescence intensity detected on the arrayed protein spots and on the background between the spots. Firstly, the incubation of the Alexa-647-BSA conjugate with the serine hydrolase activity probe resulted in a detectable fluorescence intensity of the BSA spots in the CY3 channel (Fig. 3.2.1.2. A). However, the superposition of the signal of incubated BSA with the control signal (Fig. 3.2.1.2. D) revealed that the Alexa-647-BSA spots were detected only on the basis of the channel cross-talk, as evident in the graphical illustration of both signals (Fig. 3.2.1.2. G). Secondly, in contrast to the Alexa-647-BSA conjugate, the subtraction of the cross-talk from the Alexa-647-trypsin fluorescence after probe incubation, gained a non-zero signal above the baseline (Fig. 3.2.1.2. B, E and H). Hence, after the cross-talk compensation, the fluorescence peaks of Alexa-647-trypsin spots exceeding the background were attributed to the binding of the activity probe solely to trypsin. Thirdly, the incubation of the non-labelled trypsin with the activity probe led to well defined spots of intensity twice as high as the background fluorescence (Fig. 3.2.1.2. C), while the non-labelled BSA spots incubated identically with the activity probe were not detected by the microarray analysis software (Fig. 3.2.1.2. F). Intensity profiles obtained from both, the non-labelled trypsin and BSA spots, were superimposed in the

graph in Fig. 3.2.1.2. I – in order to demonstrate the matching between the signal of BSA spots and the baseline of trypsin signal. From the analysis of spot and background intensity, we reasoned that the background fluorescence was associated with the BSA adsorbed on the surface during the blocking step of slides (10 minutes in 1 % = 150 µM BSA solution). Moreover, from the graphs H and I of Fig. 3.2.1.2., we concluded that the background fluorescence caused by the adsorption of the blocking BSA on ns-TiO_x was comparable to or even higher than the signal of probe binding to trypsin, leading to the low signal-to-background ratio approximately equal to 1.

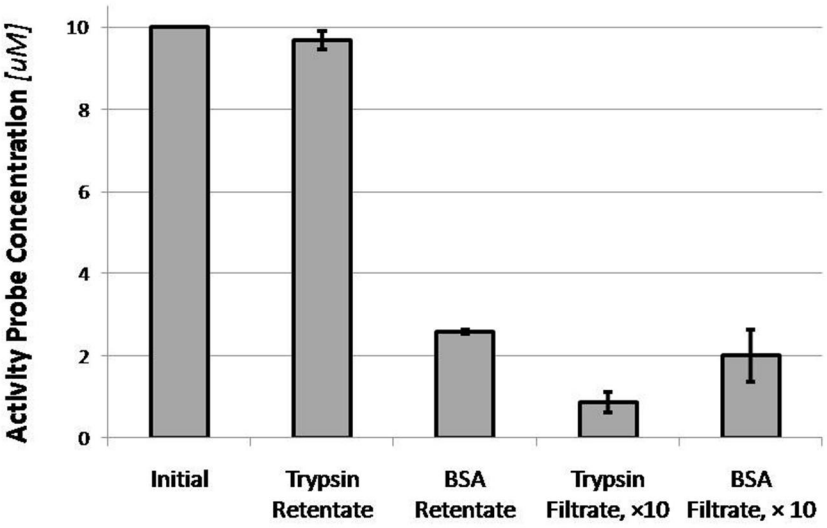

Fig. 3.2.1.3. Activity probe binding to trypsin and BSA in solution.

The initial concentration of the serine hydrolase activity probe in the reaction solutions was 10 µM. Its concentration was estimated after the filtration of reaction solutions (nominal molecular weight limit 10 kDa) to assess separately probe binding to trypsin and to BSA. Graph depicts the data of spectrophotometry measurements ± standard deviations.

We additionally tested the binding of the serine hydrolase activity probe to trypsin and to BSA in solution in order to obtain an estimation of the non-specific binding of the probe to BSA. The binding assay consisted of three main steps: (i) 30 minutes of incubation of equimolar (50 µM) trypsin and BSA solutions with 10 µM activity probe, (ii) subsequent filtration of the reaction solution for the removal of unreacted probe, and finally, (iii) spectrophotometric measurements of protein and probe concentrations in the filtrate and retentate solutions. Results of the binding

assay are shown in Fig. 3.2.1.3., where the concentration of the activity probe after the filtration was compared in case of trypsin and BSA. We found that the concentration of the activity probe in the retentate of trypsin was 9.67 ± 0.23 µM, i.e., nearly as high as the initial concentration of the probe in the reaction solution. In contrast, the activity probe concentration in the BSA retentate was 3.9 times lower than the initial concentration of the probe in the reaction solution (Fig. 3.2.1.3.). Under the given conditions of trypsin molecules being in excess, these results implied that almost all of the activity probe molecules were bound to trypsin molecules. More importantly, 3.8 times less probe was bound to BSA than to trypsin of equimolar concentration.

Based on the report of Scopelliti et al., we calculated the adsorbed amount of BSA at the isotherm plateau on ns-TiO_x of 29.5 nm roughness to be in the range of 1200 ng/cm^2. On the other hand, the amount of trypsin adsorbed on the 32 nm rough ns-TiO_x was estimated to be around 2000 ng/cm^2, according to the data of this study. Consequently, the number of immobilized trypsin molecules is by a factor of 4.6 higher than the number of immobilized BSA molecules at the isotherm plateau adsorption on circa 30 nm rough ns-TiO_x films. As already discussed in the section 3.1.5., we assumed that the non-specific adsorption of trypsin on ns-TiO_x surface proceeds via the same general mechanism as the adsorption of BSA. Hence, in microarray format, the signal of probe binding to trypsin was expected to be at least five times higher than the probe binding to BSA. Considering the specificity of the serine hydrolase probe against trypsin versus BSA, as it was confirmed in the binding assay of the activity probe to proteins in solution, the expected signal-to-background ratio of microarrays, i.e., the ratio of probe bound to trypsin versus BSA would further surpass the factor of five given by the difference in adsorption between trypsin and BSA. On the contrary, the signal-to-background ratio of trypsin arrays spotted at isotherm plateau concentration was approximately equal to 1, as mentioned regarding Fig. 3.2.1.2. However, in the simple calculation presented here, desorption of trypsin during the incubation of the activity probe (30 minutes, in this case) had not been taken into account.

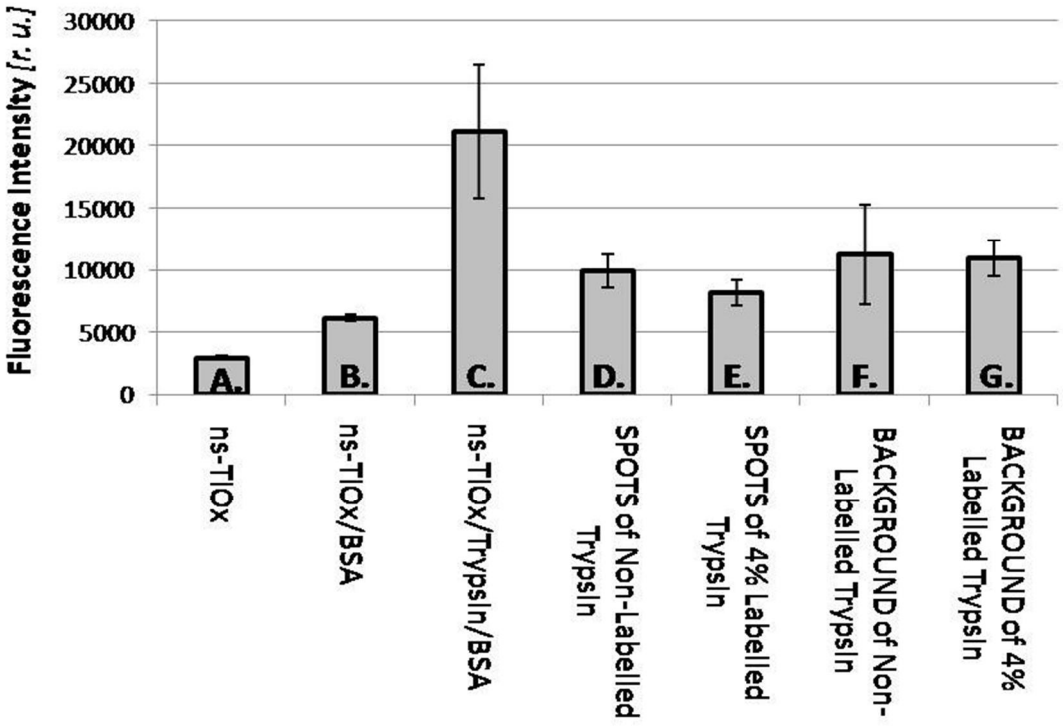

Fig. 3.2.1.4. Activity probe binding to various surfaces.

The TAMRA-tagged serine hydrolase activity probe was incubated on differently prepared ns-TiO_x surfaces (A – C) and on equimolar arrays of trypsin (D – G). The mean fluorescence intensity read in the CY3 channel was compared on the three surfaces (A – C) versus the mean intensity of trypsin array spots (D, E) and the background between the spots (F, G). ns-TiO_x film roughness was 32 nm, incubation time was 30 minutes. More specifically, the mean fluorescence intensity was detected on the following samples:

A) bare ns-TiO_x;

B) ns-TiO_x blocked with BSA;

C) ns-TiO_x incubated with non-labelled trypsin and subsequently blocked with BSA;

D) spots of non-labelled trypsin on ns-TiO_x blocked with BSA (background subtracted);

E) spots of 4 % Alexa-647 labelled trypsin (96 % non-labelled trypsin) on ns-TiO_x blocked with BSA (background subtracted and cross-talk corrected);

F) background between the spots of non-labelled trypsin on ns-TiO_x blocked with BSA;

G) background between the spots of 4 % Alexa-647 labelled trypsin (96 % non-labelled trypsin) on ns-TiO_x blocked with BSA.

Namely, at the isotherm plateau of the 32 nm rough ns-TiO_x samples, trypsin desorption was characterized by the 40 % high desorbed fraction, as shown in the section 3.1.7. (Fig. 3.1.7.2.). We carried out a further experiment to clarify the influence of trypsin desorption on the detected microarray spot and background fluorescence. The binding of the activity probe was examined under several different conditions of the nanostructured interface: (i) bare ns-TiO_x surface; (ii) ns-TiO_x surface passivated with 150 µM BSA (standard 1 % BSA blocking step); (iii) ns-TiO_x surface loaded with 150 µM trypsin and blocked with 150 µM BSA. The mean fluorescence intensity detected after the incubation with the activity probe of the prepared surfaces (i) to (iii) was compared to the mean fluorescence intensity of trypsin spots arrayed at 150 µM concentration and to the background between the spots. The results of the experiment were plotted as bar graph and displayed in Fig. 3.2.1.4.

From the bars (A – C) of the graph in Fig. 3.2.1.4., it was evident that there was 7.5 times more activity probe bound to the surface pre-incubated with trypsin than to bare ns-TiO_x, and 3.5 times more probe than on the surface subjected only to BSA blocking. These results suggest an expected signal-to-background ratio of 2.5 for equimolar trypsin arrays blocked with BSA and incubated with the activity probe. However, the results obtained from trypsin arrays disagreed with the prediction: mean fluorescence intensity between the spots, i.e., the background, was comparably high with the fluorescence intensity on the spots of trypsin, i.e., the signal, leading to signal-to-background ratio ≈ 1. Both, non-labelled and 4 % labelled trypsin exhibited similar fluorescence intensities of probe binding and background intensities between the spots. This particular finding served as proof for the negligible influence of fluorescent labelling on the proposed activity assay. Furthermore, the fluorescence intensity on ns-TiO_x surface homogenously loaded with trypsin was twice as high as the corresponding fluorescence detected on spots of equimolar trypsin. In contrast, the intensity on ns-TiO_x surface homogenously blocked with BSA was 45 % lower than the intensity detected on the background between spots of trypsin similarly blocked with BSA. We therefore concluded that the 30 minutes long incubation of the surfaces with the activity probe caused a partial desorption of trypsin. Moreover, a partial readsorption of

trypsin was indicated by the elevated background intensity detected between the spots of trypsin. Assuming that the difference in fluorescence intensity between the surface blocked with BSA and the background of trypsin arrays can be ascribed to readsorbed trypsin, the relative value of this readsorbed amount was equal to 34 % of the initial signal of trypsin spots.

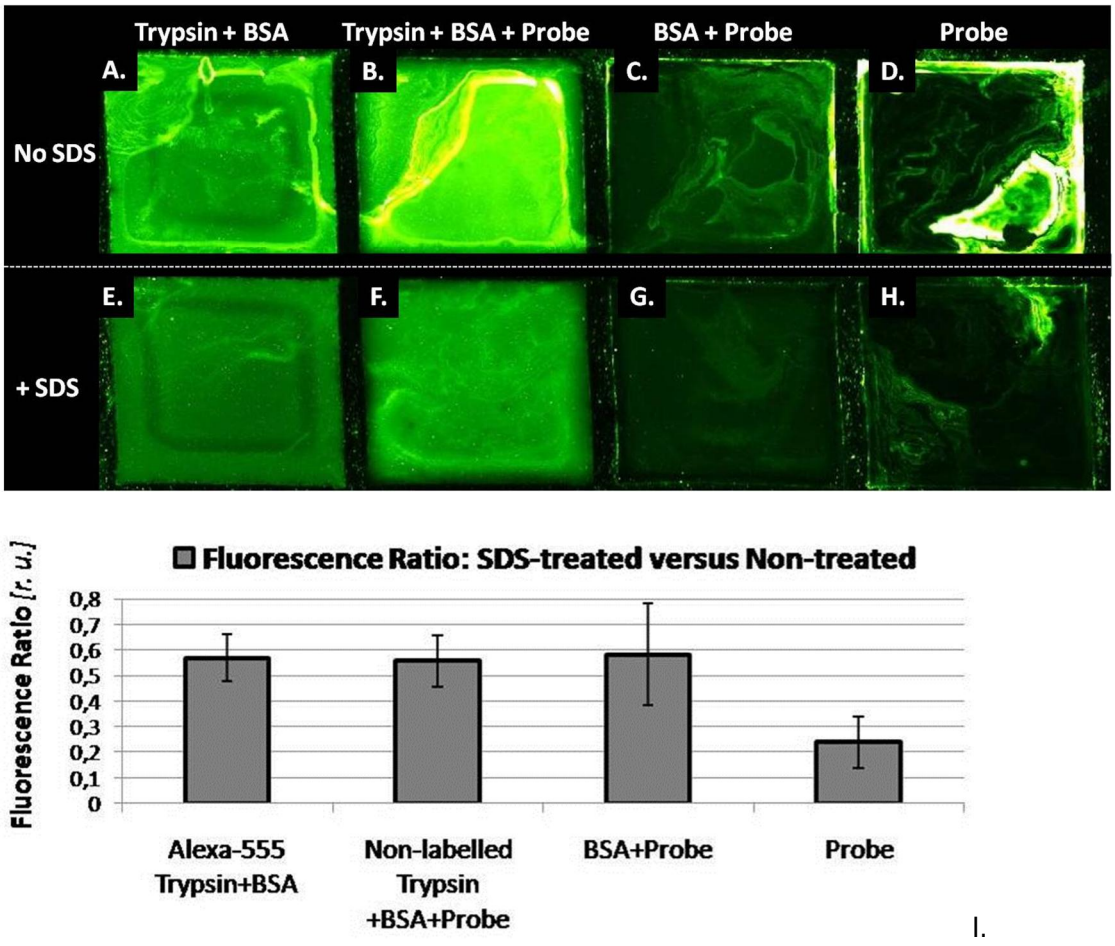

Fig. 3.2.1.5. Influence of SDS washing on the homogeneity and intensity of detected fluorescence.

Fields of deposited ns-TiO_x films of 32 nm roughness were incubated with trypsin (A, B, E, F), blocked with BSA (A – C, E – G) and incubated with the activity probe (B – D, F – H). Half of the fields were subjected to washing with 1 % SDS solution in buffer (E – H), the other half of the fields were washed with buffer only (A – D).

(I) Ratio of the mean fluorescence intensity of the fields with versus without SDS washing. The mean intensity and the standard deviation from the mean were measured on the scanned images by ImageJ.

According to desorption studies (section 3.1.7.), the desorbed fraction on ns-TiO_x of 32 nm roughness at the isotherm plateau coverage of trypsin was estimated as 40 % and hence, could account for a 34 % high readsorbed fraction. Another confirmation of the readsorption of trypsin was found by including a control test in the experiment without the incubation with activity probe. The control test was prepared by adsorbing Alexa-555-labelled trypsin on ns-TiO_x surface and blocking with 1 % BSA; thereafter the samples were subjected to the standard treatment identical with the previous experiments. The only difference was the absence of the activity probe during the 30 minutes long incubation of the adsorbed Alexa-555-trypsin in buffer solution. The scanned images of the dried slides revealed non-homogenous fluorescence intensity along the incubated surface area. In particular, the labelled trypsin that had not been washed away during the slide treatment was evident as irregular traces of bright intensity (Fig. 3.2.1.5. A).

The origin of the uneven distribution of the readsorbed trypsin was a mechanistic one: the removal of the solutions from the microwells was carried out by carefully positioning a pipet at the edge of the well. As a result of the pipetting procedure, remains of the incubation solution containing desorbed trypsin were distributed irregularly and dried out leaving trails of readsorbed trypsin on the surface. The readsorbed patches were not removed despite of subsequent slide rinsing with MilliQ water. Due to the observed effects of trypsin readsorption, it was decided: (i) to minimize the time of incubation with the activity probe to decrease the desorbed amount of trypsin; (ii) to introduce another step in the slide treatment, namely, washing of slides with a detergent solution immediately after the incubation with the activity probe for an efficient removal of any unbound trypsin and activity probe. Sodium dodecyl sulphate (SDS) was selected for the washing of slides based on the studies that have demonstrated that the presence of SDS up to concentration of 1 % does not substantially impair the activity of trypsin (Nelson, 1971a; Porter and Preston, 1975; Wills, 1954). The washing of slides with 1 % SDS was first tested on ns-TiO_x surfaces with homogenously adsorbed trypsin blocked with 1 % BSA, following the incubation either with the activity probe or with the buffer as control. The mean fluorescence intensity and

the standard deviation from the mean was compared on the fields washed with 1 % SDS solution in buffer to the fields washed with buffer only (Fig. 3.2.1.5.).

We characterized the observed non-homogeneity of the fluorescence intensity along the surface area by quantification of the mean intensity per area and the standard deviation from the mean intensity using the ImageJ software. We found that washing with 1 % SDS solution increased the homogeneity of the detected fluorescence by decreased the relative standard deviation (standard deviation normalized by the mean intensity) by a factor of 1.5 for all of the surfaces incubated with trypsin, both, with and without the activity probe (fields A, B, E, F in Fig. 3.2.1.5.). In case of the surface saturated with BSA and incubated with the activity probe, the relative standard deviation of fluorescence intensity per field area was reduced 1.3 times by SDS washing (fields C and G of Fig. 3.2.1.5.). The ns-TiO_x surfaces subjected to activity probe without pre-adsorption of proteins demonstrated equally high standard deviation relative to the mean intensity both, with and without SDS washing (fields D and H, Fig. 3.2.1.5.). Similar effect of SDS washing was observed on ns-TiO_x surfaces of 21 nm, 32 nm and 34 nm roughnesses (32 nm rough ns-$TiO_x$was represented in Fig. 3.2.1.5.). However, besides the reduction of the non-homogenous fluorescence distribution, the washing with 1 % SDS led to a decrement of the mean fluorescence intensity, as evident from the images of Fig. 3.2.1.5. The remained fluorescence intensity after SDS washing was within the boundaries from 45 to 64 % of the non-treated intensity on the fields pre-incubated with trypsin and/ or BSA on all ns-TiO_x surfaces. In contrast, when activity probe was bound directly to ns-TiO_x, 75 % of the mean fluorescence was removed by SDS washing. The remained fluorescence after SDS washing was expressed as the ratio of mean fluorescence of SDS treated versus non-treated fields and plotted in Fig. 3.2.1.5. I. Equal decrease after SDS washing was detected by both, the Alexa-555 fluorescence of the labelled trypsin and the TAMRA fluorescence of the activity probe bound to non-labelled trypsin. We therefore concluded that the non-homogenous fluorescent spikes originated from incompletely washed off readsorbed trypsin that was removed in the case of SDS washing. Thus, the usage of SDS washing could improve the quality of physisorbed trypsin microarrays by enhancement of the background homogeneity.

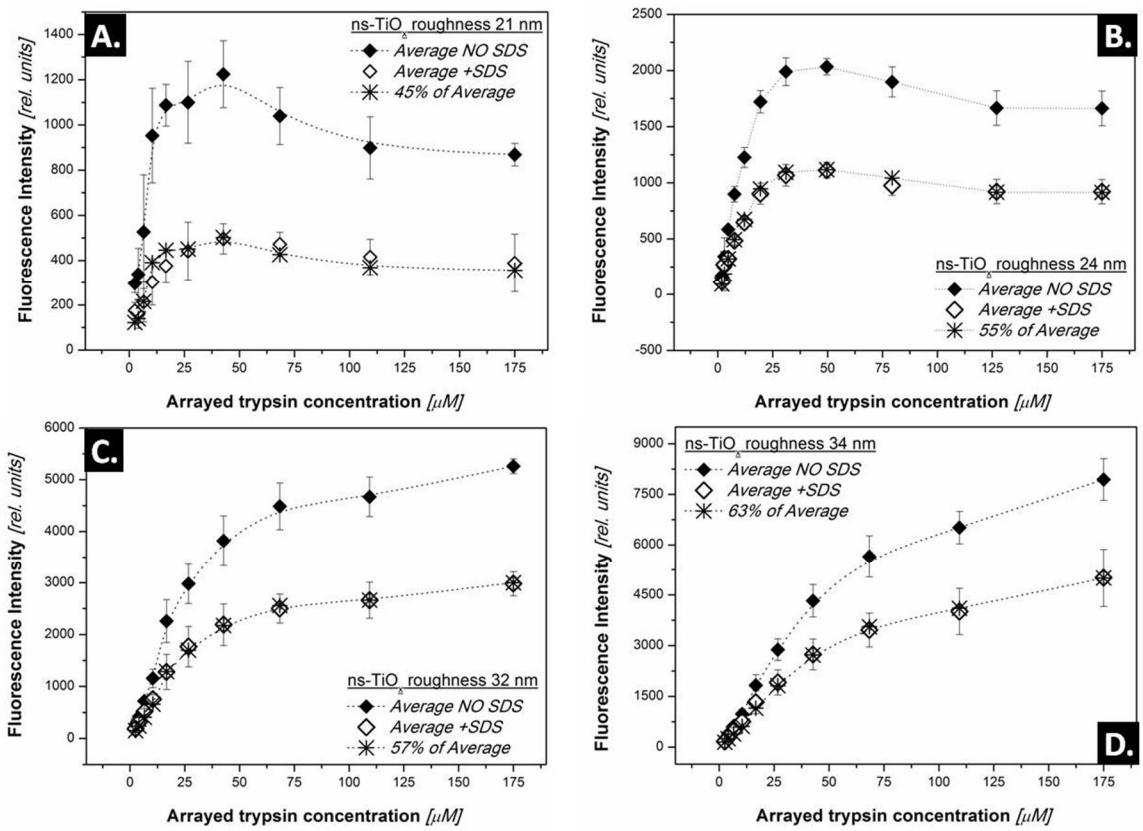

Fig. 3.2.1.6. The effect of washing with 1 % SDS on trypsin adsorption isotherms for various roughness ns-TiO_x: A) 21 nm; B) 24 nm; C) 32 nm; D) 34 nm. Trypsin was arrayed in the concentration range from 2 to 175 μM; half of the arrays were subjected to washing with 1 % SDS solution in 25 mMTris buffer, pH 8. Filled symbols denote the non-treated samples (washing with buffer only), empty symbols stand for the SDS-treated isotherms which were expressed as percentage of the non-treated isotherms and plotted with double crosses. Error bars mark the standard error of three experiments.

As mentioned in the previous paragraph, 36 to 55 % of trypsin adsorbed at the isotherm plateau coverage was removed by SDS washing. We further investigated the influence of SDS washing in the whole isotherm range on ns-TiO_x surfaces of 21, 24, 32 and 34 nm roughnesses (Fig. 3.2.1.6., A. – D.). In Fig. 3.2.1.6., adsorption isotherms of the samples washed only with 25 mM Tris buffer, i.e., the non-treated isotherms, were plotted together with the isotherms detected after washing with 1 % SDS solution in buffer. As demonstrated by the graphs A. – D., on each roughness ns-TiO_x, the SDS-treated isotherms were expressed as percentage of the non-treated isotherms. Hence, we found that SDS had diminished equal percentage of the adsorbed

amount of trypsin at any given surface coverage in the whole isotherm range. The adsorbed amount retained after SDS washing lied between 45 and 63 % for ns-TiO_x samples of different roughness and was well reproducible for every roughness value. Remarkably, the adsorbed amount removed by SDS washing was in good agreement (within the boundaries of the standard errors) with the asymptotic desorbed fraction at the plateau coverage determined by desorption studies against pure buffer (Table 3.2.1.1.). In Table 3.2.1.1., the values of the desorbed fraction estimated in desorption studies are listed together with the desorbed and retained amount after SDS washing normalized by the initial (non-treated) isotherms.

Roughness *[μm]*	**Desorbed Fraction at Plateau** ***(up to 180 min in buffer)*** *[n.u.]**	**Desorbed Amount** ***by SDS washing*** *[n.u.]**	**Retained Amount** ***after SDS washing*** *[n.u.]**
21	**0.56 ± 0.11**	**0.55 ± 0.01**	**0.45 ± 0.01**
24	**0.44 ± 0.07**	**0.45 ± 0.01**	**0.55 ± 0.01**
32	**0.40 ± 0.08**	**0.43 ± 0.04**	**0.57 ± 0.04**
34	**0.38 ± 0.07**	**0.37 ± 0.10**	**0.63 ± 0.10**
			***Units normalized against the initial adsorbed amount**

Table 3.2.1.1. Comparison of desorption upon prolonged exposure to buffer versus desorption by 1 % SDS washing. "Desorbed fraction at plateau" stands for the asymptotic desorbed fraction obtained by the exponential fitting of desorption versus time at the plateau coverage. "Desorbed amount by SDS washing" was calculated as the difference between the measured initial adsorbed amount (non-treated samples) and the retained amount after SDS washing, all expressed in units normalized against the initial isotherms. Data ± standard error of three experiments.

In contrast to desorption experiments where ns-TiO_x films with arrays of adsorbed trypsin were incubated in pure buffer solution for long time intervals (up to 180 minutes), washing with SDS solution was performed in the same buffer (25 mM Tris, pH 8) containing 1 % of SDS for a duration of 1 to 2 minutes. Moreover, the asymptotic desorbed fraction was lower at low trypsin surface coverage and grew with the coverage and with ns-TiO_x roughness. The amount desorbed by SDS treatment however, was not coverage-dependent; instead, at all coverage values, it

corresponded to the asymptotic desorbed fraction characteristic to the isotherm plateau coverage of each ns-TiO_x roughness.

It is known that anionic detergents like SDS, exhibit binding to all polypeptides – based on this phenomenon, numerous ellipsometry studies have been incorporated the elution of preadsorbed proteins by SDS, in order to probe the nature of binding between proteins and surfaces (Santos et al., 2008; Wetterö et al., 2002). It has been shown that SDS binds to proteins via its hydrophobic tail, leading to the exposure of hydrophobic residues and even denaturation under certain conditions (Deepthi et al., 2001; Nelson, 1971b; Yonath et al., 1977), like elevated temperature or high concentration of SDS (Porter and Preston, 1975). As opposed to the hydrophobic interaction between SDS and trypsin, the binding of trypsin to ns-TiO_x can be ascribed to interactions of the hydrophilic trypsin residues with the hydrated surface of ns-TiO_x, as discussed in the section 3.1.5., suggesting minor changes in the conformation of trypsin upon adsorption. The binding to SDS could however, induce changes in the conformation or even denaturation of adsorbed trypsin resulting in its release from ns-TiO_x surface. We consider the removal of trypsin by SDS to be driven by the affinity between SDS and trypsin, rather than affinity between SDS and ns-TiO_x surface, since SDS is an anionic surfactant and ns-TiO_x surface is negatively charged at pH = 8, whereas trypsin carries a net positive charge. The probability of competitive adsorption of SDS replacing trypsin on ns-TiO_x surface is therefore negligible. Instead, the correlation between the remaining adsorbed amount in both experimental setups – by prolonged desorption in buffer or by short washing with SDS – signified that at 1 % concentration, only the reversibly (low affinity) adsorbed population of trypsin was removed by SDS while the irreversibly (high affinity) adsorbed population was retained after the short exposure to 1 % SDS. We assume that at high adsorbed densities, the trypsin molecules removed by SDS belonged to the population adsorbed via low affinity binding, i.e., by protein-protein interactions within the clusters of trypsin. At low coverages however, the amount of trypsin removed by 1 % SDS exceeded the reversibly bound fraction estimated by desorption in buffer indicating that the

hydrophobic interactions between trypsin and SDS competed with the interactions between trypsin and ns-TiO_x.

The influence of the combined activity probe and SDS treatment was tested on the diameter of the arrayed spots of trypsin (Fig. 3.2.1.7.). The spot diameter was quantified for arrays of labelled, non-labelled and 4 % labelled trypsin spots after the treatment with the activity probe including washing with 1 % SDS, versus trypsin arrays that were not subjected to activity probe and SDS treatment. We found that, within the boundaries of the standard deviation, the spot diameter did not exhibit significant differences depending on the applied treatment. The similar behaviour of spot diameter in case of labelled and non-labelled trypsin confirmed that the influence of the fluorophore was negligible. Moreover, the constant size of the spot diameter approved the absence of surface mobility effects putatively induced by SDS binding.

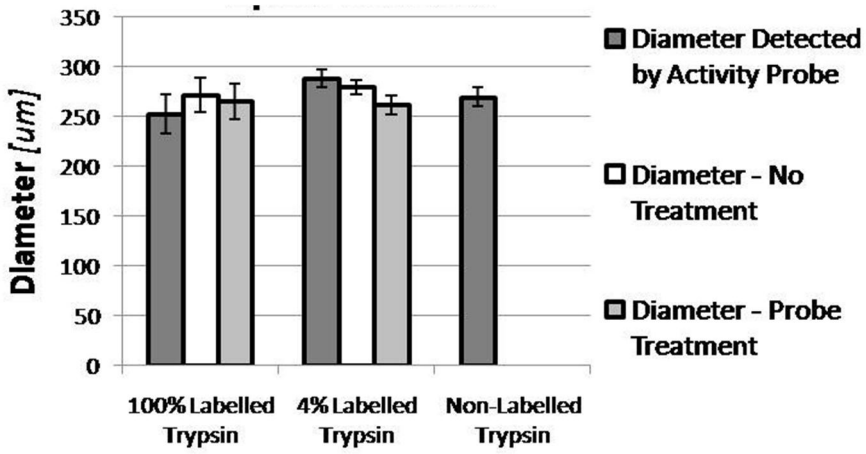

Fig. 3.2.1.7. Influence of activity probe and SDS treatment on the diameter of arrayed trypsin spots. Spot diameter, as detected by the activity probe in the CY3 channel (dark grey columns), was compared to the corresponding spot diameter detected from the signal of labeled trypsin in CY5 channel (light grey columns) and to spot diameter in the case when arrays were not treated with the activity probe and SDS washing (white columns) for labeled trypsin, trypsin containing 4 % of labeled trypsin and non-labelled trypsin.

We further investigated the influence of SDS treatment on the signal and background of trypsin arrays detected in the CY3 channel, respectively, the fluorescence of the TAMRA-labelled activity probe. Gradients of trypsin concentration were spotted as 10 × 10 patterns and incubated

for ten minutes with two concentrations of the activity probe (1 µM and 2 µM), half of the arrays were subsequently washed with 1 % SDS solution in buffer, followed by washing in buffer two times and one rinse in double-distilled water. The control fields were subjected to identical treatment except for the washing with SDS. We analyzed the CY3 channel fluorescence localized on the arrayed spots, as well as the fluorescence of the background between the spots (termed "background"). "Signal" was defined as the mean fluorescence intensity of spot corrected by the subtraction of Background and by the subtraction of the cross-talk signal. The quality of the arrays was characterized by the signal-to-background-ratio. We explored the signal, the background and the signal-to-background-ratio dependence from the arrayed trypsin concentration with and without SDS treatment on the ns-TiO_x of 32 nm roughness (Fig. 3.2.1.8.).

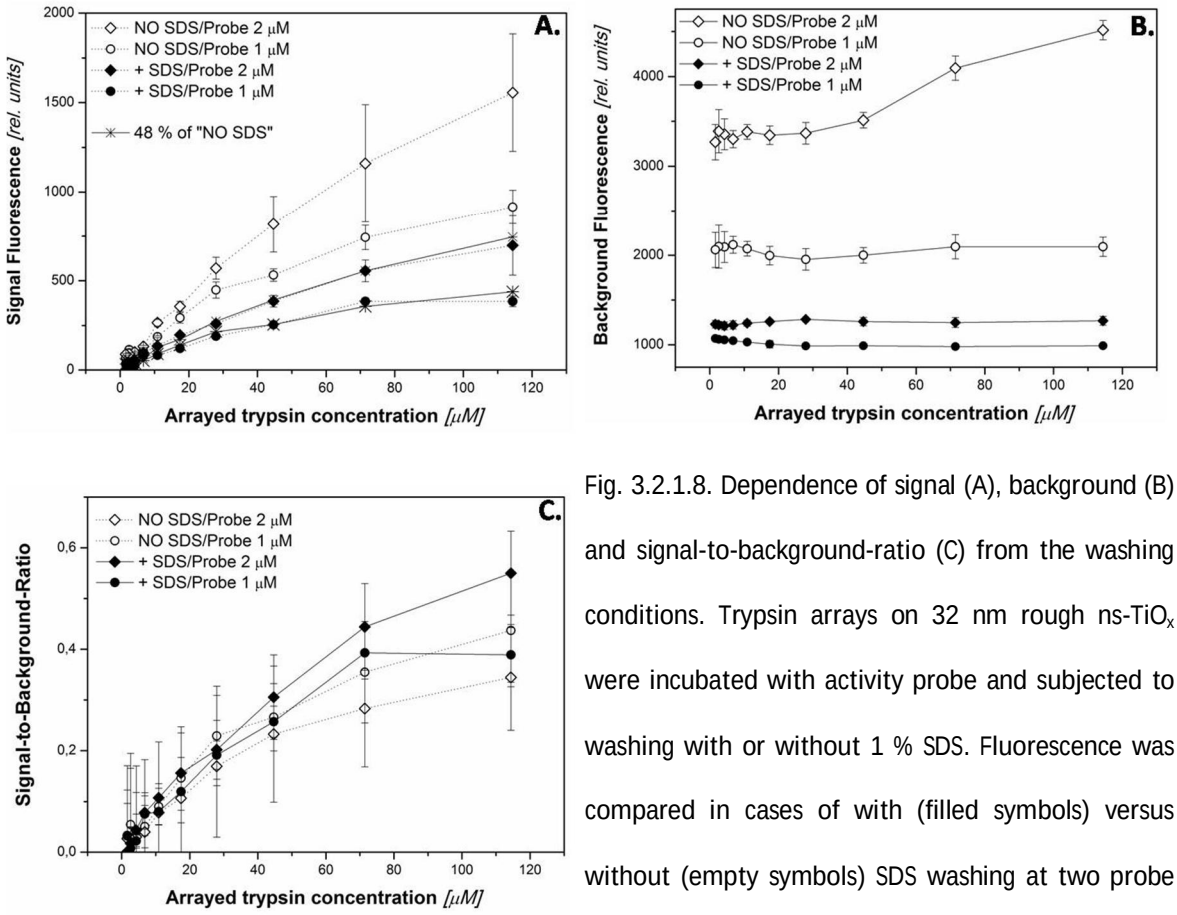

Fig. 3.2.1.8. Dependence of signal (A), background (B) and signal-to-background-ratio (C) from the washing conditions. Trypsin arrays on 32 nm rough ns-TiO_x were incubated with activity probe and subjected to washing with or without 1 % SDS. Fluorescence was compared in cases of with (filled symbols) versus without (empty symbols) SDS washing at two probe concentrations – 1 µM (circles) and 2 µM (diamonds). SDS-treated signals were expressed as 48 % of the non-treated signals (solid lines with crosses in (A)).

As evident from the graph A. in Fig. 3.2.1.8., the activity probe signal was partially removed by SDS washing; in particular, circa 48 % of the initially bound activity probe remained after SDS treatment at both applied probe concentrations, 1 µM and 2 µM. Compared to the impact of SDS treatment on the adsorption isotherms on the 32 nm rough ns-TiO_x sample, 57 % of the initially adsorbed amount of trypsin was retained after SDS washing. This would imply that the difference of 9 % from the adsorbed trypsin was not detected by the activity probe due to reasons related to steric hindrance or loss of activity. Unfortunately, we did not perform detailed studies of the effect of SDS treatment on the signal of the activity probe, in order to draw substantial conclusions about the fraction of trypsin detected by the probe on various roughness ns-TiO_x. We admit that this kind of experiment would be worthwhile to carry out.

Instead, we dedicated more attention to the background fluorescence of the arrays, since it impaired the detection of the spots of trypsin: the lowest arrayed trypsin concentration feasible to detection had to provide a signal that exceeded the relative deviation of the background from its mean value along the area of the 10 × 10 array. In case of trypsin gradient, the background fluorescence was higher at higher arrayed concentration without SDS washing (Fig. 3.2.1.8., B). As mentioned earlier in this section, we explained the occurrence of high background intensity located near the spots of higher arrayed trypsin concentration with the partial readsorption of the desorbed trypsin in the vicinity of the spots. In contrast, if 1 % SDS was applied, the background intensity was significantly reduced in the whole area of the 10 × 10 array. More importantly, however, the elevated background intensity at high trypsin concentrations was removed leaving relatively homogenous average background along the gradient of trypsin, i.e., reducing the relative deviation of the background from its mean value. As demonstrated in the graph in Fig. 3.2.1.8., C., however, the signal-to-background-ratio was improved only at high arrayed concentrations using 2 µM concentration of the activity probe, whereas in the case of 1 µM activity probe incubation, the signal-to-background-ratio remained unchanged within the boundaries of the standard errors. Despite of this, we decided to use the washing procedure with

1 % SDS solution in the further work, in order to increase the homogeneity of the background of the array spots.

We tested the dependence of trypsin microarray signal, background and the signal-to-background-ratio from the incubation time with the activity probe. In this setup, equimolar trypsin arrays at plateau concentration were spotted on ns-TiO_x surfaces of 21, 32 and 34 nm roughness. The activity probe was then applied to each 10 × 10 pattern at different time intervals resulting in up to 60 minutes of incubation time.

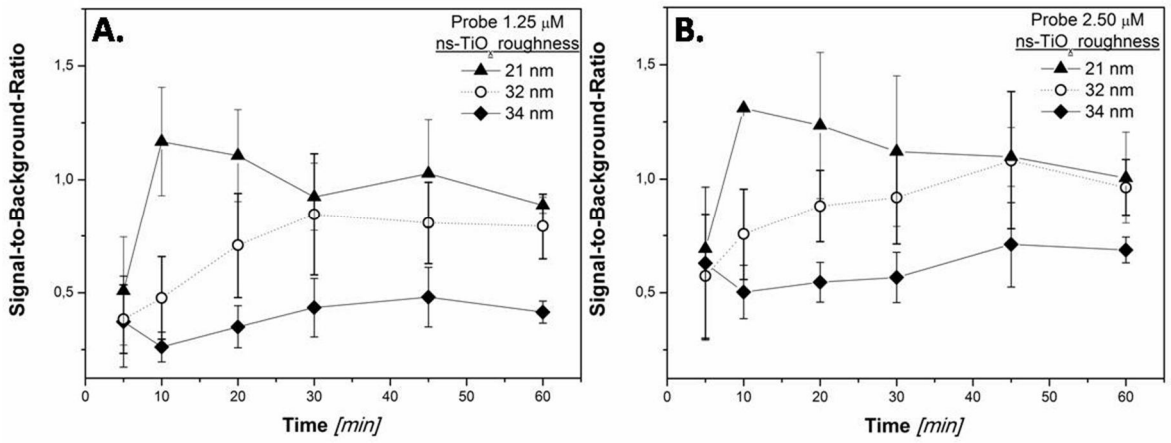

Fig. 3.2.1.9. Signal-to-background-ratio versus incubation time with the activity probe.

Trypsin was arrayed in equimolar 10 × 10 patterns, blocked with BSA and incubated for various time intervals with the activity probe at 1.25 µM (A) and 2.50 µM (B). Signal-to-background-ratio was expressed on various roughness ns-TiO_x: 21 nm (triangles), 32 nm (circles) and 34 nm (diamonds), data ± standard deviations.

The signal-to-background-ratio was different on ns-TiO_x surfaces of different roughness following the sequence: 21 nm > 32 nm > 34 nm at both tested activity probe concentrations (Fig. 3.2.1.9. A. and B.). After 10 minutes of incubation, a slight decrease of the signal-to-background-ratio was detected on the 21 nm rough samples at both probe concentrations. Instead, the signal-to-background-ratio grew with the incubation time on 32 nm rough ns-TiO_x surfaces, doubling at 1.25 µM probe concentration and increasing by a factor of 1.6 at 2.50 µM within 30 minutes. Neither a higher probe concentration, nor a longer incubation time raised the signal-to-background-ratio significantly on ns-TiO_x of 34 nm roughness.

The activity probe binding signal and background was plotted versus time on the ns-TiO_x of 32 nm roughness in Fig. 3.2.1.10. A.

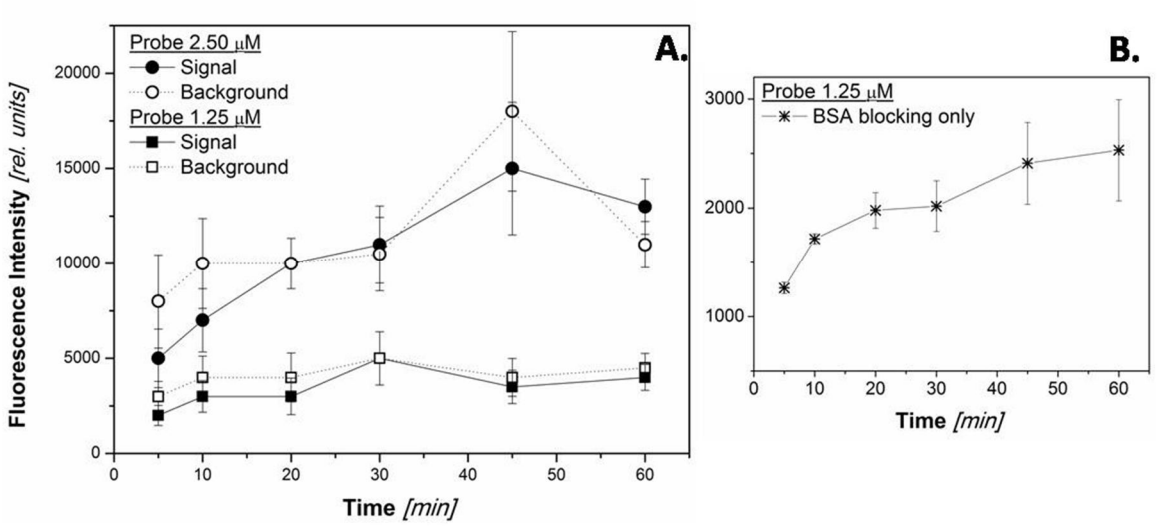

Fig. 3.2.1.10. Signal and background evolution with time.

A) Trypsin was arrayed in equimolar 10 × 10 patterns and incubated for various time intervals with the activity probe at 1.25 μM (squares) and 2.50 μM (circles). Fluorescence intensity was quantified on trypsin spots (Signal, filled symbols) and on the background adjacent to the spots (Background, empty symbols). Data from ns-TiO_x of 32 nm roughness, error bars ± standard deviations.

B) Activity probe at 1.25 μM concentration was incubated on ns-TiO_x surface blocked with 1 % BSA without the spotting of trypsin arrays.

As seen from Fig. 3.2.1.10. A., the signal of trypsin spots, as well as the background adjacent to the spots increased similarly with incubation time at both activity probe concentrations. Both, the signal and the background fluorescence of trypsin spots reached similar levels of intensity and showed similar trends of saturation. Probe binding to the trypsin located on spots became non-linear at around 10 minutes of binding reaction at 1.25 μM probe concentration and already after 5 minutes at 2.50 μM probe concentration. We ascribed the similarity between fluorescence of the spots and the background of trypsin arrays to the presence of readsorbed trypsin on the background adjacent to the spots.

In a parallel experiment, we incubated the activity probe on ns-TiO_x surfaces saturated with the 1 % blocking BSA in the absence of trypsin arrays (Fig. 3.2.1.10. B.). We found that the activity probe binding to BSA was rising likewise non-linearly with time exhibiting levelling-off as soon as after 10 minutes of binding reaction at 1.25 µM probe concentration. Therefore we concluded that the plateau of the background of trypsin arrays was formed partially by the non-linear probe binding to blocking BSA and partially to the readsorbed trypsin. The relative contribution of probe binding to BSA versus binding to readsorbed trypsin depended from the arrayed concentration of trypsin, since a higher amount of trypsin was removed by desorption and by SDS at higher adsorbed coverage. At the tested concentration of trypsin, i.e., 150 µM and the standard blocking concentration of BSA 150 µM incubated with 1.25 µM activity probe, the contribution of BSA was 48 ± 7 %, as estimated from the graphs a) and b) of Fig. 3.2.1.10. Consequently, approximately the half of the array background fluorescence resulted from trypsin readsorption.

We considered the phenomenon of trypsin readsorption to be negligible in case if the goal of the microarray-based activity assay was the assessment of the activity of trypsin that remained immobilized. The semi-quantitative data of activity probe binding was systematically analyzed in relation to the adsorption data acquired from the same microarray spots. Thus, the adsorption signal and background were equally perturbed by desorption and/or readsorption of trypsin cancelling out the differences. Moreover, the leakage of immobilized proteins from the surface is – to a certain extent – inevitable if physisorption is used as the immobilization technique. With the microarray-based activity assay proposed in this work, only the activity of trypsin localized on the array spots is accounted for, excluding the information on the activity of trypsin molecules that were initially physisorbed, but subsequently removed from the array spots due to the protocols used in the method.

On the other hand, the complete methodology of protein-surface-interaction-microarrays (PSIM) enabled us the semi-quantitative characterization of phenomena related to desorption of the physisorbed trypsin in a high-throughput approach. The relative fluorescence units of PSIM

could be further quantified by the method of fluorescence photobleaching quantification (FPQ), translating the relative fluorescence units into the absolute units of protein density or coverage for the assessment of adsorption.

In case of activity estimation of physisorbed trypsin, the relative fluorescence units gave us a direct comparative measure of the relative activity on ns-TiO_x surfaces of different roughness. Here, as well, the relative fluorescence could have been quantified by the FPQ method, expressing the binding of the activity probe in units of moles per second, thus opening the possibility to calculate the classical parameters of enzyme kinetics – the Michaelis-Menten constant and the maximum velocity. However, our setup involved non-classical conditions of the catalysis including the covalent binding of the activity probe instead of reversible binding of a substrate with subsequent product formation. The side reaction of the activity probe, namely, the binding to bovine serum albumin used for array blocking, had a rate comparable to that of probe binding to trypsin, hence the possibility of probe binding to non-active trypsin cannot be excluded, as well. Nevertheless, a validation of the activity of the irreversibly bound trypsin fraction was obtained from a control experiment by measuring the activity of physisorbed trypsin using a conventional chromogenic assay with a synthetic substrate (BAPNA). The results of this experiment will be presented in the next section 3.2.2. of the "Results and Discussion" chapter, in the context of the influence of nanotopography on the activity of adsorbed trypsin.

Unlike physisorption, covalent attachment of trypsin on ns-TiO_x surfaces would have solved the majority of issues in the establishment of a microarray-based assay for trypsin activity detection. However, physisorption was chosen in the first place, in order to explore the interaction of the biomaterial, i.e., ns-TiO_x, with the adsorbed protein. That is to say, the goal of our method was rather high-throughput material screening than enzyme profiling, the latter of which has already been demonstrated in the microarray format using activity-based probes (Chen et al., 2003; Funeriu et al., 2005). Finally, we did not study the classical enzyme kinetics, but rather focused this work on the comparative analysis of the influence of nanoscale roughness on the

activity of the physisorbed trypsin. The method established in this work, was applicable for the described objective, and the obtained results are presented in the next section 3.2.2.

3.2.2. Effect of nanometre-scale morphology on adsorbed trypsin activity

Based on our newly established method, the development of which was described in the previous section 3.2.1., (detailed protocols in the chapter "Materials and Methods"), we investigated the impact of the nanostructured surface morphology on the resulting activity of the adsorbed trypsin. Surface roughness was chosen as the variable again, owing to its role as the key-parameter in protein adsorption to cluster-assembled ns-TiO_x films.

The fluorescence intensity from both channels was detected and analyzed in parallel retaining the spatial connection between the signal localized on the spots versus the background along the gradients of arrayed trypsin concentration. The fluorescence of the CY5 channel gave a direct read-out of the relative amount of adsorbed Alexa-647-trypsin, while the CY3 channel fluorescence was expressed in relative units of the amount of bound TAMRA-activity probe after the compensation of channel cross-talk. Fluorescence intensity detected simultaneously in both channels after 10 minutes long incubation of 10 × 10 patterned trypsin gradients with the activity probe at 1.25 µM concentration was demonstrated for the ns-TiOx samples of four roughness values: 21, 24, 32 and 34 nm (Fig. 3.2.2.1.). The CY3 channel signal was plotted after the cross-talk and background subtraction, thus corresponding exclusively to the adsorption signal of trypsin localized on spots, shown in the graphs (Fig. 3.2.2.1. A., B.). Direct comparison of the relative fluorescence units was not possible since the gain of the photomultiplier tubes of the scanner was set separately to fit the dynamic range of each channel; moreover, there was an up to 25 times difference between the degree of labelling (DOL) of the TAMRA-activity probe (DOL = 1) and Alexa-647-trypsin (DOL from 0.04 to 0.1). For this reason, a direct correspondence between the amount of the surface-bound trypsin and the amount of the bound activity probe could not be derived. Instead, the adsorption signal was quantified by the FPQ method, whereas the activity signal was kept in relative units.

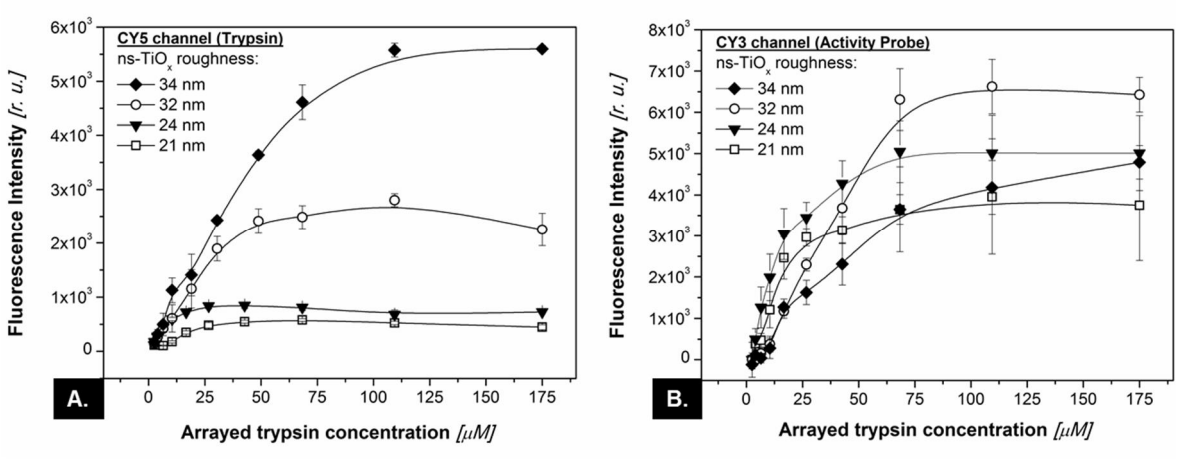

Fig. 3.2.2.1. The simultaneous double-channel detection of fluorescence intensity along trypsin gradients on a panel of ns-TiO_x films.

Alexa-647-trypsin gradients pre-adsorbed on ns-TiO_x were incubated for 10 minutes with the TAMRA-activity probe at 1.25 μM concentration. Fluorescence intensity detected in the CY5 channel (A.) reflected the adsorbed amount of Alexa-647-trypsin, while the fluorescence intensity of the CY3 channel (B.), corrected for cross-talk and background, marked the amount of the TAMRA-activity probe bound to trypsin. Samples of different roughness were assigned, as follows: 21 nm (empty squares), 24 nm (filled triangles), 32 nm (empty circles) and 34 nm (filled diamonds). Data ± standard deviations of two experiments.

Relative activity was defined as the amount of the activity probe bound to physisorbed trypsin per given time interval, having the dimension of relative fluorescence units per minute. To link the activity signal to the adsorption signal, relative activity was plotted against the adsorbed surface density of trypsin, as shown in Fig. 3.2.2.2.

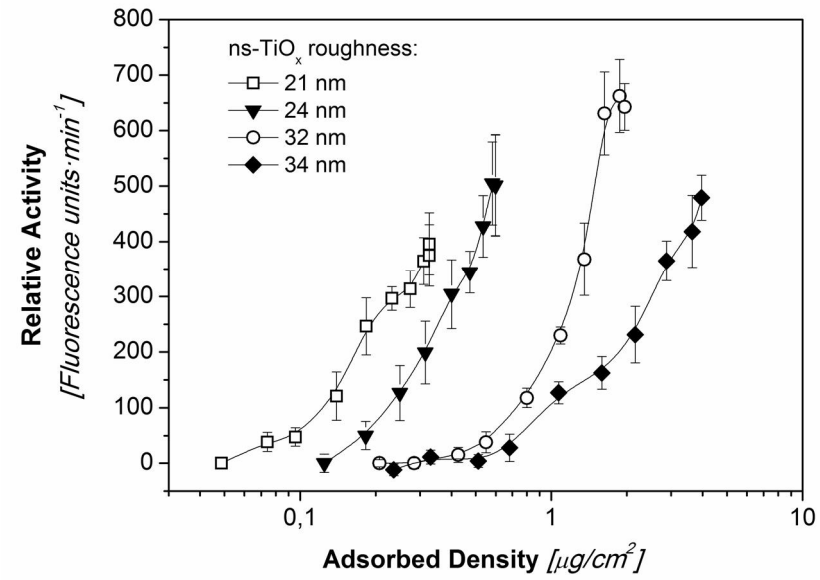

Fig. 3.2.2.2. Relative activity dependence from adsorbed trypsin surface density on ns-TiO_x surfaces of four different roughness values, denoted with symbols ± standard error bars, as follows: 21 nm (empty squares), 24 nm (filled triangles), 32 nm (empty circles) and 34 nm (filled diamonds). Adsorbed density axis was drawn in log_{10}-scale to include the whole studied coverage range.

For a clearer demonstration of all ns-TiO_x samples, adsorbed density was shown in logarithmic scale in Fig. 3.2.2.2. Tracking trypsin activity on different ns-TiO_x samples at particular surface density values revealed that the activity of immobilized trypsin at the same adsorbed density varied from sample to sample. Two main observations were evident from the graphs of Fig. 3.2.2.2.: (i) relative activity increased with trypsin surface density; (ii) relative activity depended on ns-TiOx nanotopography, since different activity was detected at equal surface density on different samples. Relative activity was then divided by the immobilized mass of trypsin corresponding to every surface density value to yield the specific activity (Fig. 3.2.2.3.).

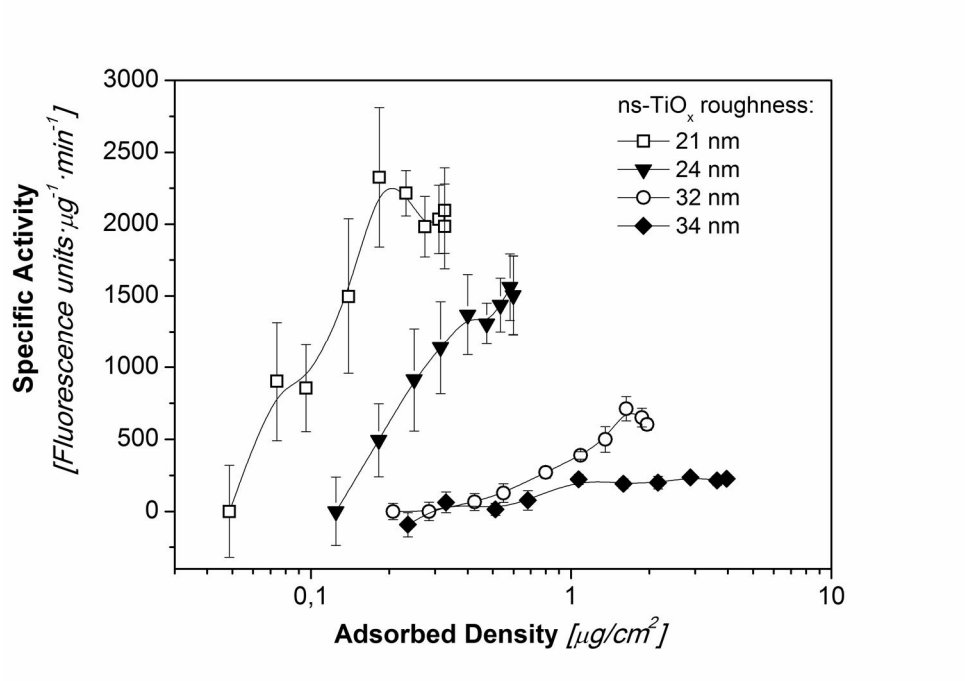

Fig. 3.2.2.3. Specific activity dependence from adsorbed trypsin surface density. Specific activity was obtained by dividing relative activity with the mass of adsorbed trypsin at every surface density value on each ns-TiO_x sample. Symbols ± standard error bars were assigned to ns-TiO_x with roughness of 21; 24; 32 and 32 nm as squares, triangles, circles and diamonds, respectively. X-axis was plotted in log_{10}-scale.

Specific activity was expressed as activity probe binding per time per mass of adsorbed trypsin, respectively relative fluorescence units per minute per microgram. The same two general statements – (i) and (ii), were valid for the specific activity versus adsorbed density curves, as in case of relative activity. Namely, identical adsorbed density values resulted in different specific activity depending on the ns-TiO_x sample. Furthermore, after the initial growth with adsorbed density, specific activity exhibited flattening in the adsorption plateau range on all ns-TiOx samples (Fig. 3.2.2.3.). Remarkably however, the maximum specific activity was detected on the lowest roughness (21 nm) sample; moreover in the whole sampled surface coverage scale, specific activity was always lower at higher ns-TiOx roughness. Instead, the highest relative activity was found at the highest coverage values of the 32 nm roughness sample (See Fig. 3.2.2.2.).

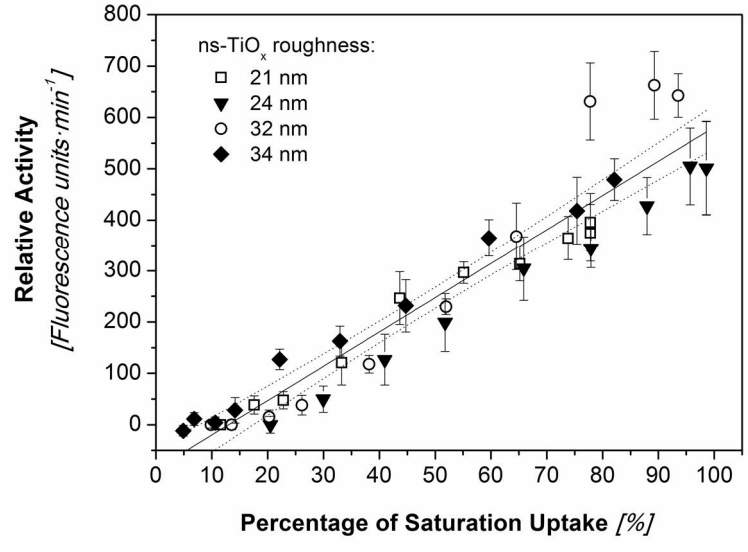

A.

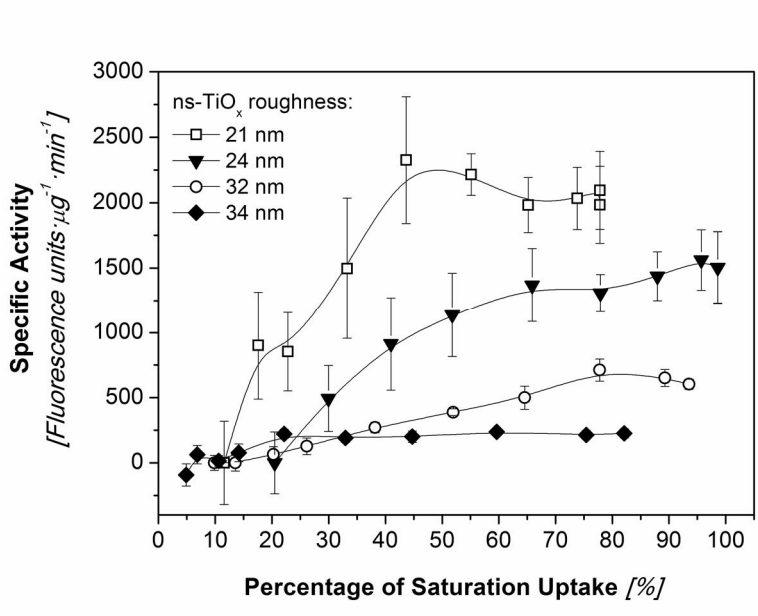

B.

Fig. 3.2.2.4. Activity dependence from the percentage of saturation uptake on various ns-TiO_x samples.

A) Relative activity of adsorbed trypsin versus percentage of saturation uptake density.

B) Specific activity versus percentage of saturation uptake.

For both, A) and B), percentage of saturation uptake was defined as the adsorbed surface density divided by the saturation uptake of every ns-TiO_x sample. In graph (A), the sum of all relative activity curves of all samples was approximated to a linear function and plotted along with its 95% confidence bands (solid and dotted lines). Data points ± standard error bars were marked as before: 21 nm (squares), 24 nm (triangles), 32 nm (circles) and 34 nm (diamonds).

To highlight the impact of the relative loading degree of the nanoporous ns-TiO_x surface on the resulting trypsin activity, we expressed it as relative surface density, respectively, as the percentage of the saturation uptake density on every ns-TiO_x surface. The corresponding relative activity and specific activity curves are displayed in Fig. 3.2.2.4. A., B.

As seen from Fig. 3.2.2.4. A., on all ns-TiO_x surfaces, relative activity was growing similarly at low adsorbed density values up to the surface density of about 75 % of the saturation uptake – described by the linear approximation of the sum of all activity curves. Only at high adsorbed surface density near the saturation uptake of every particular ns-TiO_x sample, activity curves diverged from the common linear trend.

The similarity in the rise of the relative activity with the relative surface density [percentage of saturation uptake] could be explained by the simple increase in the number of adsorbed trypsin molecules with coverage. On the other hand, the diverse levelling-off at saturation uptake density could be related to the restricted number of trypsin molecules that are accessible for the binding of the activity probe – this number of molecules is limited by the highest effective surface area formed by molecules clustering inside the nanopore volume. As reported in our previous study, a flattening of the surface nanotopography, i.e., decrease of the rms-roughness was detected by AFM morphology studies, after the ns-TiO_x surfaces were incubated with protein solutions at high (>k_D) concentrations (Scopelliti et al., 2010). We therefore assume that the effective surface area formed by the ns-TiO_x and adsorbed protein complex decreased at high adsorbed density values. This phenomenon could lead to the saturation of the detected relative activity.

The exact nature of the saturation trends was however complicated and did not scale with the roughness of the ns-TiO_x samples. A more detailed analysis of sample surface topography at high adsorbed protein density would be required in order to describe how the mechanism of pore filling contributes to the decrease of the effective surface area via the changes in the nanopore depth distribution near the saturation uptake. E.g., it would be of interest whether the near-saturation-uptake density corresponds to depletion of the higher end of the depth distribution

spectrum, or only to a shift of the spectrum towards the lower end. Furthermore, the quantitative values of the specific (effective) area near the saturation uptake on ns-TiO_x samples of various roughness would gain an important insight on the fraction of adsorbed molecules available for enzymatic activity assays. It must be noted however, that the nanoscale morphology parameters are probed by the nanometre-sized tip of the AFM apparatus and – although we have proved earlier that the tip-surface convolution effects do not perturb the estimated specific surface area (Scopelliti et al., 2010) – AFM might give an inadequate assessment. Namely, the size of the AFM tip is on the order of magnitude of trypsin molecule (≈ 5 nm) whereas the activity probe used in the enzymatic activity assay of this study is a small molecule the dimension of which is dominated by the fluorophore moiety of carboxytetramethylrhodamine (TAMRA) with the molecular weight around 40 times lower the molecular weight of trypsin. Therefore it cannot be excluded that the surface formed by adsorbed trypsin molecules would possess a higher specific area "seen" by the small molecule activity probe compared to that detected by AFM. It can be further questioned whether the decrease in the specific area accompanying the surface flattening, as we have characterized it by AFM, would result in a similar decrease in the surface area accessible to the small-molecule activity probe.

Besides the drop in the number of accessible trypsin molecules, there is another factor contributing to the reduction of the relative activity of adsorbed trypsin: the autoproteolytic activity typical of protease enzymes. It is well known that trypsin molecules are prone to cleavage by other trypsin molecules in solution (Fraser and Powell, 1950; Sipos and Merkel, 1970; Sriram et al., 1996). The probability of the self-digestion is significantly higher if trypsin molecules are located in proximity of one another, as in case of protein clustering in the ns-TiO_x nanopores. In contrast, a limiting factor for self-digestion of neighbour molecules would be the stabilization and reduced mobility facilitated by adsorption (Kim et al., 2006). From the results of the adsorption and desorption studies of trypsin, we concluded that an important fraction of adsorbed trypsin molecules were bound by protein-protein interactions only, suggesting that the attractive forces between trypsin molecules within clusters could decrease the intermolecular distances promoting

the autoproteolysis and hence, creating a population of inactive trypsin molecules. With the methods used in this study however, it was not feasible to distinguish between the population of the adsorbed molecules that were inactivated by the autoproteolysis and the rest of the adsorbed molecules.

So far, we have analysed the contribution of three major factors to the resulting activity of adsorbed trypsin on ns-TiO_x surfaces, in particular: (i) the increment of activity with the number of adsorbed molecules versus the reduction of activity via (ii) the decrease in effective accessible surface area and (iii) the autoproteolysis at high adsorbed densities. While it was difficult to decipher the behaviour of relative activity near the saturation uptake, its normalization by the adsorbed mass brought more clarity to the involvement of the three listed factors (Fig. 3.2.2.4. A, B). The graphs resulting from the normalization of the relative activity by adsorbed mass show the specific activity as a function of the relative surface density [percentage of saturation uptake] (See Fig. 3.2.2.4. B). All of the graphs displayed an increase up to a certain value of the relative surface density at which point the specific activity started to saturate or even decrease. Notably, the growth rate and the reached peak values of the specific activity were significantly higher on ns-TiO_x samples of lower roughness.

The specific activity by definition, characterizes the catalytic activity of a population of enzyme molecules per total mass or, respectively, the activity per molecule. According to the model of pore volume filling, from the total number of adsorbed molecules, only the fraction exposed on the surface is available for the binding of the activity probe. Analogous observations have often been reported for the recognition of ligands by antibodies where one of the moieties has been immobilized on solid surface: the binding of antibodies is impaired due to steric hindrance caused by the high surface coverage of the adsorbed moieties (Hovgaard et al., 2008; Zhao et al., 2011). In the case of trypsin adsorption on ns-TiO_x, the fraction of non-detected active molecules is excluded from the activity assay via steric hindrance by neighbour molecules or spatial restrictions within the adsorbed protein clusters. Considering the findings on protein multilayer formation and the flattening of the effective surface following protein adsorption, the

number of the adsorbed molecules that do not contribute to the detected enzymatic activity, grows with adsorbed density. The increase of the specific activity up to a certain value of the relative adsorbed density reveals however, that up to high density, the percentage of the surface-exposed molecules grows faster than the percentage of the non-contributing molecules, indicating that the effective surface area of ns-TiO_x and adsorbed protein complex increases faster with coverage than the pore volume filled by proteins. The latter statement holds true up to certain coverage where the levelling-off of the specific activity occurred – a finding that is in agreement with the decrease in effective surface area caused by the surface flattening observed in the high surface density range, as mentioned in the paragraph on relative activity. Furthermore, the peak specific activity was reached at lower relative density values on the two samples of lower roughness. This observation suggests that the lower k_D value, i.e., the faster saturation of protein adsorption at lower roughness could induce the surface flattening effect at lower relative density. The proposed hypothesis however, should be verified by exploring the dependence of surface flattening from ns-TiO_x sample roughness.

The observation of more rapid growth and higher peak values of the specific activity on the samples of lower roughness is directly linked to the mechanism of protein adsorption on ns-TiO_x surfaces. We described previously that the nanopore depth distribution shifts towards higher depth at higher ns-TiO_x roughness while retaining similar pore width distribution, moreover, both, the total nanopore volume and the number of protein molecules per cluster increase with ns-TiO_x roughness (Scopelliti et al., 2010). We conclude that as a consequence of the mentioned effects, the percentage of the non-contributing molecules is higher at higher ns-TiO_x roughness leading to lower specific activity at higher roughness.

Considering the impact of auto-proteolysis on the specific activity of immobilized trypsin, we expect the inactivation of adsorbed molecules by self-digestion to be more pronounced on the samples of higher roughness, as a consequence to the higher absolute surface density of trypsin. Additionally, adsorption isotherms in the roughness range from 24 to 34 nm were characterized by a Hill coefficient larger than 1, signifying cooperative trypsin adsorption accompanied by

attractive protein-protein interactions. Such interactions between the neighbour molecules within the adsorbed clusters would have a high probability of the occurrence of autoproteolysis. To assess the effects induced by autoproteolysis selectively, it would be necessary to quantitatively estimate the relative increase in the filled volume fraction as well as the relative decrease of the effective surface area at high coverage, e.g., by AFM morphology characterization. Since we have not performed this analysis, it remains questionable whether the growth rate of specific activity versus relative surface density was lower due to autoproteolysis on the ns-TiO_x samples of higher roughness.

To highlight the role of ns-TiO_x roughness in the resulting catalytic activity of adsorbed trypsin, we examined as function of roughness both, the relative and the specific activity detected near the saturation uptake (Fig. 3.2.2.5. A.) Within the sampled roughness range, relative activity was at first growing, reaching its maximum around 30-32 nm roughness and decreasing at the highest roughness (Fig. 3.2.2.5. A., empty symbols). The occurrence of a peak activity can be understood as a result of two controversial trends. Relative activity rises with sample roughness benefiting from the increment of the adsorbed amount of trypsin with roughness. On the other hand, the decrease of the relative activity at the highest probed ns-TiO_x roughness is not fully understood – a hypothetical cause could be the autoproteolytic inactivation of a fraction of trypsin molecules facilitated by the high adsorbed density reached on the rougher surface. In order to verify this hypothesis, it would be interesting to extend the probed range of adsorbed trypsin surface density in a controlled manner, as well as the range of ns-TiO_x sample roughness.

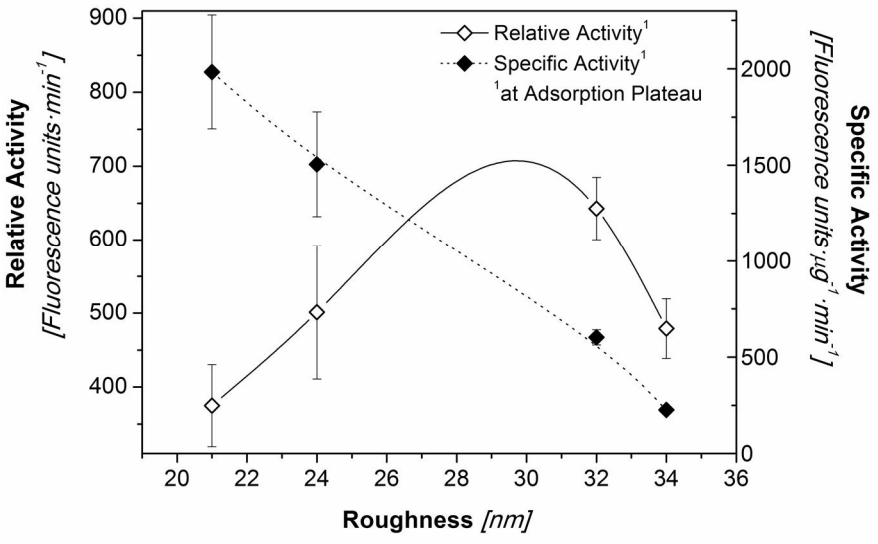

A.

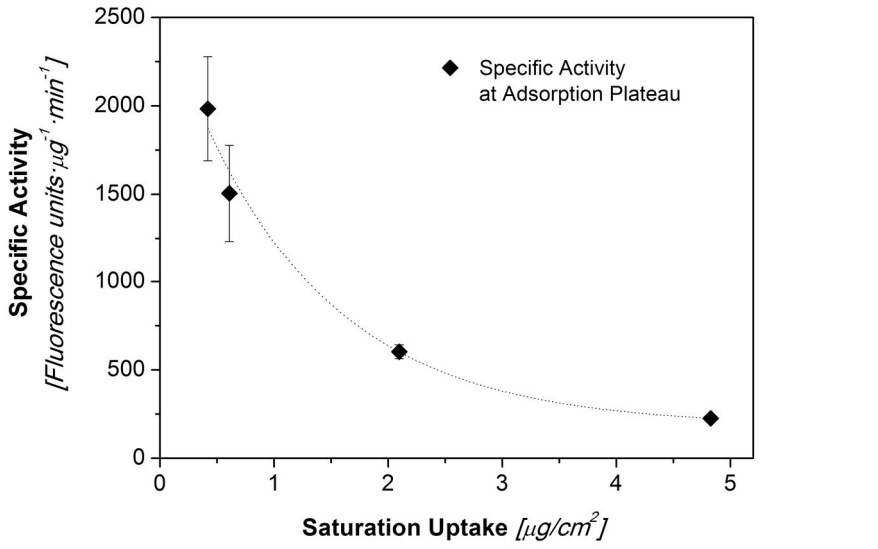

B.

Fig. 3.2.2.5. Dependence of trypsin activity from ns-TiO_x roughness and saturation uptake. Both, the relative and the specific activity correspond to the plateau coverage of adsorbed trypsin.

A) Relative (empty symbols) and specific (filled symbols) activity versus roughness.

B) Specific activity versus saturation uptake surface density expressed in µg/cm^2.

Data points ± standard error bars were obtained from three experiments.

Remarkably, the specific activity dropped almost linearly with roughness (Fig. 3.2.2.5. A., filled symbols). We already pondered on the close linkage between the ns-TiO_x roughness and the mean depth of the surface nanopores, and the adsorbed trypsin density determined by the latter

two nanoscale topography parameters (discussion of the adsorption results, section 3.1.5.). Here, we reckon that the decrease of the specific activity with roughness is in accordance with the respective increase of the adsorbed density with roughness, which, in turn, indicates that, a growing fraction of the catalytic sites within the nanopores become inaccessible for the binding of the activity probe. We have demonstrated this relation directly in Fig. 3.2.2.5. B., where specific activity was plotted against the adsorbed density at the isotherm plateau, i.e., against the saturation uptake. A similar finding of specific activity drop with the growth of the immobilized mass was reported by Shtelzer et al. who explored the effect of encapsulation on activity of trypsin in mesoporous sol-gel glass matrices (Shtelzer et al., 1992). The authors interpreted the decline in activity by the formation of trypsin aggregates within the matrix pores that limited the access of catalytic substrate molecules.

In order to cross-check the results on physisorbed trypsin activity obtained by the newly proposed microarray-based approach, in parallel, we performed measurements with the well-established method of chromogenic synthetic substrate Nα-Benzoyl- DL -arginine 4-nitroanilide hydrochloride, shortly termed BAPNA. Assays that imply the usage of chromogenic or fluorometric enzyme substrates, are optimized for the detection of activity of free enzymes in solution. In case of physisorbed enzymes, the solution-based assays suffer from the occurrence of desorption and hence, lack of distinction between the activity originating from bound versus unbound enzyme species. To avoid the co-detection of desorbed trypsin, ns-TiO_x surfaces were subjected to extensive washing after two hours of incubation with trypsin solution and prior to the colorimetric activity test, thus removing the reversibly adsorbed population, as found in the desorption studies (Section 3.1.7.).

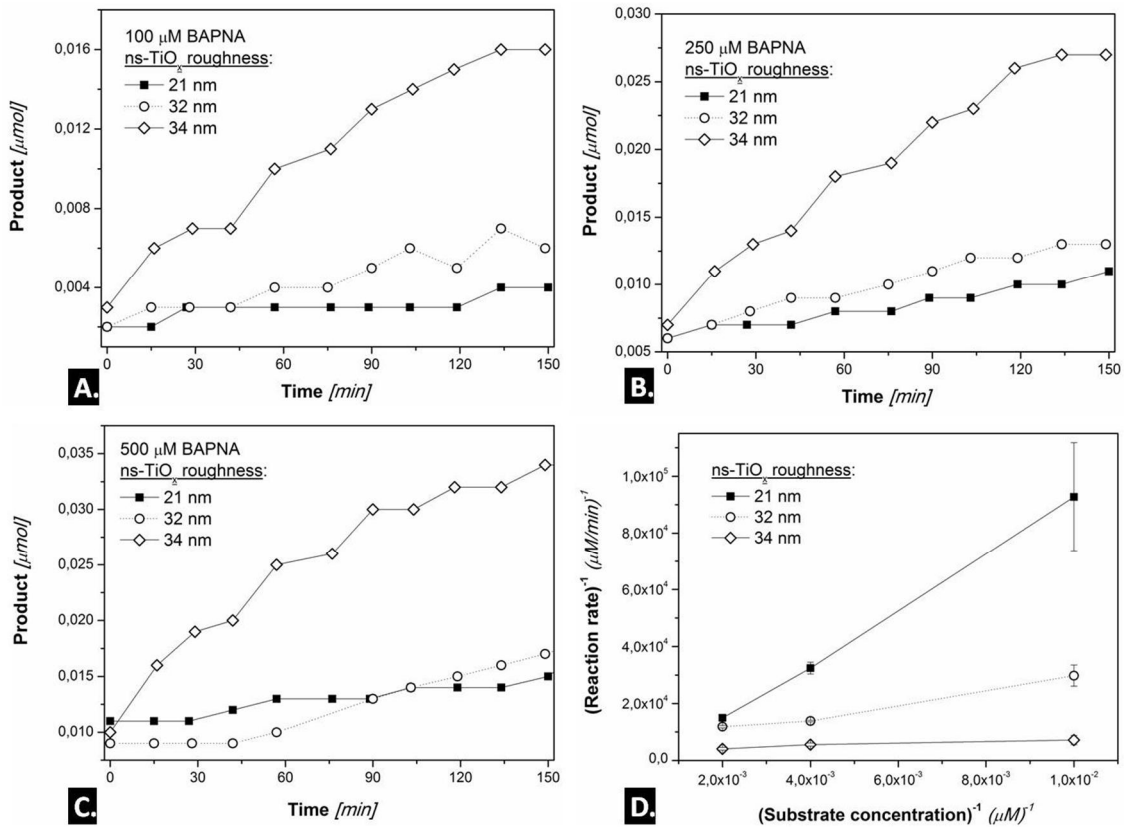

Fig. 3.2.2.6. Adsorbed trypsin activity measurement by conventional chromogenic substrate BAPNA assay.

(A) – (C) The concentration of the reaction product was detected as increase of the absorbance at 410 nm of the reaction solution incubated on top of ns-TiO_x surfaces pre-incubated with trypsin and washed for the removal of the reversibly bound fraction prior to the activity assay at three BAPNA concentrations: 100 μM (A), 250 μM (B) and 500 μM (C). The reciprocal (Lineweaver-Burk) plot of reaction velocity versus reciprocal substrate concentration was used to determine the kinetic parameters of adsorbed trypsin (D). Roughness of ns-TiO_x: 21 nm (squares), 32 nm (circles) and 34 nm (diamonds).

Activity assay was performed on ns-TiO_x of 21, 32 and 34 nm roughness probing three BAPNA concentrations (Fig. 3.2.2.6. A – C) and measuring the absorbance of the cleaved reaction product p-nitroaniline at distinct time intervals. As seen from the reaction curves in Fig. 3.2.2.6., the amount of the created product increased slowly with time showing saturation trends within the time scale of an hour due to the minute amount of trypsin present on the surfaces, resulting in the effective molar concentrations in the nanomolar range. Product concentration grew significantly more rapidly on the ns-TiO_x surface of 34 nm roughness, compared to the other two surfaces. To obtain quantitative measures of adsorbed trypsin activity, we used the Lineweaver-

Burk linearization of Michaelis-Menten kinetics and constructed a reciprocal plot of the reaction velocity versus the reciprocal of the initial BAPNA concentration, as demonstrated in Fig. 3.2.2.6. D.

The experimentally determined kinetic parameters for adsorbed trypsin were listed in Table 3.2.2.1. and compared to the typical range of kinetic parameter values for trypsin reported in literature. We found that the maximum reaction velocity increased with ns-TiO_x roughness, thus disagreeing with the sequence 21 nm < 34 nm < 32 nm of activity increase determined by the microarray-based approach. This result implied that the relative activity, obtained as the amount of activity probe bound to trypsin per unit of time in the microarray setup, cannot be directly translated into the reaction velocity units of BAPNA cleavage. The explanation could be the different principles of the two activity assays: the former is taking the advantage of an irreversible binding reaction, while the latter one is measuring the outcome of a second order reaction kinetics. Nevertheless, we expected that the relative activity measured by both methods would obey similar trends.

The Michaelis constant K_M, in turn, decreased with ns-TiO_x roughness suggesting a faster approaching of the maximum reaction rate with increasing surface roughness, whereby the values of K_M were in the range of and slightly lower than the values published in literature for trypsin interaction with BAPNA as substrate (Dallas Johnson et al., 2002; Goradia et al., 2005). The turnover number k_{cat} corresponds to the forward reaction rate of the enzyme-substrate complex conversion to product and free enzyme characterizing the activity in terms of the number of substrate molecules that can be transformed into product per second. We observed an impaired turnover rate of adsorbed trypsin: k_{cat} was approximately one order of magnitude lower than its values reported for free trypsin in solution (Dallas Johnson et al., 2002; Treetharnmathurot et al., 2008). The value of k_{cat} was lower at high roughness values – an observation that could be interpreted by steric hindrance of the active site of trypsin molecules at high adsorbed densities, i.e., on ns-TiO_x of higher roughness. The specific activity defined as the maximum reaction rate per total amount of the enzyme, was found to decrease with roughness and its absolute value at

21 nm roughness was within the range reported for trypsin in solution, while on higher roughness surfaces, the specific activity of trypsin dropped below the level typical of trypsin in solution (Seabra and Gil, 2007; Yiu et al., 2001a) (Table 3.2.2.1.). The quantitative values obtained by the BAPNA assay confirmed that the irreversibly adsorbed fraction of trypsin maintained on ns-TiO_x surface after washing, exhibited catalytic activity slightly lower and comparable to that of trypsin in solution. These results indicate that the major fraction of trypsin retained an active conformation upon adsorption on ns-TiO_x surfaces.

ns-TiO_x Roughness	Adsorbed enzyme	Maximum velocity Vm	Michaelis constant K_M	Turnover number k_{cat}	Specific Activity
nm	µg/cm²	nmol · min⁻¹	mM	s⁻¹	µmol · min⁻¹ · mg⁻¹
21 nm	0.12 ± 0.01	0.18 ± 0.06	1.8 ± 0.6	0.5 ± 0.1	1.1 ± 0.4
32 nm	0.49 ± 0.09	0.16 ± 0.06	0.4 ± 0.2	0.10 ± 0.03	0.26 ± 0.09
34 nm	0.60 ± 0.06	0.27 ± 0.04	0.10 ± 0.04	0.14 ± 0.02	0.35 ± 0.06
Literature data			*0.77[1] - 1.72[2]*	*1.44[2] - 6.1[3]*	*0.46[4] - 2.89[5]*

Table 3.2.2.1. Kinetic constants of adsorbed trypsin on various roughness ns-TiO_x.

The maximum velocity V_m, Michaelis constant K_M and turnover number k_{cat} were determined according to standard Michaelis-Menten kinetics. Specific activity was expressed as the maximum velocity per total mass of adsorbed trypsin. The range of the values reported in literature on trypsin activity with BAPNA as substrate, are given for K_M, k_{cat} and the specific activity from the following sources: (1) Goradia et al. 2005; (2) Dallas Johnson et al. 2002; (3) Treetharnmaturot et al. 2008; (4) Yiu et al. 2001; (5) Seabra & Gil. 2007.

To enable a direct comparison of the two diverse approaches to the detection of adsorbed trypsin activity, we expressed the specific activity estimated by both methods in relative units normalized against its highest value (Fig. 3.2.2.7.). As seen in the graph in Fig. 3.2.2.7., the activity values measured for ns-TiOx samples of 32 nm and 34 nm roughness were significantly different, however, the average specific activity values in the 32 to 34 nm roughness region converged to similar specific activity determined by both methods.

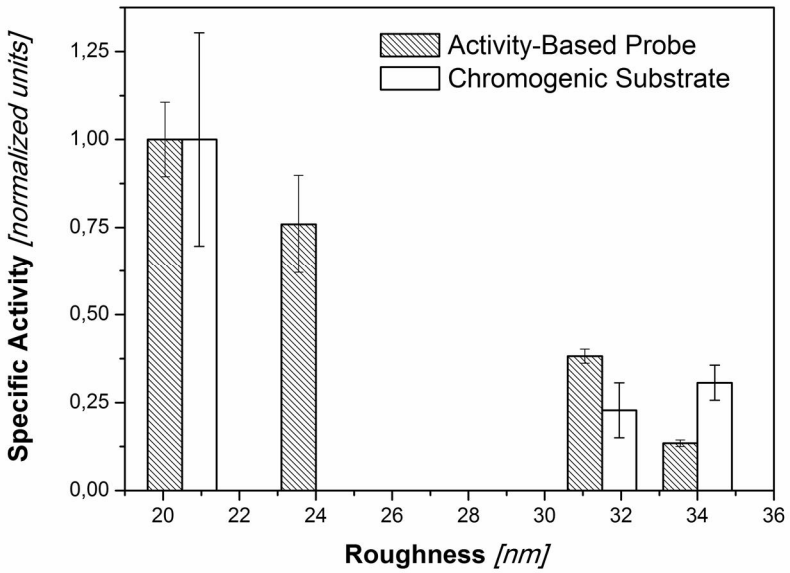

Fig. 3.2.2.7. Specific activity as function of ns-TiO_x roughness estimated by two conceptually different methods: the activity-based probe binding in microarray format (dark columns) versus the standard chromogenic substrate BAPNA assay (bright columns).

The activity of immobilized trypsin has mostly been studied with the aim to optimize the methods of protein digestion for mass spectrometry. Up to date, protein digestion by trypsin in solution is the standard protocol of peptide preparation prior to further analysis. Meanwhile, there have been numerous attempts to improve the efficiency and to accelerate the tryptic digestion process (Kim et al., 2010). One of the key ideas in reaching the mentioned goals is the spatial confinement of trypsin which in some cases can lead to an enhanced stability and even a higher catalytic activity of trypsin (Kim et al., 2009; Liu et al., 2005). However, within the scope of trypsin implementation for proteomics tools, the immobilization by physical adsorption has been of least interest due to the leakage of physisorbed enzyme during multiple operation cycles. Instead, the covalent binding (Huckel et al., 1996) or the cross-linking (Migneault et al., 2004) of trypsin on solid substrates, including nanoparticles (Li et al., 2007), as well as the encapsulation of trypsin in sol-gels (Braun et al., 1991; Braun et al., 1992; Park and Clark, 2002; Pluskal et al., 2002; Shtelzer et al., 1992) has been among the preferred methods to achieve stable immobilization.

For covalent binding, crosslinking and encapsulation, the chemical properties of the immobilization substrate and reactants are of primary importance for the resulting activity and stability of trypsin; additionally for encapsulation – the spatial dimensions of the matrix play a key role. In few cases, physical adsorption has been chosen as the immobilization method, in particular, for the entrapment of trypsin in siliceous molecular sieves, taking advantage of the ordered network of pores with tailored diameter (Díaz and Balkus Jr, 1996; Gómez et al., 2003; Goradia et al., 2005; Jang et al., 2006; Matsuura et al., 2010; Yiu et al., 2001b). The central issue of these studies has been the immobilization chemistry and the pore diameter sufficiently large to accommodate trypsin. The influence of the size of nanoscale pores on the adsorption and activity of adsorbed trypsin has been analyzed within the scope of the applicability of these immobilized trypsin systems as microreactors for proteomic digestion, emphasizing the leakage of enzyme. To prevent the leakage, physisorption is almost exclusively accompanied by silanization (Díaz and Balkus Jr, 1996), otherwise silicate surfaces are functionalized with reactive groups (Casadonte et al., 2010; Jang et al., 2006; Yiu et al., 2001b). In some cases, the activity of trypsin encapsulated inside the mesoporous silicates has been reported higher than or comparable to that of aqueous trypsin (Gómez et al., 2003; Goradia et al., 2005), whereas elsewhere the lowered activity has been attributed to steric blockage of trypsin active site upon adsorption (Díaz and Balkus Jr, 1996). In the context of trypsin immobilization on ns-TiO_x surfaces, the lesson from the numerous enzyme encapsulation studies is the concern about the restricted accessibility of the immobilized enzymes, since this was proven to occur in the same manner to trypsin adsorbed on the randomly-rough nanoporous surface of ns-TiO_x (Braun et al., 1992; Shtelzer et al., 1992).

In contrast to the aforementioned studies, our intention was to dissect the means of nanometre-scale surface topography influence on the activity of the physisorbed trypsin. Considering the nature of trypsin binding to ns-TiO_x surfaces, the non-specific adsorption occurs presumably via coordinated covalent bonding between carboxyl-terminated amino acid residues and undercoordinated titanium atoms, as proposed in the earlier work by our group (Giorgetti et al., 2008; Vyas et al., 2011). Hydrogen bonds resulting from the opposite surface charges of

trypsin and ns-TiO_x at the used buffer pH = 8, could also contribute to trypsin adsorption to ns-TiO_x., as noted in the discussion of section 3.1.5.

In the current study however, we focused on the topographical determinants of the non-specific protein adsorption on ns-TiO_x. We have characterized the impact of surface roughness and specific area on the activity of physisorbed trypsin, as the main parameters of the nanoscale topography. Moreover, we have linked the observed activity dependence with the particular geometrical constraints of the nanopores in relation to the adsorption mechanism known from our previous study. The evolution of the specific activity of adsorbed trypsin with the nanometre-scale roughness of ns-TiO_x surfaces was confirmed by the standard colorimetric activity assay validating the findings of the newly established microarray-based method.

The findings of the current study have relevance in the general knowledge on the behaviour of enzymes at nanostructured material interfaces – the effect of the detailed nanopore geometry on the adsorbed enzyme activity has never been analysed before, to our knowledge. Furthermore, these results are directly applicable to screening of biomaterials and enzyme immobilization techniques that can be extended beyond the trypsin-ns-TiO_x model used here. In particular, we have demonstrated that the nanometre-scale surface topography parameters can be optimized thanks to a trade-off between the amount of enzyme that can be immobilized and its peak activity.

4. CONCLUSIONS AND PERSPECTIVES

4.1. Conclusions

4.1.1. Development of a new approach for high-throughput surface-bound enzyme activity detection in microarray format

- A new microarray-based method for the detection of the catalytic activity of surface-bound enzymes has been proposed and validated using the model system of trypsin, a proteolytic enzyme of serine hydrolase family, immobilized by physical adsorption on the surfaces of cluster-assembled nanostructured titanium oxide thin films. The activity was read-out as the fluorescence signal of the binding of a commercially available activity-based small-molecule probe to trypsin pre-adsorbed on the material surfaces under investigation.

- The newly established technique opens the possibility of the simultaneous detection of the amount and the activity of enzymes immobilized on slide surfaces coated with materials of interest in a high-throughput manner.

- The novel methodology was verified by a standard colorimetric activity assay showing agreement in terms of the estimated specific activity.

- In contrast to existing activity assays aimed at the characterization of *enzymes*, the goal of the proposed method is the high-throughput screening of biomaterial libraries for the characterization of *enzyme-surface interactions*. In this sense, our method is a novelty.

- The major advantage distinguishing the proposed method from other existing activity assays is its applicability to enzymes immobilized by physisorption without the requirement of surface functionalization, covalent attachment or encapsulation, as opposed to the majority of microarray-based techniques.

- The requirements of the method include: (i) any material of interest provided that it can be fabricated into a transparent coating of standard array slides; (ii) choice of the immobilization method depending on the studied material surface; (iii) fluorescent labelling of the enzyme

molecules of interest; (iv) fluorescently-tagged activity-based probes synthesized for the studied group of enzymes.

4.1.2. Nanometre-scale topography effects on trypsin adsorption characteristics

- The adsorption of trypsin on nanostructured titanium oxide has been characterized by the high-throughput PSIM method covering the enzyme concentration range from 0.5 to 150 µM on a panel of ns-TiO_x thin films of six different nanometre-scale surface topographies within the roughness interval from 15 to 34 nm.
- The adsorbed amount of trypsin overstepped the value predicted by the geometric increase in surface area of ns-TiO_x films.
- The saturation uptake of ns-TiO_x samples – with the exception of the lowest roughness surface – exceeded the theoretical value of one full monolayer reaching up to 22 theoretical monolayers on the highest roughness sample.
- Adsorption isotherms on the two lowest roughness samples were described with accuracy with the Langmuir adsorption model, whereas on higher roughness samples, adsorption behaviour was in accordance with the Hill model.
- The values of the Hill coefficient indicated cooperative adsorption.
- The non-linear increase of the saturation uptake and the equilibrium dissociation constant with ns-TiO_x roughness was in agreement with the findings of the earlier work by our group suggesting that trypsin adsorption proceeded as the clustering of molecules inside the volume of nanopores, as opposed to homogenous surface coverage.
- Homogenous exchange of trypsin was studied by FRAP in the low quasi-linear sub-monolayer range of the adsorption isotherm.
- The exchange reaction was a desorption-rate limited process described with a monoexponential model.
- Desorption against buffer was studied by PSIM in the whole isotherm range up to saturation plateau coverage.

- Desorption was modelled as monoexponential decrease of the adsorbed surface density, implying the co-existence of one reversibly bound and one irreversibly bound population on ns-TiO_x surfaces.

- The irreversibly adsorbed fraction increased with ns-TiO_x roughness and decreased with trypsin surface density suggesting that the irreversibly bound population can be attributed to trypsin bound to ns-TiO_x whereas the reversibly bound population can be ascribed to trypsin molecules within the clusters bound by protein-protein interactions.

4.1.3. Influence of nanometre-scale morphology on the activity of adsorbed trypsin

- At equal adsorbed densities, the relative activity of trypsin was higher on ns-TiO_x samples of lower roughness – according to the pore filling model of adsorption, this implied the loss of activity due to steric hindrance on higher roughness samples characterized by higher average pore depth.

- At the saturation uptake densities, the relative activity grew with ns-TiO_x roughness according to the sequence 21 nm < 24 nm < 34 nm < 32 nm exhibiting a peak at 32 nm roughness.

- The specific activity expressed per mass of adsorbed enzyme, decreased linearly with ns-TiO_x roughness reflecting the reciprocal increase with roughness of the population of immobilized molecules that were rendered inactive by steric hindrance due to clustering inside the nanopores.

4.2. Perspectives

4.2.1. Possibilities towards a better understanding of the studied model system

- Trypsin adsorption on flat titanium oxide surface with the proposed methodology

- Usage of nanofabricated titania surfaces with nanometre-scale pores with a well defined geometrically ordered shape, as opposed to the stochastically-rough nanoporous surfaces used in this study.

- Additional studies that would shed light on the role of nanometre-scale surface topography in the mechanism of protein adsorption include the AFM investigation of the relative change in the surface specific area upon adsorption of proteins on various roughness ns-TiO_x surfaces. The evaluation of the specific area formed by the complex of adsorbed enzymes on top of titanium oxide surface is a non-trivial question, since the adsorption does not proceed as homogenous coverage of a planar surface. Moreover, it would be of particular interest to assess the relative change in the effective surface area upon enzyme adsorption because the detected enzyme activity is directly related to the availability of active sites, i.e., to the effective area formed by enzyme molecules exposed on the surface.

- Additional methods, such as scanning electron microscopy or transmission electron microscopy, might give a more adequate picture of the nanoporosity, the nanopore shape and volume, as well as the specific area of the studied cluster-assembled titanium oxide films, since these methods are not limited by the finite size of the scanning probe, as it is the case in scanning probe microscopies.

- Antibody detection of the adsorbed enzymes using our high-throughput microarray-based setup would aid relevant complementary information about the relative amount of enzymes available on the surface for antibody recognition.

- The quantification of the fluorescence signal of the TAMRA-activity probe would gain the absolute values of trypsin activity. This quantification can be performed by the confocal microscopy-based FPQ setup.

- Valuable insights into the state of activity of the adsorbed enzyme would be provided by acquiring enzyme inhibition profiles using the proposed microarray-based activity assay by detecting the signal of the activity probe applied to enzyme arrays pre-incubated with various concentrations of inhibitor.

4.2.2. Potential improvements and applications of the microarray-based enzymatic activity assay

- Multiplexing of the non-contact arraying system is absolutely necessary in order to ensure the time-resolved assessment of enzyme kinetics with a good accuracy and in high-throughput. The lack of the multiplexing capability restricted the number of samples per time that could have been processed by our setup; furthermore, it strongly impaired our temporal resolution. This technical problem can be solved by introducing multiple dispenser units for simultaneous spotting of multiple enzyme arrays.

- Moreover, if the multiplexing requirement is fulfilled, activity probes can be spotted on top of the spots of enzymes at well-defined time points and with a good spatial resolution. This would enhance the accuracy of the estimation of the kinetic constants of enzymes, as well as solve the major drawback associated with microarrays of physisorbed enzymes: the high non-specific background.

- The high non-specific background could be diminished by applying anti-fouling coating around the spots, e.g., by using soft lithography techniques with fabricated polymer moulds.

- Immobilization methods other than physisorption could be applied, e.g., the glutaraldehyde cross-linking of enzymes within well-defined spatial boundaries of the arrayed spots.

- Innumerable perspectives for biomaterial screening in terms of their interactions with enzymes, most importantly, applicable to nanostructured materials.

5. REFERENCES

Abbas, A., Vercaigne-Marko, D., Supiot, P., Bocquet, B., Vivien, C., and Guillochon, D. (2009). Covalent attachment of trypsin on plasma polymerized allylamine. Colloids and Surfaces B: Biointerfaces *73*, 315-324.

Adamczyk, Z., Weronski, P., and Musial, E. (2002). Particle adsorption under irreversible conditions: kinetics and jamming coverage. Colloids and Surfaces A: Physicochemical and Engineering Aspects *208*, 29-40.

Angenendt, P., Lehrach, H., Kreutzberger, J., and Glökler, J. (2005). Subnanoliter enzymatic assays on microarrays. PROTEOMICS *5*, 420-425.

Armelao, L., Pascolini, M., Biasiolo, E., Tondello, E., Bottaro, G., Carbonare, M.D., D'Arrigo, A., and Leon, A. (2008). Innovative metal oxide-based substrates for DNA microarrays. Inorganica Chimica Acta *361*, 3603-3608.

Atkins, G.L., and Nimmo, I.A. (1975). A comparison of seven methods for fitting the Michaelis-Menten equation. Biochem J *149*, 775-777.

Axelrod, D., Koppel, D.E., Schlessinger, J., Elson, E., and Webb, W.W. (1976). Mobility measurement by analysis of fluorescence photobleaching recovery kinetics. Biophys J *16*, 1055-1069.

Bachovchin, W.W. (1986). Nitrogen-15 NMR spectroscopy of hydrogen-bonding interactions in the active site of serine proteases: evidence for a moving histidine mechanism. Biochemistry *25*, 7751-7759.

Badre, C., Pauporté, T., Turmine, M., and Lincot, D. (2007). Tailoring the wetting behavior of zinc oxide films by using alkylsilane self-assembled monolayers. Superlattices and Microstructures *42*, 99-102.

Ball, V., Bentaleb, A., Hemmerle, J., Voegel, J.C., and Schaaf, P. (1996). Dynamic Aspects of Protein Adsorption onto Titanium Surfaces: Mechanism of Desorption into Buffer and Release in the Presence of Proteins in the Bulk, pp. 1614-1621.

Ball, V., Huetz, P., Elaissari, A., Cazenave, J.P., Voegel, J.C., and Schaaf, P. (1994). Kinetics of exchange processes in the adsorption of proteins on solid surfaces, pp. 7330-7334.

Balme, S., Janot, J.-M., Déjardin, P., Vasina, E.N., and Seta, P. (2006). Potentialities of confocal fluorescence for investigating protein adsorption on mica and in ultrafiltration membranes. Journal of Membrane Science *284*, 198-204.

Barborini, E., Conti, A.M., Kholmanov, I., Piseri, P., Podestà, A., Milani, P., Cepek, C., Sakho, O., Macovez, R., and Sancrotti, M. (2005). Nanostructured TiO2 Films with 2 eV Optical Gap. Advanced Materials *17*, 1842-1846.

Barborini, E., Piseri, P., and Milani, P. (1999). A pulsed microplasma source of high intensity supersonic carbon cluster beams. Journal of Physics D: Applied Physics *32*, L105.

Baschong, W., Suetterlin, R., Hefti, A., and Schiel, H. (2001). Confocal laser scanning microscopy and scanning electron microscopy of tissue Ti-implant interfaces. Micron *32*, 33-41.

Belicchi, M., Erratico, S., Razini, P., Meregalli, M., Cattaneo, A., Jacchetti, E., Farini, A., Villa, C., Bresolin, N., Porretti, L., *et al.* (2010). Ex vivo expansion of human circulating myogenic progenitors on cluster-assembled nanostructured TiO2. Biomaterials *31*, 5385-5396.

Benesch, T., Yiacoumi, S., and Tsouris, C. (2003). Brownian motion in confinement. Physical Review E *68*, 021401.

Bentaleb, A., Ball, V., Haikel, Y., Voegel, J.C., and Schaaf, P. (1997). Kinetics of the Homogeneous Exchange of Lysozyme Adsorbed on a Titanium Oxide Surface, pp. 729-735.

Bentaleb, A., Haikel, Y., Voegel, J.C., and Schaaf, P. (1998). Kinetics of the homogeneous exchange of alpha-lactalbumin adsorbed on titanium oxide surface. Journal of biomedical materials research *40*, 449-457.

Bergman, A.A., Buijs, J., Herbig, J., Mathes, D.T., Demarest, J.J., Wilson, C.D., Reimann, C.T., Baragiola, R.A., Hull, R., and Oscarsson, S.O. (1998). Nanometer-Scale Arrangement of Human Serum Albumin by Adsorption on Defect Arrays Created with a Finely Focused Ion Beam. Langmuir *14*, 6785-6788.

Biloivan, O.A., Dzyadevych, S.V., El'skaya, A.V., Jaffrezic-Renault, N., Zine, N., Bausells, J., Samitier, J., and Errachid, A. (2007). Development of bi-enzyme microbiosensor based on solid-contact ion-selective microelectrodes for protein detection. Sensors and Actuators B: Chemical *123*, 1096-1100.

Binnig, G., Quate, C.F., and Gerber, C. (1986). Atomic Force Microscope. Physical Review Letters *56*, 930-933.

Blanco, E.M., Horton, M.A., and Mesquida, P. (2008). Simultaneous Investigation of the Influence of Topography and Charge on Protein Adsorption Using Artificial Nanopatterns. Langmuir *24*, 2284-2287.

Bonneil, E., and Waldron, K.C. (2000). On-line system for peptide mapping by capillary electrophoresis at sub-micromolar concentrations. Talanta *53*, 687-699.

Bowen, W.R., Hilal, N., Lovitt, R.W., and Wright, C.J. (1998). Direct Measurement of Interactions between Adsorbed Protein Layers Using an Atomic Force Microscope. Journal of Colloid and Interface Science *197*, 348-352.

Bras, M., Dugas, V., Bessueille, F., Cloarec, J.P., Martin, J.R., Cabrera, M., Chauvet, J.P., Souteyrand, E., and Garrigues, M. (2004). Optimisation of a silicon/silicon dioxide substrate for a fluorescence DNA microarray. Biosensors and Bioelectronics *20*, 797-806.

Braun, S., Rappoport, S., Shtelzer, S., Zusman, R., Druckmann, S., Avnir, D., and Ottolenghi, M. (1991). Design and Properties of Enzymes Immobilized in Sol-Gel Glass Matrices. In Biotechnology: Bridging Research and Applications, D. Kamely, A. Chakrabarty, and S. Kornguth, eds. (Springer Netherlands), pp. 205-218.

Braun, S., Shtelzer, S., Rappoport, S., Avnir, D., and Ottolenghi, M. (1992). Biocatalysis by sol-gel entrapped enzymes. Journal of Non-Crystalline Solids *147–148*, 739-743.

Briggs, G.E., and Haldane, J.B. (1925). A Note on the Kinetics of Enzyme Action. Biochem J *19*, 338-330.

Brunette, D., Tengvall, P., and Textor, M. (2001). Titanium in Medicine: Material Science, Surface Science, Engineering, Biological Responses and Medical Applications (Engineering Materials) (Springer).

Buck, F.F., Vithayathil, A.J., Bier, M., and Nord, F.F. (1962). On the mechanism of enzyme action. LXXIII. Studies on trypsins from beef, sheep and pig pancreas. Archives of Biochemistry and Biophysics *97*, 417-424.

Bulinski, J.C., Odde, D.J., Howell, B.J., Salmon, T.D., and Waterman-Storer, C.M. (2001). Rapid dynamics of the microtubule binding of ensconsin in vivo. Journal of Cell Science *114*, 3885-3897.

Burghardt, T.P., and Axelrod, D. (1981). Total internal reflection/fluorescence photobleaching recovery study of serum albumin adsorption dynamics. Biophysical journal *33*, 455-467.

Cai, K., Bossert, J., and Jandt, K.D. (2006). Does the nanometre scale topography of titanium influence protein adsorption and cell proliferation? Colloids Surf B Biointerfaces *49*, 136-144.

Calonder, C., Tie, Y., and Van Tassel, P.R. (2001). History dependence of protein adsorption kinetics. Proc Natl Acad Sci U S A *98*, 10664-10669.

Campbell, D.A., and Szardenings, A.K. (2003). Functional profiling of the proteome with affinity labels. Curr Opin Chem Biol *7*, 296-303.

Carbone, R., De Marni, M., Zanardi, A., Vinati, S., Barborini, E., Fornasari, L., and Milani, P. (2009). Characterization of cluster-assembled nanostructured titanium oxide coatings as substrates for protein arrays. Analytical Biochemistry *394*, 7-12.

Carbone, R., Giorgetti, L., Zanardi, A., Marangi, I., Chierici, E., Bongiorno, G., Fiorentini, F., Faretta, M., Piseri, P., Pelicci, P.G.*, et al.* (2007). Retroviral microarray-based platform on nanostructured TiO2 for functional genomics and drug discovery. Biomaterials *28*, 2244-2253.

Carbone, R., Marangi, I., Zanardi, A., Giorgetti, L., Chierici, E., Berlanda, G., Podesta, A., Fiorentini, F., Bongiorno, G., Piseri, P.*, et al.* (2006). Biocompatibility of cluster-assembled nanostructured TiO2 with primary and cancer cells. Biomaterials *27*, 3221-3229.

Caro, A., Humblot, V., Méthivier, C., Minier, M., Barbes, L., Li, J., Salmain, M., and Pradier, C.-M. (2010). Bioengineering of stainless steel surface by covalent immobilization of enzymes. Physical characterization and interfacial enzymatic activity. Journal of Colloid and Interface Science *349*, 13-18.

Casadonte, F., Pasqua, L., Savino, R., and Terracciano, R. (2010). Smart Trypsin Adsorption into N-(2-Aminoethyl)-3-aminopropyl-Modified Mesoporous Silica for Ultra Fast Protein Digestion. Chemistry – A European Journal *16*, 8998-9001.

Cedervall, T., Lynch, I., Lindman, S., Berggård, T., Thulin, E., Nilsson, H., Dawson, K.A., and Linse, S. (2007). Understanding the nanoparticle–protein corona using methods to quantify exchange rates and affinities of proteins for nanoparticles. Proceedings of the National Academy of Sciences *104*, 2050-2055.

Chan, V., Graves, D.J., Fortina, P., and McKenzie, S.E. (1997). Adsorption and Surface Diffusion of DNA Oligonucleotides at Liquid/Solid Interfaces. Langmuir *13*, 320-329.

Chang, I.N., Lin, J.-N., Andrade, J.D., and Herron, J.N. (1995). Adsorption Mechanism of Acid Pretreated Antibodies on Dichlorodimethylsilane-Treated Silica Surfaces. Journal of Colloid and Interface Science *174*, 10-23.

Chayen, N.E., Saridakis, E., El-Bahar, R., and Nemirovsky, Y. (2001). Porous silicon: an effective nucleation-inducing material for protein crystallization. Journal of Molecular Biology *312*, 591-595.

Chayen, N.E., Saridakis, E., and Sear, R.P. (2006). Experiment and theory for heterogeneous nucleation of protein crystals in a porous medium. Proc Natl Acad Sci U S A *103*, 597-601.

Chen, G.Y., Uttamchandani, M., Zhu, Q., Wang, G., and Yao, S.Q. (2003). Developing a strategy for activity-based detection of enzymes in a protein microarray. Chembiochem *4*, 336-339.

Chen, Y.Z., Yang, C.T., Ching, C.B., and Xu, R. (2008). Immobilization of Lipases on Hydrophobilized Zirconia Nanoparticles: Highly Enantioselective and Reusable Biocatalysts, pp. 8877-8884.

Dabrowski, A. (2001). Adsorption -- from theory to practice. Advances in Colloid and Interface Science *93*, 135-224.

Dallas Johnson, K., Clark, A., and Marshall, S. (2002). A functional comparison of ovine and porcine trypsins. Comparative Biochemistry and Physiology Part B: Biochemistry and Molecular Biology *131*, 423-431.

De Feijter, J.A., Benjamins, J., and Veer, F.A. (1978). Ellipsometry as a tool to study the adsorption behavior of synthetic and biopolymers at the air–water interface. Biopolymers *17*, 1759-1772.

de la Garza, L., Saponjic, Z.V., Dimitrijevic, N.M., Thurnauer, M.C., and Rajh, T. (2005). Surface States of Titanium Dioxide Nanoparticles Modified with Enediol Ligands. The Journal of Physical Chemistry B *110*, 680-686.

Deepthi, S., Johnson, A., and Pattabhi, V. (2001). Structures of porcine [beta]-trypsin-detergent complexes: the stabilization of proteins through hydrophilic binding of polydocanol. In Acta Crystallographica Section D, pp. 1506-1512.

Deng, J., Davies, D.R., Wisedchaisri, G., Wu, M., Hol, W.G.J., and Mehlin, C. (2004). An improved protocol for rapid freezing of protein samples for long-term storage. Acta Crystallographica Section D *60*, 203-204.

Denis, F.A., Hanarp, P., Sutherland, D.S., Gold, J., Mustin, C., Rouxhet, P.G., and Dufrêne, Y.F. (2002). Protein Adsorption on Model Surfaces with Controlled Nanotopography and Chemistry. Langmuir *18*, 819-828.

Diaspro, A., Federici, F., and Robello, M. (2002). Influence of Refractive-Index Mismatch in High-Resolution Three-Dimensional Confocal Microscopy. Appl Opt *41*, 685-690.

Díaz, J.F., and Balkus Jr, K.J. (1996). Enzyme immobilization in MCM-41 molecular sieve. Journal of Molecular Catalysis B: Enzymatic *2*, 115-126.

Diebold, U. (2003). The surface science of titanium dioxide. Surface Science Reports *48*, 53-229.

Dixon, M.C. (2008). Quartz crystal microbalance with dissipation monitoring: enabling real-time characterization of biological materials and their interactions. Journal of biomolecular techniques : JBT *19*, 151-158.

Dolatshahi-Pirouz, A., Kolman, N., Arpanaei, A., Jensen, T., Foss, M., Chevallier, J., Kingshott, P., Baas, J., Søballe, K., and Besenbacher, F. (2011). The adsorption characteristics of osteopontin on hydroxyapatite and gold. Materials Science and Engineering: C *31*, 514-522.

Dolatshahi-Pirouz, A., Skeldal, S., Hovgaard, M.B., Jensen, T., Foss, M., Chevallier, J., and Besenbacher, F. (2009). Influence of Nanoroughness and Detailed Surface Morphology on Structural Properties and Water-Coupling Capabilities of Surface-Bound Fibrinogen Films. The Journal of Physical Chemistry C *113*, 4406-4412.

Dufrene, Y.F. (2008). Towards nanomicrobiology using atomic force microscopy. Nat Rev Micro *6*, 674-680.

Dufrêne, Y.F., Marchal, T.G., and Rouxhet, P.G. (1999). Probing the organization of adsorbed protein layers: complementarity of atomic force microscopy, X-ray photoelectron spectroscopy and radiolabeling. Applied Surface Science *144–145*, 638-643.

Ellingsen, J.E. (1991). A study on the mechanism of protein adsorption to TiO2. Biomaterials *12*, 593-596.

Elwing, H. (1998). Protein absorption and ellipsometry in biomaterial research. Biomaterials *19*, 397-406.

Evans, M.J., and Cravatt, B.F. (2006). Mechanism-Based Profiling of Enzyme Families. Chem Rev *106*, 3279-3301.

Fonovic, M., and Bogyo, M. (2007). Activity based probes for proteases: applications to biomarker discovery, molecular imaging and drug screening. Curr Pharm Des *13*, 253-261.

Fraser, D., and Powell, R.E. (1950). THE KINETICS OF TRYPSIN DIGESTION, pp. 803-820.

Funeriu, D.P., Eppinger, J., Denizot, L., Miyake, M., and Miyake, J. (2005). Enzyme family-specific and activity-based screening of chemical libraries using enzyme microarrays. Nat Biotechnol *23*, 622-627.

Gallagher, W.M., Lynch, I., Allen, L.T., Miller, I., Penney, S.C., O'Connor, D.P., Pennington, S., Keenan, A.K., and Dawson, K.A. (2006). Molecular basis of cell–biomaterial interaction: Insights gained from transcriptomic and proteomic studies. Biomaterials *27*, 5871-5882.

Galli, C., Collaud Coen, M., Hauert, R., Katanaev, V.L., Gröning, P., and Schlapbach, L. (2002). Creation of nanostructures to study the topographical dependency of protein adsorption. Colloids and Surfaces B: Biointerfaces *26*, 255-267.

Garbers, E., Mitlöhner, R., Georgieva, R., and Bäumler, H. (2007). Activity of Immobilized Trypsin in the Layer Structure of Polyelectrolyte Microcapsules (PEMC). Macromolecular Bioscience *7*, 1243-1249.

Garipcan, B., Winters, J., Atchison, J.S., Cathell, M.D., Schiffman, J.D., Leaffer, O.D., Nonnenmann, S.S., Schauer, C.L., Piskin, E., Nabet, B.*, et al.* (2008). Controllable formation of nanoscale patterns on TiO2 by conductive-AFM nanolithography. Langmuir *24*, 8944-8949.

Gaspers, P.B., Robertson, C.R., and Gast, A.P. (1994). Enzymes on Immobilized Substrate Surfaces: Diffusion. Langmuir *10*, 2699-2704.

Gill, I., and Ballesteros, A. (1998). Encapsulation of Biologicals within Silicate, Siloxane, and Hybrid Sol–Gel Polymers: An Efficient and Generic Approach. Journal of the American Chemical Society *120*, 8587-8598.

Giorgetti, L., Bongiorno, G., Podesta, A., Berlanda, G., Scopelliti, P.E., Carbone, R., and Milani, P. (2008). Adsorption and stability of streptavidin on cluster-assembled nanostructured TiOx films. Langmuir *24*, 11637-11644.

Gómez, J., M. , Ma. Dolores, R., Gassan, H., and Elena de la, P. (2009). Adsorption of trypsin on commercial silica gel, pp. 336-341.

Gómez, J.M., Deere, J., Goradia, D., Cooney, J., Magner, E., and Hodnett, B.K. (2003). Transesterification Catalyzed by Trypsin Supported on MCM-41. Catalysis Letters *88*, 183-186.

Goradia, D., Cooney, J., Hodnett, B.K., and Magner, E. (2005). The adsorption characteristics, activity and stability of trypsin onto mesoporous silicates. Journal of Molecular Catalysis B: Enzymatic *32*, 231-239.

Gray, J.J. (2004). The interaction of proteins with solid surfaces. Current Opinion in Structural Biology *14*, 110-115.

Green, N.M., and Neurath, H. (1953). The effects of divalent cations on trypsin. J Biol Chem *204*, 379-390.

Guerin, S., Hayden, B.E., Lee, C.E., Mormiche, C., and Russell, A.E. (2006). High-Throughput Synthesis and Screening of Ternary Metal Alloys for Electrocatalysis. The Journal of Physical Chemistry B *110*, 14355-14362.

Han, M., Sethuraman, A., Kane, R.S., and Belfort, G. (2003). Nanometer-Scale Roughness Having Little Effect on the Amount or Structure of Adsorbed Protein. Langmuir *19*, 9868-9872.

Harke, M., Teppner, R., Schulz, O., Motschmann, H., and Orendi, H. (1997). Description of a single modular optical setup for ellipsometry, surface plasmons, waveguide modes, and their corresponding imaging techniques including Brewster angle microscopy. Review of Scientific Instruments *68*, 3130-3134.

Harris, L.G., Tosatti, S., Wieland, M., Textor, M., and Richards, R.G. (2004). Staphylococcus aureus adhesion to titanium oxide surfaces coated with non-functionalized and peptide-functionalized poly(l-lysine)-grafted-poly(ethylene glycol) copolymers. Biomaterials *25*, 4135-4148.

Hehemann, J.H., Redecke, L., Murugaiyan, J., von Bergen, M., Betzel, C., and Saborowski, R. (2008). Autoproteolytic stability of a trypsin from the marine crab Cancer pagurus. Biochem Biophys Res Commun *370*, 566-571.

Hell, S., Reiner, G., Cremer, C., and Stelzer, E.H.K. (1993). Aberrations in confocal fluorescence microscopy induced by mismatches in refractive index. Journal of Microscopy *169*, 391-405.

Hibbs, A.R., MacDonald, G., and Garsha, K. (2006). Practical Confocal Microscopy

Handbook Of Biological Confocal Microscopy. In, J.B. Pawley, ed. (Springer US), pp. 650-671.

Holmes, P.F., Bohrer, M., and Kohn, J. (2008). Exploration of polymethacrylate structure–property correlations: Advances towards combinatorial and high-throughput methods for biomaterials discovery. Progress in Polymer Science *33*, 787-796.

Holmlin, R.E., Haag, R., Chabinyc, M.L., Ismagilov, R.F., Cohen, A.E., Terfort, A., Rampi, M.A., and Whitesides, G.M. (2001). Electron Transport through Thin Organic Films in Metal−Insulator−Metal Junctions Based on Self-Assembled Monolayers. Journal of the American Chemical Society *123*, 5075-5085.

Homola, J. (2003). Present and future of surface plasmon resonance biosensors. Analytical and Bioanalytical Chemistry *377*, 528-539.

Hook, A.L., Anderson, D.G., Langer, R., Williams, P., Davies, M.C., and Alexander, M.R. (2010). High throughput methods applied in biomaterial development and discovery. Biomaterials *In Press, Corrected Proof*.

Hook, F., Voros, J., Rodahl, M., Kurrat, R., Boni, P., Ramsden, J.J., Textor, M., Spencer, N.D., Tengvall, P., Gold, J., *et al.* (2002). A comparative study of protein adsorption on titanium oxide surfaces using in situ ellipsometry, optical waveguide lightmode spectroscopy, and quartz crystal microbalance/dissipation. Colloids and Surfaces B: Biointerfaces *24*, 155-170.

Hovgaard, M.B., Rechendorff, K., Chevallier, J., Foss, M., and Besenbacher, F. (2008). Fibronectin Adsorption on Tantalum: The Influence of Nanoroughness. The Journal of Physical Chemistry B *112*, 8241-8249.

Huckel, M., Wirth, H.J., and Hearn, M.T. (1996). Porous zirconia: a new support material for enzyme immobilization. J Biochem Biophys Methods *31*, 165-179.

Huetz, P., Ball, V., Voegel, J.C., and Schaaf, P. (1995). Exchange Kinetics for a Heterogeneous Protein System on a Solid Surface, pp. 3145-3152.

Hung, A., Mwenifumbo, S., Mager, M., Kuna, J.J., Stellacci, F., Yarovsky, I., and Stevens, M.M. (2011). Ordering Surfaces on the Nanoscale: Implications for Protein Adsorption. Journal of the American Chemical Society *133*, 1438-1450.

Imamura, K., Shimomura, M., Nagai, S., Akamatsu, M., and Nakanishi, K. (2008). Adsorption characteristics of various proteins to a titanium surface. J Biosci Bioeng *106*, 273-278.

Inoue, T., Irifune, T., Higo, Y., Sanehira, T., Sueda, Y., Yamada, A., Shinmei, T., Yamazaki, D., Ando, J., Funakoshi, K., *et al.* (2006). The phase boundary between wadsleyite and ringwoodite in Mg₂SiO₄ determined by in situ X-ray diffraction. Physics and Chemistry of Minerals *33*, 106-114.

Jackson, D.R., Omanovic, S., and Roscoe, S.G. (2000). Electrochemical Studies of the Adsorption Behavior of Serum Proteins on Titanium. Langmuir *16*, 5449-5457.

Jang, S., Kim, D., Choi, J., Row, K., and Ahn, W. (2006). Trypsin immobilization on mesoporous silica with or without thiol functionalization. Journal of Porous Materials *13*, 385-391.

Jennissen, H.P. (1976). Evidence for negative cooperativity in the adsorption of phosphorylase b on hydrophobic agaroses. Biochemistry *15*, 5683-5692.

Jiang, H., Zou, H., Wang, H., Ni, J., Zhang, Q., and Zhang, Y. (2000). On-line characterization of the activity and reaction kinetics of immobilized enzyme by high-performance frontal analysis. Journal of Chromatography A *903*, 77-84.

Jin, G., Tengvall, P., Lundström, I., and Arwin, H. (1995). A Biosensor Concept Based on Imaging Ellipsometry for Visualization of Biomolecular Interactions. Analytical Biochemistry *232*, 69-72.

Johnson, D.S., Weerapana, E., and Cravatt, B.F. (2010). Strategies for discovering and derisking covalent, irreversible enzyme inhibitors. Future medicinal chemistry *2*, 949-964.

Johnson, P., and Whateley, T.L. (1981). The effects of surface and macromolecular interactions on the kinetics of inactivation of trypsin and alpha-chymotrypsin. Biochem J *193*, 285-294.

Kang, K., Kan, C., Yeung, A., and Liu, D. (2006). The immobilization of trypsin on soap-free P(MMA-EA-AA) latex particles. Materials Science and Engineering: C *26*, 664-669.

Kang, M., and Kenworthy, A.K. (2008). A closed-form analytic expression for FRAP formula for the binding diffusion model. Biophys J *95*, L13-15.

Kaufman, E.N., and Jain, R.K. (1992). In vitro measurement and screening of monoclonal antibody affinity using fluoroscence photobleaching. Journal of Immunological Methods *155*, 1-17.

Khang, D., Kim, S.Y., Liu-Snyder, P., Palmore, G.T.R., Durbin, S.M., and Webster, T.J. (2007). Enhanced fibronectin adsorption on carbon nanotube/poly(carbonate) urethane: Independent role of surface nano-roughness and associated surface energy. Biomaterials *28*, 4756-4768.

Kholmanov, I.N., Barborini, E., Vinati, S., Piseri, P., Podestà, A., Ducati, C., Lenardi, C., and Milani, P. (2003). The influence of the precursor clusters on the structural and morphological evolution of nanostructured TiO 2 under thermal annealing. Nanotechnology *14*, 1168.

Kim, B.C., Lopez-Ferrer, D., Lee, S.-M., Ahn, H.-K., Nair, S., Kim, S.H., Kim, B.S., Petritis, K., Camp, D.G., Grate, J.W.*, et al.* (2009). Highly stable trypsin-aggregate coatings on polymer nanofibers for repeated protein digestion. PROTEOMICS *9*, 1893-1900.

Kim, J., Grate, J.W., and Wang, P. (2006). Nanostructures for enzyme stabilization. Chemical Engineering Science *61*, 1017-1026.

Kim, J., Kim, B.C., Lopez-Ferrer, D., Petritis, K., and Smith, R.D. (2010). Nanobiocatalysis for protein digestion in proteomic analysis. PROTEOMICS *10*, 687-699.

Klinger, A., Steinberg, D., Kohavi, D., and Sela, M.N. (1997). Mechanism of adsorption of human albumin to titanium in vitro. Journal of biomedical materials research *36*, 387-392.

Kobayashi, T., and Laidler, K.J. (1974). Theory of the kinetics of reactions catalyzed by enzymes attached to membranes. Biotechnology and Bioengineering *16*, 77-97.

Koutsopoulos, S., Patzsch, K., Bosker, W.T.E., and Norde, W. (2007). Adsorption of Trypsin on Hydrophilic and Hydrophobic Surfaces. Langmuir *23*, 2000-2006.

Kunitz, M., Anson, M.L., and Northrop, J.H. (1934). MOLECULAR WEIGHT, MOLECULAR VOLUME, AND HYDRATION OF PROTEINS IN SOLUTION. The Journal of General Physiology *17*, 365-373.

Kurosawa, S., Kamo, N., Aizawa, H., and Muratsugu, M. (2007). Adsorption of 125I-labeled immunoglobulin G, its F(ab')2 and Fc fragments onto plasma-polymerized films. Biosensors and Bioelectronics *22*, 2598-2603.

Kurrat, R., Textor, M., Ramsden, J.J., Boni, P., and Spencer, N.D. (1997). Instrumental improvements in optical waveguide light mode spectroscopy for the study of biomolecule adsorption. Review of Scientific Instruments *68*, 2172-2176.

Langmuir, I. (1918). THE ADSORPTION OF GASES ON PLANE SURFACES OF GLASS, MICA AND PLATINUM. Journal of the American Chemical Society *40*, 1361-1403.

Langmuir, I., and Schaefer, V.J. (1937). OPTICAL MEASUREMENT OF THE THICKNESS OF A FILM ADSORBED FROM A SOLUTION. Journal of the American Chemical Society *59*, 1406-1406.

Lausmaa, J., Kasemo, B., and Hansson, S. (1985). Accelerated oxide growth on titanium implants during autoclaving caused by fluorine contamination. Biomaterials *6*, 23-27.

Lavalle, P., DeVries, A.L., Cheng, C.C.C., Scheuring, S., and Ramsden, J.J. (2000). Direct Observation of Postadsorption Aggregation of Antifreeze Glycoproteins on Silicates. Langmuir *16*, 5785-5789.

Lee, G., Chrisey, L., and Colton, R. (1994). Direct measurement of the forces between complementary strands of DNA. Science *266*, 771-773.

Lee, H.J., Wark, A.W., Goodrich, T.T., Fang, S., and Corn, R.M. (2005). Surface enzyme kinetics for biopolymer microarrays: a combination of Langmuir and Michaelis-Menten concepts. Langmuir *21*, 4050-4057.

Li, F.-Y., Xing, Y.-J., and Ding, X. (2007). Immobilization of papain on cotton fabric by sol-gel method. Enzyme and Microbial Technology *40*, 1692-1697.

Li, J., and Yeung, E.S. (2008). Real-Time Single-Molecule Kinetics of Trypsin Proteolysis. Analytical Chemistry *80*, 8509-8513.

Li, X.-F., Nie, X., and Tang, J.-G. (1998). Anti-autolysis of Trypsin by Modification of Autolytic Site Arg117. Biochem Biophys Res Commun *250*, 235-239.

Lindan, P.J.D., Harrison, N.M., and Gillan, M.J. (1998). Mixed Dissociative and Molecular Adsorption of Water on the Rutile (110) Surface. Physical Review Letters *80*, 762-765.

Linderbäck, P., Harmankaya, N., Askendal, A., Areva, S., Lausmaa, J., and Tengvall, P. (2010). The effect of heat- or ultra violet ozone-treatment of titanium on complement deposition from human blood plasma. Biomaterials *31*, 4795-4801.

Linfoot, E.H., and Wolf, E. (1953). Diffraction Images in Systems with an Annular Aperture. Proceedings of the Physical Society Section B *66*, 145.

Liu, C.-G., Desai, K.G.H., Chen, X.-G., and Park, H.-J. (2005). Preparation and Characterization of Nanoparticles Containing Trypsin Based on Hydrophobically Modified Chitosan. Journal of Agricultural and Food Chemistry *53*, 1728-1733.

Liu, T., Wang, S., and Chen, G. (2009). Immobilization of trypsin on silica-coated fiberglass core in microchip for highly efficient proteolysis. Talanta *77*, 1767-1773.

Liu, Y.-X., Wang, X.-J., Lu, J., and Ching, C.-B. (2007). Influence of the Roughness, Topography, and Physicochemical Properties of Chemically Modified Surfaces on the Heterogeneous Nucleation of Protein Crystals. The Journal of Physical Chemistry B *111*, 13971-13978.

Liu, Y., Patricelli, M.P., and Cravatt, B.F. (1999). Activity-based protein profiling: The serine hydrolases. Proceedings of the National Academy of Sciences *96*, 14694-14699.

Lubarsky, G.V., Davidson, M.R., and Bradley, R.H. (2007). Hydration–dehydration of adsorbed protein films studied by AFM and QCM-D. Biosensors and Bioelectronics *22*, 1275-1281.

Luo, Q., and Andrade, J.D. (1998). Cooperative Adsorption of Proteins onto Hydroxyapatite. Journal of Colloid and Interface Science *200*, 104-113.

Ma, J., Zhang, L., Liang, Z., Zhang, W., and Zhang, Y. (2009). Recent advances in immobilized enzymatic reactors and their applications in proteome analysis. Anal Chim Acta *632*, 1-8.

MacBeath, G. Protein microarrays and proteomics. Nat Genet.

MacBeath, G., and Schreiber, S.L. (2000). Printing Proteins as Microarrays for High-Throughput Function Determination. Science *289*, 1760-1763.

Malek, K., and Coppens, M.-O. (2001). Effects of Surface Roughness on Self- and Transport Diffusion in Porous Media in the Knudsen Regime. Physical Review Letters *87*, 125505.

Malmsten, M., and Larsson, A. (2000). Immobilization of trypsin on porous glycidyl methacrylate beads: effects of polymer hydrophilization. Colloids and Surfaces B: Biointerfaces *18*, 277-284.

Mant, A., Tourniaire, G., Diaz-Mochon, J.J., Elliott, T.J., Williams, A.P., and Bradley, M. (2006). Polymer microarrays: Identification of substrates for phagocytosis assays. Biomaterials *27*, 5299-5306.

Mathur, S., Erdem, A., Cavelius, C., Barth, S., and Altmayer, J. (2009). Amplified electrochemical DNA-sensing of nanostructured metal oxide films deposited on disposable graphite electrodes functionalized by chemical vapor deposition. Sensors and Actuators B: Chemical *136*, 432-437.

Matsuura, S.-i., Ishii, R., Itoh, T., Hanaoka, T., Hamakawa, S., Tsunoda, T., and Mizukami, F. (2010). Direct visualization of hetero-enzyme co-encapsulated in mesoporous silicas. Microporous and Mesoporous Materials *127*, 61-66.

Merkel, R., Nassoy, P., Leung, A., Ritchie, K., and Evans, E. (1999). Energy landscapes of receptor-ligand bonds explored with dynamic force spectroscopy. Nature *397*, 50-53.

Migneault, I., Dartiguenave, C., Vinh, J., Bertrand, M.J., and Waldron, K.C. (2004). Comparison of two glutaraldehyde immobilization techniques for solid-phase tryptic peptide mapping of human hemoglobin by capillary zone electrophoresis and mass spectrometry. ELECTROPHORESIS *25*, 1367-1378.

Milani, P., Piseri, P., Barborini, E., Podesta, A., and Lenardi, C. (2001). Cluster beam synthesis of nanostructured thin films (AVS).

Miyahara, M., Vinu, A., Hossain, K.Z., Nakanishi, T., and Ariga, K. (2006). Adsorption study of heme proteins on SBA-15 mesoporous silica with pore-filling models. Thin Solid Films *499*, 13-18.

Möller, C., Allen, M., Elings, V., Engel, A., and Müller, D.J. (1999). Tapping-Mode Atomic Force Microscopy Produces Faithful High-Resolution Images of Protein Surfaces. Biophys J *77*, 1150-1158.

Mrksich, M., Sigal, G.B., and Whitesides, G.M. (1995). Surface Plasmon Resonance Permits in Situ Measurement of Protein Adsorption on Self-Assembled Monolayers of Alkanethiolates on Gold. Langmuir *11*, 4383-4385.

Muller, B., Riedel, M., Michel, R., De Paul, S.M., Hofer, R., Heger, D., and Grutzmacher, D. (2001). Impact of nanometer-scale roughness on contact-angle hysteresis and globulin adsorption. Journal of Vacuum Science & Technology B: Microelectronics and Nanometer Structures *19*, 1715-1720.

Nakanishi, K., Sakiyama, T., and Imamura, K. (2001). On the adsorption of proteins on solid surfaces, a common but very complicated phenomenon. J Biosci Bioeng *91*, 233-244.

Neal, W.E.J., and Fane, R.W. (1973). Ellipsometry and its applications to surface examination. Journal of Physics E: Scientific Instruments *6*, 409.

Nelson, C.A. (1971a). The Binding of Detergents to Proteins. Journal of Biological Chemistry *246*, 3895-3901.

Nelson, C.A. (1971b). The binding of detergents to proteins. I. The maximum amount of dodecyl sulfate bound to proteins and the resistance to binding of several proteins. The Journal of biological chemistry *246*, 3895-3901.

Nijdam, A.J., Ming-Cheng Cheng, M., Geho, D.H., Fedele, R., Herrmann, P., Killian, K., Espina, V., Petricoin Iii, E.F., Liotta, L.A., and Ferrari, M. (2007). Physicochemically modified silicon as a substrate for protein microarrays. Biomaterials *28*, 550-558.

Nygren, H., Kaartinen, M., and Stenberg, M. (1986). Determination by ellipsometry of the affinity of monoclonal antibodies. Journal of Immunological Methods *92*, 219-225.

Olsen, J.V., Ong, S.-E., and Mann, M. (2004). Trypsin Cleaves Exclusively C-terminal to Arginine and Lysine Residues. Molecular & Cellular Proteomics *3*, 608-614.

Orschel, M., Katerkamp, A., Meusel, M., and Cammann, K. (1998). Evaluation of several methods to quantify immobilized proteins on gold and silica surfaces. Colloids and Surfaces B: Biointerfaces *10*, 273-279.

Pan, J.M., Maschhoff, B.L., Diebold, U., and Madey, T.E. (1992). Interaction of water, oxygen, and hydrogen with TiO[sub 2](110) surfaces having different defect densities (Seattle, Washington (USA): AVS).

Park, C.B., and Clark, D.S. (2002). Sol-gel encapsulated enzyme arrays for high-throughput screening of biocatalytic activity. Biotechnol Bioeng *78*, 229-235.

Patricelli, M.P., Giang, D.K., Stamp, L.M., and Burbaum, J.J. (2001). Direct visualization of serine hydrolase activities in complex proteomes using fluorescent active site-directed probes. Proteomics *1*, 1067-1071.

Pertaya, N., Marshall, C.B., DiPrinzio, C.L., Wilen, L., Thomson, E.S., Wettlaufer, J.S., Davies, P.L., and Braslavsky, I. (2007). Fluorescence Microscopy Evidence for Quasi-Permanent Attachment of Antifreeze Proteins to Ice Surfaces. Biophys J *92*, 3663-3673.

Petersen, L.K., Sackett, C.K., and Narasimhan, B. (2010). High-throughput analysis of protein stability in polyanhydride nanoparticles. Acta Biomaterialia *6*, 3873-3881.

Pluskal, M.G., Bogdanova, A., Lopez, M., Gutierrez, S., and Pitt, A.M. (2002). Multiwell in-gel protein digestion and microscale sample preparation for protein identification by mass spectrometry. Proteomics *2*, 145-150.

Podesta, A., Bongiorno, G., Scopelliti, P.E., Bovio, S., Milani, P., Semprebon, C., and Mistura, G. (2009). Cluster-Assembled Nanostructured Titanium Oxide Films with Tailored Wettability. The Journal of Physical Chemistry C *113*, 18264-18269.

Polgár, L. (2005). The catalytic triad of serine peptidases. Cellular and Molecular Life Sciences *62*, 2161-2172.

Porter, W.H., and Preston, J.L. (1975). Retention of trypsin and chymotrypsin proteolytic activity in sodium dodecyl sulfate solutions. Analytical Biochemistry *66*, 69-77.

Porter, W.R., and Trager, W.F. (1977). Improved non-parametric statistical methods for the estimation of Michaelis-Menten kinetic parameters by the direct linear plot. Biochem J *161*, 293-290.

Qiao, L., Liu, Y., Hudson, S.P., Yang, P., Magner, E., and Liu, B. (2008). A Nanoporous Reactor for Efficient Proteolysis. Chemistry – A European Journal *14*, 151-157.

Rechendorff, K., Hovgaard, M.B., Foss, M., Zhdanov, V.P., and Besenbacher, F. (2006). Enhancement of protein adsorption induced by surface roughness. Langmuir *22*, 10885-10888.

Riedel, M., Müller, B., and Wintermantel, E. (2001). Protein adsorption and monocyte activation on germanium nanopyramids. Biomaterials *22*, 2307-2316.

Roach, P., Farrar, D., and Perry, C.C. (2006). Surface Tailoring for Controlled Protein Adsorption: Effect of Topography at the Nanometer Scale and Chemistry. Journal of the American Chemical Society *128*, 3939-3945.

Roba, M., Naka, M., Gautier, E., Spencer, N.D., and Crockett, R. (2009). The adsorption and lubrication behavior of synovial fluid proteins and glycoproteins on the bearing-surface materials of hip replacements. Biomaterials *30*, 2072-2078.

Roemer, T., Davies, J., Giaever, G., and Nislow, C. (2012). Bugs, drugs and chemical genomics. Nat Chem Biol *8*, 46-56.

Rondelez, Y., Tresset, G., Tabata, K.V., Arata, H., Fujita, H., Takeuchi, S., and Noji, H. (2005). Microfabricated arrays of femtoliter chambers allow single molecule enzymology. Nat Biotech *23*, 361-365.

Roth, C.M., and Lenhoff, A.M. (1993). Electrostatic and van der Waals contributions to protein adsorption: computation of equilibrium constants. Langmuir *9*, 962-972.

Rusmini, F., Zhong, Z., and Feijen, J. (2007). Protein Immobilization Strategies for Protein Biochips. Biomacromolecules *8*, 1775-1789.

Russo, G., Zegar, C., and Giordano, A. (0000). Advantages and limitations of microarray technology in human cancer. Oncogene *22*, 6497-6507.

Saal, K., Tätte, T., Tulp, I., Kink, I., Kurg, A., Mäeorg, U., Rinken, A., and Lõhmus, A. (2006). Sol–gel films for DNA microarray applications. Materials Letters *60*, 1833-1838.

Sakai-Kato, K., Kato, M., and Toyo'oka, T. (2003). Creation of an On-Chip Enzyme Reactor by Encapsulating Trypsin in Sol−Gel on a Plastic Microchip. Analytical Chemistry *75*, 388-393.

Sakai-Kato, K., Kato, M., Utsunomiya-Tate, N., and Toyo'oka, T. (2006). Encapsulated Biomolecules Using Sol-Gel Reaction for High-Throughput Screening. Frontiers in Drug Design & Discovery *2*, 273-294.

Salakhutdinov, I., VandeVord, P., Palyvoda, O., Matthew, H., Tatagiri, G., Handa, H., Mao, G., Auner, G.W., and Newaz, G. (2008). Fibronectin Adsorption to Nanopatterned Silicon Surfaces. Journal of Nanomaterials *2008*.

Salisbury, C.M., Maly, D.J., and Ellman, J.A. (2002). Peptide Microarrays for the Determination of Protease Substrate Specificity. Journal of the American Chemical Society *124*, 14868-14870.

Sanjines, R., Tang, H., Berger, H., Gozzo, F., Margaritondo, G., and Levy, F. (1994). Electronic structure of anatase TiO[sub 2] oxide. Journal of Applied Physics *75*, 2945-2951.

Santos, O., Kosoric, J., Hector, M.P., Anderson, P., and Lindh, L. (2008). Adsorption behavior of statherin and a statherin peptide onto hydroxyapatite and silica surfaces by in situ ellipsometry. Journal of Colloid and Interface Science *318*, 175-182.

Sanz, R., and et al. (2010). Patterning of rutile TiO 2 surface by ion beam lithography through full-solid masks. Nanotechnology *21*, 235301.

Schaub, R., Thostrup, P., Lopez, N., Lægsgaard, E., Stensgaard, I., Nørskov, J.K., and Besenbacher, F. (2001). Oxygen Vacancies as Active Sites for Water Dissociation on Rutile TiO_{2}(110). Physical Review Letters *87*, 266104.

Scherp, H.W. (1933). THE DIFFUSION COEFFICIENT OF CRYSTALLINE TRYPSIN. The Journal of General Physiology *16*, 795-800.

Schlesinger, R., and Bruns, M. (2000). Quality control of gas sensor microarrays using Auger electron spectroscopy. Thin Solid Films *366*, 265-271.

Schwert, G.W., Neurath, H., Kaufman, S., and Snoke, J.E. (1948). THE SPECIFIC ESTERASE ACTIVITY OF TRYPSIN. Journal of Biological Chemistry *172*, 221-239.

Scopelliti, P.E., Borgonovo, A., Indrieri, M., Giorgetti, L., Bongiorno, G., Carbone, R., Podestà, A., and Milani, P. (2010). The Effect of Surface Nanometre-Scale Morphology on Protein Adsorption. PLoS ONE *5*, e11862.

Scott, E.A., and Elbert, D.L. (2007). Mass spectrometric mapping of fibrinogen conformations at poly(ethylene terephthalate) interfaces. Biomaterials *28*, 3904-3917.

Seabra, I.J., and Gil, M.H. (2007). Cotton gauze bandage: a support for protease immobilization for use in biomedical applications. Revista Brasileira de Ciências Farmacêuticas *43*, 535-542.

Sela, M.N., Badihi, L., Rosen, G., Steinberg, D., and Kohavi, D. (2007). Adsorption of human plasma proteins to modified titanium surfaces. Clin Oral Implants Res *18*, 630-638.

Senger, B., Voegel, J.C., and Schaaf, P. (2000). Irreversible adsorption of colloidal particles on solid substrates. Colloids and Surfaces A: Physicochemical and Engineering Aspects *165*, 255-285.

Senkan, S.M. (1998). High-throughput screening of solid-state catalyst libraries. Nature *394*, 350-353.

Shtelzer, S., Rappoport, S., Avnir, D., Ottolenghi, M., and Braun, S. (1992). Properties of trypsin and of acid phosphatase immobilized in sol-gel glass matrices. Biotechnology and Applied Biochemistry *15*, 227-235.

Sieber, S.A., and Cravatt, B.F. (2006). Analytical platforms for activity-based protein profiling - exploiting the versatility of chemistry for functional proteomics. Chemical Communications, 2311-2319.

Sieber, S.A., Mondala, T.S., Head, S.R., and Cravatt, B.F. (2004). Microarray Platform for Profiling Enzyme Activities in Complex Proteomes. Journal of the American Chemical Society *126*, 15640-15641.

Sipos, T., and Merkel, J.R. (1970). An effect of calcium ions on the activity, heat stability, and structure of trypsin. Biochemistry *9*, 2766-2775.

Sit, P.S., and Marchant, R.E. (2001). Surface-dependent differences in fibrin assembly visualized by atomic force microscopy. Surface Science *491*, 421-432.

Sobek, J., Bartscherer, K., Jacob, A., Hoheisel, J.D., and Angenendt, P. (2006). Microarray technology as a universal tool for high-throughput analysis of biological systems. Comb Chem High Throughput Screen *9*, 365-380.

Sousa, S.R., Brás, M.M., Moradas-Ferreira, P., and Barbosa, M.A. (2007). Dynamics of Fibronectin Adsorption on TiO2 Surfaces. Langmuir *23*, 7046-7054.

Sprague, B.L., Pego, R.L., Stavreva, D.A., and McNally, J.G. (2004). Analysis of binding reactions by fluorescence recovery after photobleaching. Biophys J *86*, 3473-3495.

Sriram, P., Kalogerakis, N., and Behie, L.A. (1996). Experimental determination of the rate of autolysis of trypsin at 37 °C. Biotechnology Techniques *10*, 601-606.

Steiner, G. (2004). Surface plasmon resonance imaging. Analytical and Bioanalytical Chemistry *379*, 328-331.

Stigter, E., de Jong, G., and van Bennekom, W. (2007). Development of an open-tubular trypsin reactor for on-line digestion of proteins. Analytical and Bioanalytical Chemistry *389*, 1967-1977.

Stroud, R.M. (1974). A family of protein-cutting proteins. Scientific American *231*, 74-88.

Suh, C.W., Kim, M.Y., Choo, J.B., Kim, J.K., Kim, H.K., and Lee, E.K. (2004). Analysis of protein adsorption characteristics to nano-pore silica particles by using confocal laser scanning microscopy. Journal of Biotechnology *112*, 267-277.

Sun, H., Chattopadhaya, S., Wang, J., and Yao, S. (2006). Recent developments in microarray-based enzyme assays: from functional annotation to substrate/inhibitor fingerprinting. Analytical and Bioanalytical Chemistry *386*, 416-426.

Takeda, S., Nakamura, C., Miyamoto, C., Nakamura, N., Kageshima, M., Tokumoto, H., and Miyake, J. (2003). Lithographing of Biomolecules on a Substrate Surface Using an Enzyme-Immobilized AFM Tip. Nano Letters *3*, 1471-1474.

Talbot, J., Tarjus, G., Van Tassel, P.R., and Viot, P. (2000). From car parking to protein adsorption: an overview of sequential adsorption processes. Colloids and Surfaces A: Physicochemical and Engineering Aspects *165*, 287-324.

Templin, M.F., Stoll, D., Schrenk, M., Traub, P.C., Vohringer, C.F., and Joos, T.O. (2002). Protein microarray technology. Trends Biotechnol *20*, 160-166.

Thompson, N.L., Burghardt, T.P., and Axelrod, D. (1981). Measuring surface dynamics of biomolecules by total internal reflection fluorescence with photobleaching recovery or correlation spectroscopy. Biophysical journal *33*, 435-454.

Tie, Y., Calonder, C., and Van Tassel, P.R. (2003). Protein adsorption: Kinetics and history dependence. Journal of Colloid and Interface Science *268*, 1-11.

Tilton, R.D., Robertson, C.R., and Gast, A.P. (1990). Lateral diffusion of bovine serum albumin adsorbed at the solid-liquid interface. Journal of Colloid and Interface Science *137*, 192-203.

Togashi, D.M., Ryder, A.G., and Heiss, G. (2009). Quantifying adsorbed protein on surfaces using confocal fluorescence microscopy. Colloids and Surfaces B: Biointerfaces *72*, 219-229.

Treetharnmathurot, B., Ovartlarnporn, C., Wungsintaweekul, J., Duncan, R., and Wiwattanapatapee, R. (2008). Effect of PEG molecular weight and linking chemistry on the biological activity and thermal stability of PEGylated trypsin. International Journal of Pharmaceutics *357*, 252-259.

Uttamchandani, M., Huang, X., Chen, G.Y.J., and Yao, S.Q. (2005). Nanodroplet profiling of enzymatic activities in a microarray. Bioorg Med Chem Lett *15*, 2135-2139.

Uttamchandani, M., Lu, C.H.S., and Yao, S.Q. (2009). Next Generation Chemical Proteomic Tools for Rapid Enzyme Profiling. Accounts of Chemical Research *42*, 1183-1192.

Vegas, A.J., Fuller, J.H., and Koehler, A.N. (2008). Small-molecule microarrays as tools in ligand discovery, pp. 1385-1394.

Vertegel, A.A., Siegel, R.W., and Dordick, J.S. (2004). Silica Nanoparticle Size Influences the Structure and Enzymatic Activity of Adsorbed Lysozyme. Langmuir *20*, 6800-6807.

Viot, P., Tarjus, G., Ricci, S.M., and Talbot, J. (1992). Random sequential adsorption of anisotropic particles. I. Jamming limit and asymptotic behavior. J Chem Phys *97*, 5212-5218.

Vörös, J. (2004). The Density and Refractive Index of Adsorbing Protein Layers. Biophysical journal *87*, 553-561.

Vroman, L., and Adams, A.L. (1969). Identification of rapid changes at plasma-solid interfaces. Journal of biomedical materials research *3*, 43-67.

Vyas, V., Podesta, A., and Milani, P. (2011). Probing nanoscale interactions on biocompatible cluster-assembled titanium oxide surfaces by atomic force microscopy. Journal of nanoscience and nanotechnology *11*, 4739-4748.

Wahlström, E., Lopez, N., Schaub, R., Thostrup, P., Rønnau, A., Africh, C., Lægsgaard, E., Nørskov, J.K., and Besenbacher, F. (2003). Bonding of Gold Nanoclusters to Oxygen Vacancies on Rutile TiO_{2}(110). Physical Review Letters *90*, 026101.

Wälivaara, B., Askendal, A., Lundström, I., and Tengvall, P. (1997). Imaging of the Early Events of Classical Complement Activation Using Antibodies and Atomic Force Microscopy. Journal of Colloid and Interface Science *187*, 121-127.

Wälivaara, B., Warkentin, P., Lundström, I., and Tengvall, P. (1995). Aggregation of IgG on Methylated Silicon Surfaces Studied by Tapping Mode Atomic Force Microscopy. Journal of Colloid and Interface Science *174*, 53-60.

Walsh, K.A., Ericsson, L.H., Bradshaw, R.A., and Neurath, H. (1970). Chemical evidence of a disulfide bond in bovine carboxypeptidase A. Biochemistry *9*, 219-225.

Wegner, K., Piseri, P., Tafreshi, H.V., and Milani, P. (2006). Cluster beam deposition: a tool for nanoscale science and technology. Journal of Physics D: Applied Physics *39*, R439-R459.

Wetterö, J., Askendal, A., Bengtsson, T., and Tengvall, P. (2002). On the binding of complement to solid artificial surfaces in vitro. Biomaterials *23*, 981-991.

Wills, E.D. (1954). The effect of anionic detergents and some related compounds on enzymes. The Biochemical journal *57*, 109-120.

Yang, J., Mei, Y., Hook, A.L., Taylor, M., Urquhart, A.J., Bogatyrev, S.R., Langer, R., Anderson, D.G., Davies, M.C., and Alexander, M.R. (2010). Polymer surface functionalities that control human embryoid body cell adhesion revealed by high throughput surface characterization of combinatorial material microarrays. Biomaterials *31*, 8827-8838.

Yang, X.Y., Li, Z.Q., Liu, B., Klein-Hofmann, A., Tian, G., Feng, Y.F., Ding, Y., Su, D.S., and Xiao, F.S. (2006). "Fish-in-Net" Encapsulation of Enzymes in Macroporous Cages for Stable, Reusable, and Active Heterogeneous Biocatalysts. Advanced Materials *18*, 410-414.

Yiu, H.H.P., Wright, P.A., and Botting, N.P. (2001a). Enzyme immobilisation using SBA-15 mesoporous molecular sieves with functionalised surfaces. Journal of Molecular Catalysis B: Enzymatic *15*, 81-92.

Yiu, H.H.P., Wright, P.A., and Botting, N.P. (2001b). Enzyme immobilisation using siliceous mesoporous molecular sieves. Microporous and Mesoporous Materials *44–45*, 763-768.

Yonath, A., Podjarny, A., Honig, B., Traub, W., Sielecki, A., Herzberg, O., and Moult, J. (1977). Structural analysis of denaturant-protein interactions: comparison between the effects of bromoethanol and SDS on denaturation and renaturation of triclinic lysozyme. Biophysics of structure and mechanism *4*, 27-36.

Yuan, Y., Velev, O.D., and Lenhoff, A.M. (2003). Mobility of Adsorbed Proteins Studied by Fluorescence Recovery after Photobleaching. Langmuir *19*, 3705-3711.

Zhao, C., Jiang, H., Smith, D.R., Bruckenstein, S., and Wood, T.D. (2006). Integration of an on-line protein digestion microreactor to a nanoelectrospray emitter for peptide mapping. Analytical Biochemistry *359*, 167-175.

Zhao, X., Pan, F., Cowsill, B., Lu, J.R., Garcia-Gancedo, L., Flewitt, A.J., Ashley, G.M., and Luo, J. (2011). Interfacial Immobilization of Monoclonal Antibody and Detection of Human Prostate-Specific Antigen. Langmuir *27*, 7654-7662.